On Low Frequency Conducted EMI: Interference Mitigation with Focus on the DC Switching Harmonic in the Time and Frequency Domains

Submitted July 2023, to obtain the double degree of
Doctor of Philosophy
in
Electrical and Electronic Engineering.

Angel Eduardo Pena Quintal
20198414

Supervised by
University of Nottingham:
Prof. M. Sumner & Dr. S. Greedy
Leibniz University Hannover:
Prof. Dr. H. Garbe
Jade University of Applied Sciences:
Prof. Dr. S. Koj

George Green Institute for Electromagnetic Research
Power Electronics Machines and Control
Department of Electrical and Electronic Engineering

Signature _____

Date _____ / _____ / _____

The University of Nottingham, University Park, UK

Abstract

English:

The recent increase of interconnected electrical systems such as power supplies and communication links are creating problems associated with electromagnetic fields generated at different voltage levels and frequencies. Semiconductor switches used in for example Switched Mode Power Supplies are constantly increasing in power rating and frequency limits. In addition, wired communication links are also increasing the working bandwidth and channel capability to transfer more information in less time.

Smart grids are receiving much attention from companies and researchers all over the world. Two concerns that drive the research carried out on smart grids are Power Quality and Signal Integrity. This work presents an analysis of conducted emissions with two aims.

Firstly, an analysis is made of the simulated and measured data when a DC system generates electromagnetic interference and how to improve or mitigate it with certain frequency modulation techniques by spreading the spectrum of the switching frequency in agreement to an established standard.

Secondly, a demonstration of the coupling effects as one of the major concerns when dealing with Electromagnetic Interference sources is presented experimentally. Statistical analyses for these tests are performed to understand the main causes and possible actions to suppress interference and to address Electromagnetic Compatibility between devices.

The work presents the following findings.

1. An understanding of the important parameters for frequency modulation techniques called as Spread Spectrum. These parameters are the rate of change for the modulating signal and the modulation index that controls the switching frequency of a modulated DC-DC converter to mitigate the interference measured.

2. The importance of an auxiliary time domain (Bit Error Rate) analysis to measure the interference of a DC-DC converter modulated by Spread Spectrum to understand the main drawback in the emissions measured from a different point of view by means of a Crosstalk environment.

3. The conclusion that Bit Error Rate measurement of a communication signal cannot be decreased using Spread Spectrum Modulation for the power converter as the EMI source.

The results obtained use data measured using an EMI receiver and where possible a simulation describing the most important parameters. This work provides interesting and useful points to analyse the Spread Spectrum technique applied to DC power converters and the main advantages and disadvantages.

German:

In jüngster Zeit führen die zunehmend vernetzten elektrischen Systeme wie Stromversorgungen und Kommunikationsverbindungen zu Problemen, die mit elektromagnetischen Feldern verbunden sind, die bei verschiedenen Spannungsebenen und Frequenzen erzeugt werden. Halbleiterschalter, die beispielsweise in geschalteten Stromversorgungen verwendet werden, nehmen stetig an Leistungsfähigkeit und Frequenzgrenzen zu. Zudem werden kabelgebundene Kommunikationsverbindungen zunehmend erweitert, um mehr Informationen in kürzerer Zeit zu übertragen.

Smart Grids erlangen weltweit große Aufmerksamkeit von Unternehmen und Forschern. Zwei wesentliche Anliegen, die die Forschung in Bezug auf Smart Grids antreiben, sind die Netzqualität (Power Quality) und die Signalintegrität. Diese Arbeit präsentiert eine Analyse der leitungsgebundenen Emissionen mit zwei Zielen.

Erstens wird eine Analyse der simulierten und gemessenen Daten durchgeführt, wenn ein Gleichstromsystem elektromagnetische Interferenzen erzeugt, und wie diese mit bestimmten Frequenzmodulationstechniken verbessert oder reduziert werden können, indem das Spektrum der Schaltfrequenz gemäß eines etablierten Standards verbreitert wird.

Zweitens wird experimentell eine Demonstration der Kopplungseffekte als eine der Hauptursachen für elektromagnetische Interferenzquellen präsentiert. Statistische Analysen für diese Tests werden durchgeführt, um die Hauptursachen zu verstehen und mögliche Maßnahmen zur Unterdrückung von Interferenzen und zur Behandlung der elektromagnetischen Verträglichkeit zwischen Geräten zu ermitteln.

Die Arbeit präsentiert folgende Ergebnisse:

1. Ein Verständnis der wichtigen Parameter für Frequenzmodulationstechniken, die als Spread Spectrum bezeichnet werden. Diese Parameter sind die Änderungsrate des modulierenden Signals und der Modulationsindex, der die Schaltfrequenz eines modulierten DC-DC-

Wandlers zur Verringerung der gemessenen Interferenzen steuert.

2. Die Bedeutung einer zusätzlichen zeitorientierten (Bitfehlerrate) Analyse zur Messung der Interferenzen eines durch Spread Spectrum modulierten DC-DC-Wandlers, um das Hauptproblem bei den gemessenen Emissionen aus einer anderen Perspektive in einer Kreuzkopplungsumgebung zu verstehen.

3. Die Schlussfolgerung besagt, dass die Bitfehlerrate-Messung eines Kommunikationssignals durch Spread Spectrum-Modulation für den Leistungswandler als EMI-Quelle nicht verringert werden kann.

Die erzielten Ergebnisse basieren auf den gemessenen Daten mit einem EMI-Empfänger und gegebenenfalls einer Simulation, die die wichtigsten Parameter beschreibt. Diese Arbeit liefert interessante und nützliche Aspekte für die Analyse der Spread Spectrum-Technik, die auf Gleichstromwandler angewendet wird, sowie deren Hauptvorteile und -nachteile."

Publications

Publications of 2022

J-1 A. Pena-Quintal, Waseem El Sayed, Mark Sumner, Seda Ustun Ercan, Steve Greedy, Dave Thomas, Robert Smolenski, "On Spread Spectrum for DC grids: Low Frequency Conducted EMI Mitigation and Signal Integrity Disruption in Serial Communication Links".
Pusblished in: IEEE Transactions on Electromagnetic Compatibility.
DOI: 10.1109/TEMC.2023.3273111

M-1 A. Pena-Quintal, Hermes Loschi, Robert Smolenski, Mark Sumner, Dave Thomas, Piotr Lezynski, "Impact of Pseudo-Random Modulation on Measured Conducted EMI".
Published in: IEEE Electromagnetic Compatibility Magazine (Volume: 11, Issue: 2, 2nd Quarter 2022).
DOI: 10.1109/MEMC.2022.9873829

C-1 A. Pena-Quintal, A. Khilnani, L. Sandrolini, M. Sumner, D. Thomas and S. Greedy, "EMI Spectral Aggregation of Modulation Schemes in a lab-based DC Microgrid".
Published in: 2022 IEEE International Symposium on Electromagnetic Compatibility & Signal/Power Integrity (EMCSI).
DOI: 10.1109/EMCSI39492.2022.9889337

C-2 A. D. Khilnani, A. E. Pena-Quintal, E. Ballukja, M. Sumner, D. W. P. Thomas, L. Sandrolini, A. Mariscotti, "Influence of Impedance Interaction & Comparability on Spectral Aggregation (2–150 kHz) in DC Grids".
Published in: 2022 International Symposium on Electromagnetic Compatibility – EMC Europe.
DOI: 10.1109/EMCEurope51680.2022.9900988

C-3 E. Ballukja, K. Niewiadomski, A. Pena-Quintal, D. W. P. Thomas, S. Sumsurooah and M. Sumner, "Stochastic Modelling of Power Electronic Converters under Uncertainties".
Published in: 2022 IEEE International Symposium on Electromagnetic Compatibility & Signal/Power Integrity (EMCSI).
DOI: 10.1109/EMCSI39492.2022.9889372

Publications of 2021

C-4 A. Pena-Quintal, K. Niewiadomski, S. Greedy, M. Sumner, D.W.P. Thomas, "The Influence of the Number of Frequencies and the Frequency Repetitions Rates in Spread Spectrum Sigma-Delta Modulated DC-DC Converters".
Published in: 2021 Asia-Pacific International Symposium on Electromagnetic Compatibility (APEMC).
DOI: 10.1109/APEMC49932.2021.9597184

C-5 A. Pena-Quintal, K. Niewiadomski, V. Muneeswaran, S. Greedy, M. Sumner, D.W.P. Thomas, "The Effect of Spread Spectrum Modulation for a Buck Converter Coupled with a Single Wired Communication Link".
Published in: 2021 IEEE International Joint EMC/SI/PI and EMC Europe Symposium.
DOI: 10.1109/EMC/SI/PI/EMCEurope52599.2021.9559276

C-6 K. Niewiadomski, A. Pena-Quintal, D.W.P. Thomas, S. Sumsurooah, "Sensitivity Analysis of Parasitics in Power Electronic Circuit Through Sobol' Indices".
Published in: 2021 Asia-Pacific International Symposium on Electromagnetic Compatibility (APEMC).
DOI: 10.1109/APEMC49932.2021.9597088

Publications of 2020

C-7 A. E. Pena-Quintal, M. J. Basford, K. Niewiadomski, S. Greedy, M. Sumner, D. W. P. Thomas, "Data Links Modelling under Radiated EMI and its Impact on Sampling Errors in the Physical Layer".
Published in: 2020 International Symposium on Electromagnetic Compatibility - EMC EUROPE.
DOI: 10.1109/EMCEUROPE48519.2020.9245670

C-8 M. J. Basford, A. E. Pena-Quintal, S. Greedy, M. Sumner, D. W. P. Thomas, "Open Source Bit Error Rate FPGA-based Tester for Serial Communications".
Published in: 2020 International Symposium on Electromagnetic Compatibility - EMC EUROPE.
DOI: 10.1109/EMCEUROPE48519.2020.9245786

J - Journal publication, **M** - Magazine publication, **C** - Conference publication

Acknowledgements

I would like to thank all the people who helped me during this journey. I will always be grateful to Prof. Dave Thomas for giving me the opportunity to be part of the ETOPIA (European Training network Of PhD researchers on Innovative EMI analysis and power Applications) project and guiding my research.

I would also thank my supervisors, especially Prof Mark Summner who always helped me and suggested points to improve in my research. Finally, a special thanks to Dr. Alessandro Costabeber who, although no longer with us, helped me a lot and continues to inspire me every day.

I really appreciate the support and help of my colleagues at the PEMC (professors, researchers and technicians) and GGIEMR laboratories, thank you all for making my journey easier with their ideas and for the time we spent together.

Finally, words will never be enough to thank my family. My parents (Freddy and Maria) always were there to support me and dream with me about my goals. This achievement is also yours. I am extremely grateful to my brothers (Irving and Guillermo) for their advise and time to speak with me during difficult times. You all inspired me to pursue this goal in my academic career knowing that we can go further everyday if you believe in yourself.

This project has received funding from the European Union's Horizon 2020 research and innovation programme under the Marie Skłodowska-Curie grant agreement No 812753

List of Figures

List of Tables

List of Abbreviations

ΣΔM . . . . . Sigma Delta Modulator

AC . . . . . Alternating Current

ADC . . . . . Analogue to Digital Converter

AV . . . . . Average Value

AWG . . . . . American Wire Gauge

BER . . . . . Bit Error Rate

BERT . . . . . Bit Error Rate Tester

CENELEC . . Comité Européen de Normalisation Électrotechnique

CF . . . . . Constant Frequency

CFL . . . . . Compact Fluorescent Lamps

CISPR . . . . International Special Committee on Radio Interference

CL . . . . . Confidence Level

CM . . . . . Common Mode

DC . . . . . Direct Current

DetM . . . . . Deterministic Modulation

DFT . . . . . Discrete Fourier Transform

DM . . . . . Differential Mode

DUT . . . . . Device Under Test

EC . . . . . European Commission

EMC . . . . . Electromagnetic Compatibility

EMI . . . . . Electromagnetic Interference

FACTS . . . . Flexible AC Transmission Systems

FCC . . . . . Federal Communications Commission

FD . . . . . Frequency domain

FFT . . . . . Fast Fourier Transform

FPGA . . . . Field Programmable Gate Array

HV . . . . . High Voltage

IC . . . . . Integrated Circuit

IEMI . . . . . Intentional Electromagnetic Interference

IF . . . . . Intermediate Frequency

IGBT . . . . . Insulated Gate Bipolar Transistor

IR . . . . . Infra Red

LCG . . . . . Linear Congruential Generator

LFSR . . . . . Linear Feedback Shift Register

LISN . . . . . Line Impedance Stabilisation Network

LV . . . . . Low Voltage

NI . . . . . National Instruments

NRZ . . . . . Non Return to Zero

OSI . . . . . Open Systems Interconnection Model

PAM . . . . . Pulse Amplitude Modulation

PC . . . . . Personal Computer

PCB . . . . . Printed Circuit Board

PEI . . . . . Power Electronic Interfaces

PK . . . . . Peak Value

PLC . . . . . Power Line Communication

PQ . . . . . Power Quality

PRF . . . . . Pulse Repetition Frequency

PSU . . . . . Power System Unit

PV . . . . . Photovoltaic

PWM . . . . . Pulse Width Modulation

QP . . . . . Quasi-Peak Value

RanM . . . . . Random Modulation

RBW . . . . . Resolution Bandwidth

RF . . . . . Radio Frequency

SI . . . . . Signal Integrity

SMPS . . . . . Switched Mode Power Supply

SSFW . . . . . Square Series Fourier Wave

SSM . . . . . Spread Spectrum Modulation

STFT . . . . . Short Time Fourier Transform

TD . . . . . Time domain

TI . . . . . Texas Instruments

TTL . . . . . Transistor–Transistor Logic

UV . . . . . Ultra Violet

WPT . . . . . Wireless Power Transfer

Contents

Chapter 1

Introduction

1.1 Main Issues in Modern Grids

The state-of-the-art electrical and electronic devices are changing their current operation to have more interconnected systems and complexity. This fast-growing trend has been pushed by the microgrid concept. In fact, microgrid usage has increased over the past years. On the one hand, the main reasons behind it are the transition to non-fossil fuels such as photovoltaic (PV), wind turbines, fuel cells and storage devices (batteries and supercapacitors). It is during recent years that microgrids have been providing solutions to meet the local demands of distributed power systems [1]. On the other hand, the human need to communicate along other areas with or without cables has encouraged new and challenging ways to transfer data over considerable distances using cables or high gain antennas. However this can create interference between all of the devices involved in a certain area or environment.

According to the synthesis report titled, "Scenarios for the Development of Smart Grids in the UK" [2], Smart Grids employ concepts such as new kinds of power company, time-of-use tariffs to create a new paradigm for managing and distributing electrical power, with the main focus of

decarbonising the UK's electricity system. This approach is being developed in other countries as well to move to a more sustainable future.

In reality, sustainable energy is one of the main drivers for the use of smart grids all over the world as is presented in Figure 1.1, in this graph it can be seen the investments of countries such as China (approximately 400 USD billion), United States (approximately 350 USD billion) and Europe (approximately 200 USD billion) in energy as the main leaders in the technology with a clear focus on Fossil fuel supply, Power sector, Energy efficiency and Renewables for transport and heat.

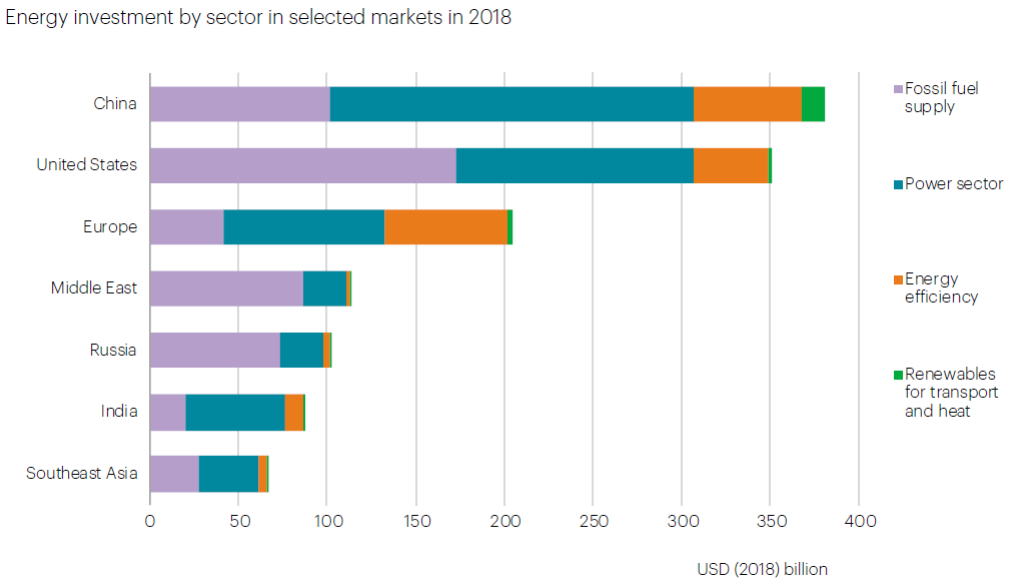

Figure 1.1: Energy investment by sector in selected markets for 2018.

Considering this increasing trend towards power networks which include a high penetration of Power Conversion and Integrated Circuit (IC) technology, issues related to Electromagnetic Interference (EMI) become important for reliable system operation. EMI is generally classified as conducted and/or radiated interference. For both classifications, these issues can impact performance on; digital devices, converters, cables, smart devices, communications and plenty of other systems, as devices working on the same system all generate and can be susceptible to EMI. As illustrated in Figure 1.2, it can be seen the two main paths for EMI in which there is a

source and a victim.

Therefore, EMI analysis is a task that should be considered very seriously when designing electrical and electronic systems since one system can affect the behaviour of other systems through the different EMI coupling paths.

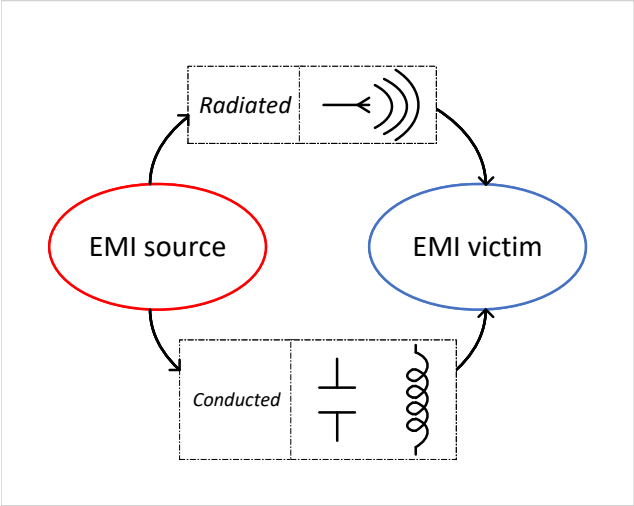

Figure 1.2: Interference of different devices over a common point.

Another important topic that encourages the study of EMI is the use of Power Line Communications (PLC) applied to smart grids [3]. In fact, a new topic called Supraharmonics has been taking attention nowadays due to the frequency bandwidth 9-150 kHz covered. This band will be considered as an important part for researching purposes in the low frequency band.

The IEEE 1901.2 "Standard for Low-Frequency (less than 500kHz) Narrowband Power-Line Communications for Smart-Grid Applications" [4], provides the most important recommendations to avoid interference and to address a balanced and efficient channel for PLC technologies. For example, technologies which can create or to be susceptible to EMI when PLC is present are grid to utility meters, electric vehicle to charging stations, lighting and solar panels, and other equipment requiring PLC communications for data or control [4].

1.1.1 Electromagnetic Interference Issues

Over the recent years, there has been an increase of grid connected power electronic converters (e.g. for renewable energy, motor drives, power supplies for electronic devices). These devices can cause high frequency currents and high rates of changes of current and voltage, which can combine at different parts of the distribution systems. The frequencies emitted by a particular piece of equipment might be bounded within the limits given by the manufacturer of the device or between the most suitable frequency limits for the power system to maintain correct functioning without any disruption in other devices, particularly for communications systems, medical equipment and aircrafts [5]. A brief list of the most common issues of EMI according to [6] and [7], is usually identified as listed below.

- Related to Power Electronic Interfaces (PEI):
  Power converters's switching frequency used for renewable sources.
  Errors in communication for Smart Meter.
- Power Line Communication (PLC):
  EMI generation and signal propagation along the power lines.
- Flexible AC Transmission System (FACTS):
  Continuous transient operation due to switching devices.
- Other Communication technologies:
  Ever increasing network capacity to cover demands in challenging and changing environments given by the electric car market.

1.1.2 Power Quality Issues

In order to define what are the main Power Quality (PQ) issues in power systems the general meaning of PQ should be defined. According to the IEEE Recommended Practice for Monitoring Electric Power Quality [8],

PQ refers to a variety of electromagnetic phenomena that can characterise the voltage and current at a given time and at given location on the power system. It can be applied to any Low Voltage (LV) or High Voltage (HV) system that is able to generate electrical energy. Most of the PQ analyses and standards are currently based on AC systems and refer to the system fundamental frequency. One of the most important standards is the EN- 50160 [9] which explains the voltage characteristics in the Public Distribution. The main characteristics of the supply power are given by,

- Frequency
- Magnitude
- Waveform
- Symmetry of three phase voltages

These characteristics are applied for both LV and HV systems to determine the main issues generated in AC. According to G. T. Heydt, the most common power quality engineering indices are listed in [10]. However, the application of these standards to a DC system requires a complete rethink of the nature of a switching device in both Time and Frequency domains in order to create systematic standards.

The possible standardisation of DC power has been a topic which is attracting attention due to the EMI issues created by noise and the nonlinear effects from the devices used. In [11], a set of different indices based on statistical analyses is presented, however the results might be dependant on the recorded time of the signal to be analysed. The main cause for the EMI in DC microgrid systems is due to Switched Mode Power Supplies (SMPS), these systems tend to generate considerable levels of EMI because of its switching nature. There are no specified Electromagnetic Compatibility (EMC) limits for DC rails, so there are no specific tests, for example in the

European Commission (EC) or in the Comité Européen de Normalisation Électrotechnique (CENELEC) regulations that can be applied directly to this situation. Likewise, a Power System Unit (PSU) and the DC supplied circuit may be considered as sub-systems, possibly even components; as a result, they may be exempt from the EC directive [12].

1.1.3 Signal Integrity Issues

Signal Integrity (SI) is an important topic to provide reliable communication in today's systems. According to [13], SI is considered a set of measures of the quality of an electrical signal transmitted through the interconnects. However, as the definition states it can have a double relationship considering the quality and degradation (at the same time) of a signal for a communication link. The authors in [13] and [14] present important parameters when signal integrity is studied. These issues are:

- Losses
- Impedance mismatch
- Crosstalk

Losses are caused by the dielectric (electrical field) and conductor losses (skin effect and conductivity). Impedance mismatch depends on the geometry and materials for the transmission line model and the impedance used for termination, also the nature of the connections or connectors. Crosstalk is a more complex issue which depends mostly on the coupling effects (conducted and inductive) from two or more conductors and can vary according to different frequencies.

In fact, the important issue of EMI that will be addressed in this work is how the interference generated by a converter can affect the quality of a signal on a nearby communication link by means of Crosstalk. In recent

research focused on DC converters that will be discussed in this thesis, it has been demonstrated that coupling methods are an important aspect of understanding how EMI generates between devices. Moreover, both capacitive and inductive couplings are important paths for EMI activity, and the cable coupling that happens in real applications can be a combination of both effects.

1.2 Low Frequency Issues: Supraharmonics

In the recent literature a problem with regards to low frequency distortion is referred to as Supraharmonics [3], [15], [16]. In this context, the interference generated appears to include all the frequency content that is above the well-known harmonics bands as stated in AC standards. However the usage of this bandwidth is analysed for frequencies ranging from 2 kHz to 150 kHz [3]. To understand better this issue, [15] has compared different spectrums for three different load test cases for specific SMPS; no load, 25% load and 90% load. As inferred, bigger amplitudes are generated in the frequency domain areas where loads were higher. [16] states that different devices tend to generate a particular band of interference, this is more noticeable in non linear devices which defines an interesting path to research about standardisation in these kinds of devices. Due to the nature of the low frequency band to be analysed in this thesis, it seems important to account for EMI in the Supraharmonics and standardisation of limits as suggested in [17].

In [18] the interference generated to a PLC channel when it is tested in a low voltage network is analysed under five different testing cases. This work concludes that the frequency range from 9 kHz to 95 kHz is the most affected by the most common interactions such as high voltage/current levels, low impedance path at the communication frequency, overheating

of components in the voltage systems, non-linear equipment that generate harmonics and waveform distortion.

The mitigation of EMI in the Supraharmonics range for Power Electronics was considered in [19]. In this research it is concluded that different topologies can generate different harmonic content and it is important to account for the methods used to drive them. This work [19], analysed the usage of methods for spreading the spectrum is introduced to overcome an undesired interference caused by Supraharmonics in conventional PWM power converters.

1.3 Research Objectives

This research work is aimed at developing an understanding of EMI issues in DC micro grids to account for mitigation techniques in both the time and frequency domains applied to DC power converters. The investigation is focused on one converter having a switching frequency modulation technique, however different techniques are applied and analysed on the same device in order to understand how these interactions can generate different EMI.

The task of understanding the EMI generated by a switching converter will be performed by investigating the nature of modulation techniques to reduce the EMI impact on DC converters. This thesis will provide valuable points on how these switching devices can potentially have considerable impact on other devices such as wired communication links.

Finally, the points and conclusions obtained in this thesis can be used to inform for future standardisation for DC micro grids and create new frameworks to measure and understand the EMI generated in emerging DC complex systems.

1.3.1 Specific Objectives

This research work has the following specific objectives:

- Test two Spread Spectrum Modulation techniques to determine advantages and disadvantages in the time and frequency domains for the DC converter.
- Assess the effects of the Spread Spectrum Modulation technique for a DC converter by considering the CISPR-16 Standard framework of measurement.
- Determine the impact or the side effects of Spread Spectrum Modulation for a DC converter in a Crosstalk interaction to a communication channel by measuring the Bit Error Rate.
- Design a controlled pseudorandom variant of Spread Spectrum Modulation for an FPGA to shape the noise by considering a repetition rate control of switching frequencies over time.

1.4 Main Contributions

The knowledge gathered from the experimental tests supported by the main theory and simulations in this thesis has led to the main contributions listed below:

1. The first contribution is the understanding of the trade-offs when modulation techniques such as Spread Spectrum are used as a solution to reduce EMI. The EMI energy is being re-distributed over a wider range of the frequency spectrum. However, many researchers consider only the benefits in the frequency domain (FD) while there are important drawbacks which can be observed in the time domain (TD).

2. A second important contribution of this work is the demonstration of the signal integrity for a communication data link over a cable which is coupled to an EMI source such as a power converter. The Bit Error Rate (BER), figure of merit is used to quantify the channel quality of these EMI effects of power systems to data systems. Crosstalk between conductors/devices is a situation that happens frequently and must be minimised or avoided while possible. The use of different modulation techniques applied for power converters has shown that the impact on the BER value is not mitigated, in fact, it can generate a considerable increase in the error rate figure.

3. Finally, this work aims to define the main parameters which influence the propagation of interference when a system as a DC-DC converter is modulated using switching frequency modulation techniques. These parameters can be used as recommendations for researchers or companies that are interested in strategies to mitigate the effects of the switching frequency of a power converter knowing about the drawback effect seen in time domain.

1.5 Thesis Structure

The structure of this thesis is so as to provide a practical and useful study about the use of modulation techniques and its influence on different environments that can exist in real cases. To address these points, the thesis is divided into seven chapters:

In Chapter II, a literature survey of main EMI concepts and issues with special focus on EMI for DC power converters is presented. In this chapter the required background theory is presented as well as important EMI definitions, frequency limits, standards and main interactions given by cable coupling (capacitive and inductive) mainly used for transmission line models

to address Crosstalk. All of these topics are taken into consideration to define how a DC converter can be analysed as an EMI source by understanding the generation, propagation and mitigation.

In Chapter III, a broad explanation of Spread Spectrum Modulation (SSM) considering the most important parameters is presented. In this chapter the theoretical background is presented along with information about the importance of time and frequency domains. The signals used to modulate a converter are considered as well as the modulator to be used. A simulation is presented based on the formulas presented in the chapter.

The measured results obtained with an EMI receiver are presented in Chapter IV along with a discussion about the best mitigation profile to be used as well as the best modulating signal parameters for CISPR-16 Band A with regards to mitigation purposes. In addition, this chapter considers the information of the previous chapter to discuss the experimental results about mitigation for modulating signal in the frequency range covered in the frequency range from 9 kHz to 150 kHz.

In Chapter V, an analysis based on BER is carried out to determine the effect of different parameters when SSM is used with a power converter, the Crosstalk between cables (power and data) is tested under different parameters in order to determine the impact of this technique for two different modulating signals. Crosstalk interaction is usually found in modern smart grids when the switching frequency of a converter creates interference that must be considered to meet EMC.

A different approach for the SSM technique is presented in Chapter VI. A Pseudorandom signal with a controlled repetition rate of switching frequency is used to drive a converter under a similar environment as the converter used in Chapter IV. This chapter demonstrates the importance of the EMI receiver parameters such as the resolution bandwidth and the dwell time of the instrument. Different test cases are shown to support the

idea of different rates of change for the generation of the driving signal and its relationship to the mitigation of the switching interference.

Finally, Chapter VII presents the conclusions of the thesis mainly based on the EMI issues found in DC systems and its possible mitigation strategies. The chapter includes conclusions for the use of SSM with a single converter with regards to time and frequency domains. In addition, recommendations are provided for Spread Spectrum techniques and the need for time domain standards for DC systems with a focus on frequency domain procedures is highlighted.

Chapter 2

EMI in DC Microgrids

In this chapter, the main theory behind EMI for DC microgrid technology is introduced and explained. The chapter contains theoretical information about the nature of the emissions, the electrical and electronic devices that can generate EMI, the valid standards and set-ups for measuring EMI as well as the coupling methods that can generate issues in microgrid technology. In addition, there is a section with information about common EMI mitigation techniques such as filtering and modulation in frequency, but mainly focused on the latter. These topics are necessary to introduce and explain the generation, propagation, and mitigation of EMI presented in the next chapters of the thesis.

2.1 EMI Basic Concepts

Theoretically, there are two main types of emissions generated by any electrical or electronic device. According to Clayton's book, "Introduction to Electromagnetic Compatibility" [20], the EMI can be radiated or conducted.

In Table 2.1, the explanation of both situations can be seen with the main limits or frequency ranges and common listed cases. The limits are according to the Federal Communications Commission (FCC) in the United

States.

Table 2.1: Common emissions limits and examples.

Emission Type	**Frequency Range**	**Examples**
Conducted	9 kHz - 30 MHz	AC Power cords and cables (50 or 60 Hz frequency), light bulbs, compact fluorescent lamps (CFL).
Radiated	30 MHz - 40 GHz	Antennas, radio communication disturbance (radars), resonances of passive devices, damped oscillatory magnetic fields.

Considering the nature of the two given cases that generate emissions, there exist coupling mechanisms that must be addressed as well. This is due to the nature of any conductor which has resistive, capacitive (related to electric field) and inductive (related to magnetic field) behaviour at different frequencies. It is important to mention that wire insulations do not affect magnetic field properties caused by the currents in the cables.

In the frequency band for conducted emissions there are two main paths for noise flow as can be seen in Figure 2.1. Firstly, the Differential Mode (DM) noise (Figure 2.1a) is the noise generated the go and return in two conductors, for example an AC system which has Phase and Neutral.

However, this is not the only path for noise flow, another path is given by the Common Mode (CM) noise (Figure 2.1b). Considering the same case of an AC system with two main conductors, if both conductors have the same current then that is a common current and there must be an return current in a separate third conductor. Common mode noise is often flowing to the lowest potential, in this case the physical ground via the stray capacitance.

With regards to parallel conductors, the coupling mechanisms are conductive, capacitive and inductive leading to Crosstalk. The transmission line models are often used to demonstrate these effects for a pair of cables with similar geometrical properties [20], and for simplicity cylindrical conductors

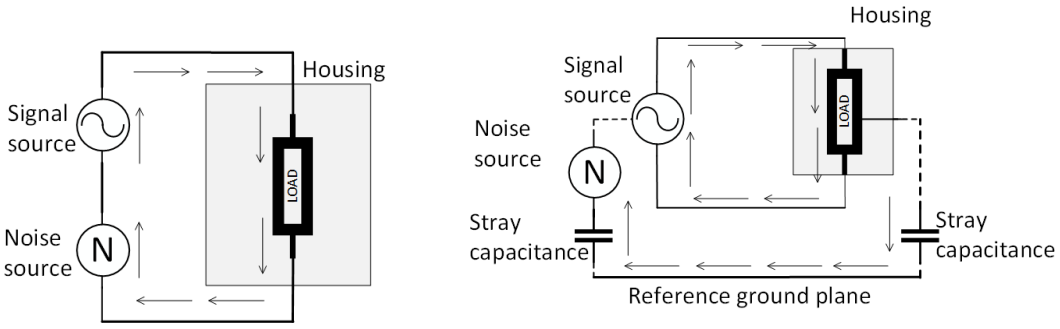

(a) Differential mode noise path. (b) Common mode noise path.

Figure 2.1: Noise propagation along two different paths.

are considered.

2.2 Crosstalk Effects

The conductors (cables) can be represented as a transmission line with lumped parameters. Consider the case that the wires might have the same radius (r_w) and length ($\mathscr{L}$), with a separation (s) between them. The interaction of these two conductors are graphically presented in Figure 2.2. In here, the capacitive (2.1) and inductive (2.2) coupling effects are highlighted in red with the corresponding differential equations representing the relation in the transmission line model.

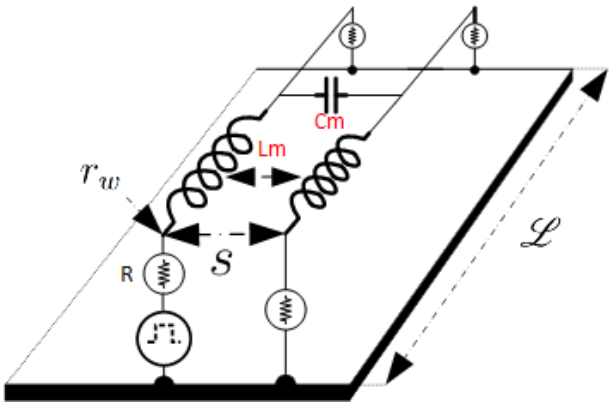

Figure 2.2: Cable conductor model, on the left the EMI "aggressor", on the right the "victim".

$$I_{Cm} = C_m \frac{dV}{dt}, \tag{2.1}$$

$$V_{Lm} = L_m \frac{dI}{dt}, \tag{2.2}$$

Equations (2.1) and (2.2) show that coupling to a victim conductor is related to the rate of the change of voltages and currents on the interference source conductor. The lumped circuit model can be useful for analysing for both radiated and conducted cases.

The DC resistance R of a round wire of radius r_w, conductivity σ, and total length $\mathscr{L}$ is [20].

$$R = \frac{\mathscr{L}}{\sigma \pi r_w^2} \tag{2.3}$$

In Figure 2.2, referring to one of the cylindrical conductors, higher frequencies will make the electrons flow towards the outside. This is the skin phenomenon or skin depth. The skin depth of the conductor is then given by [20],

$$\delta = \frac{1}{\sqrt{\pi f \mu \sigma}}, \tag{2.4}$$

where $\mu = 4\pi x 10^{-7} H/m$ represents the permeability of the conductor, σ is the conductor conductivity and f is the the frequency of the wave flowing across it. The skin depth phenomenon will cause the inductance and resistance to be frequency dependant.

2.2.1 Capacitive Coupling

This coupling mechanism is generated by an electric field. In order to have a capacitive relationship between a source of EMI and a victim the conductors must be in close proximity.

Considering the capacitive effect in which both conductors have similar characteristics, the contribution to capacitance (c) in F/m is given by [21],

$$c = \frac{\pi \epsilon_0}{\ln(s/r_w)}, \tag{2.5}$$

where, r_w represents the radius of the two conductors, s represents the distance between them and ϵ_0 is the relative permittivity of the conductor. The capacitive relationship explained in [22] of the two conductors is shown in Figure 2.3.

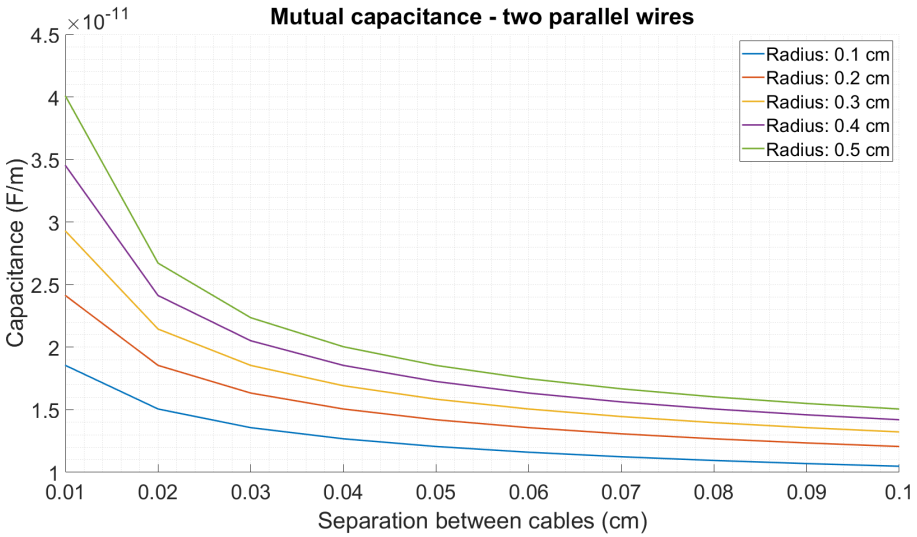

Figure 2.3: Capacitive behaviour of two parallel wires with different separations.

2.2.2 Inductive Coupling

This coupling mechanism has similarities with the capacitive coupling. However, the inductive behaviour is found when the two cables couple by a magnetic field. If we assume that the wires are sufficiently separated the mutual inductance (H/m) with a ground plane placed below the conductors is given by [21],

$$L_m = \frac{\mu_0}{4 \cdot \pi} \ln\left(1 + 4\frac{h_G\ h_R}{S^2}\right), \tag{2.6}$$

where h_G is the height above ground of the first cable, h_R is the height above ground of the second cable and S is the separation between cables. The graphical result presented in [22] of the equation above can be seen in Figure 2.4.

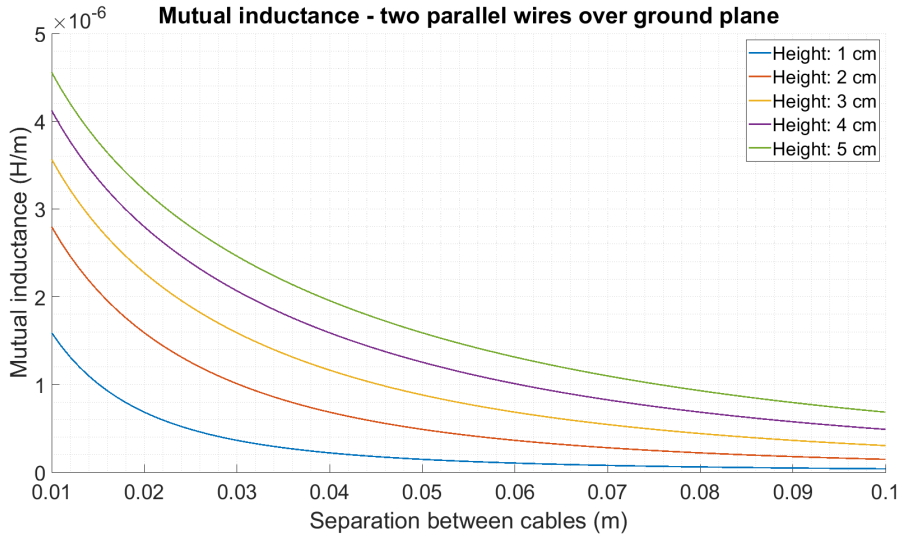

Figure 2.4: Inductive behaviour of two parallel wires over a ground plane.

Here it can be noticed a relationship of distance and mutual inductance, when the separation exceeds a few centimeters the mutual inductance becomes less significant.

2.2.3 Multiconductor Transmission Line Equations

In [23], the explanation of the multiconductor transmission line model equation focused on Spice simulation software is presented. This model is based on the theory stated by [20]. The authors consider an arrangement of cables as shown in Figure 2.2. In this figure there exist two conductors and one ground plane which composes a cable bundle.

If the per-unit length parameters are considered, the matrices of the transmission line model for inductance [L], capacitance [C], resistance [R] and conductance [G] are obtained. The voltage and current on the cylindrical conductors widely spaced along the z axis may be described in time by the

following equations [23]:

$$\begin{aligned}\frac{\delta}{\delta z}[V(z,)]] &= -[R][I(z,t)] - [L]\frac{\delta}{\delta z}[I(z,t)],\\ \frac{\delta}{\delta z}[I(z,t)] &= -[G][V(z,t)] - [C]\frac{\delta}{\delta z}[V(z,t)],\end{aligned} \tag{2.7}$$

where $[V(z,t)]$ and $[I(z,t)]$ are vectors of the conductors time domain voltage and current at a distance z along the bundle. The frequency domain equations are expressed as:

$$\begin{aligned}\frac{d}{dz}[\tilde{V}(z)] &= -[R][\tilde{I}(z)] - j\omega[L][\tilde{I}(z)],\\ \frac{d}{dz}[\tilde{I}(z)] &= -[G][\tilde{V}(z)] - j\omega[C][\tilde{V}(z)],\end{aligned} \tag{2.8}$$

The resistance and conductance can be combined into a single matrix with frequency dependence, and the same can be applied for the capacitance and conductance which yields.

$$\begin{aligned}\frac{d}{dz}[\tilde{V}(z)] &= -[\tilde{Z}][\tilde{I}(z)],\\ \frac{d}{dz}[\tilde{I}(z)] &= -[\tilde{Y}][\tilde{V}(z)],\end{aligned} \tag{2.9}$$

where

$$\begin{aligned}[\tilde{Z}] &= [\tilde{R}] + j\omega[\tilde{L}],\\ [\tilde{Y}] &= [\tilde{G}] + j\omega[\tilde{C}],\end{aligned} \tag{2.10}$$

Equations (2.7) to (2.10) fully express how the the conductors in a bundle couple.

Having considered the coupling methods and the transmission line model, it is clear that Crosstalk is the resulting effect of the coupling given by

the mutual inductance and mutual capacitance between conductors. There exist accepted methods to mitigate Crosstalk such as cable shielding, wider separation between conductors, decrease of edge rates, etc [13]. However, the intention of this research work is to decrease the EMI seen in the aggressor (the power converter) and address the effects of such a procedure with a time domain index seen in the victim (the communication link).

A practical example of the Crosstalk phenomena between conductors can be simulated and measured experimentally by considering a cable bundle with inputs and outputs in which 3 cables (transferring predefined signals) are placed in parallel above a ground plane with a certain separation between them and with certain height, the interference between cables can be simulated by employing state-of-the-art tools such as SACAMOS [24]. This is a software to generate cable bundles for Spice simulating softwares like Ltspice [25]. The results obtained were presented in [26] and are used in here to demonstrate a simple effect of interference. The block diagram in Figure 2.5 shows the Crosstalk-based set-up used for simulations and experimental tests, where the "Bit Sampling Error" is used as a the Crosstalk metric.

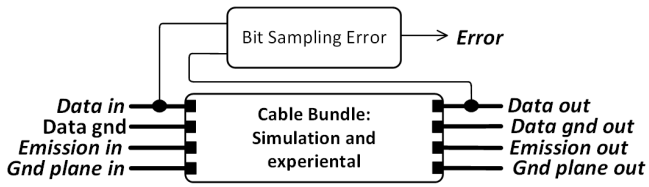

Figure 2.5: Crosstalk set-up with three conductors for simulation and experimental test.

The cables are labelled as follows along with the resulting effect of the "Bit Sampling Error" function block providing the *Error*.

- *Data in*, is the input signal of the victim, for simulation purposes digital pulses are used.
- *Data gnd in*, is the ground reference of *Data in*.

- *Emission in*, is the signal injected (EMI source) to the bundle to interfere *Data in*.
- *Gnd plane in*, is the input of the ground plane.
- *Data out*, is the output signal after being interfered by the *Emission* cable.
- *Data gnd output*, is the output ground of *Data out*.
- *Emission out*, is the output emission injected to the cable bundle.
- *Gnd plane out*, is the output of the ground plane.
- *Error*, considers a digital system that is able to read an error if a certain threshold is reached.

The simulation results can be seen in Figure 2.6, while the experimental measurement can be seen in Figure 2.7. Both the simulation and the experimental tests consider Data In (in orange) and Emission (in blue) without phase delay, in the top panel, Figure 2.6a and Figure 2.7a, respectively. A phase delay of approximately 50% of the time period is added for the two cases analysed in order to determine the effect at a different moment. The simulation result is shown in Figure 2.6b and the experimental measurement is shown in Figure 2.7b.

When a phase delay of zero is used (Figure 2.6a and Figure 2.7a), the effect of interference in the victim (Data in/Data out) can be easily appreciated if the Emission changes from negative to positive amplitude, a bump is generated in the falling edge of Data out (in green). For the experimental tests measurement, a considerable noise added by means of the equipment used and non-ideal effects can be noticed. However no errors are generated (purple). In the case of 50% phase delay added (Figure 2.6b

and Figure 2.7b), errors can be generated due to the fast change of the electromagnetic field from the EMI source to the victim (Data out in green).

In summary, the effects shown previously are an interesting problem in EMC for digital devices that are mainly caused for the rapid change of $\frac{dv}{dt}$ of the given interfering signal (Emission) and can lead to digital errors as is shown in both cases with a bump present when Data out has zero potential being interfered by the EMI source change from positive to negative voltage.

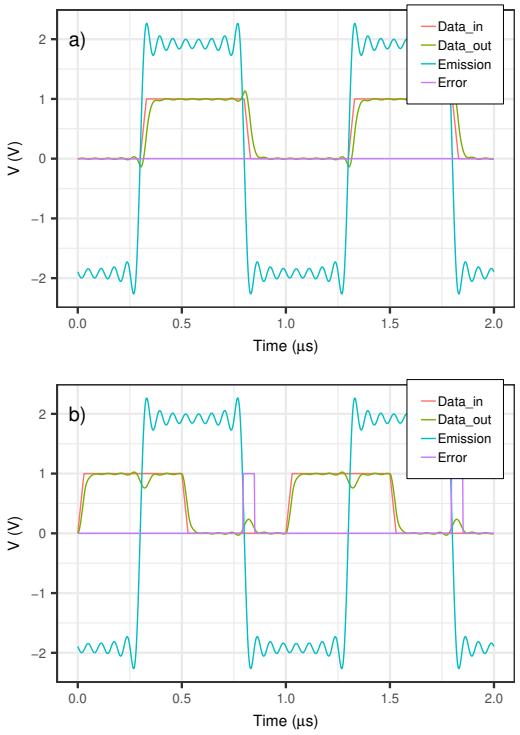

Figure 2.6: Simulation test: Crosstalk issue for a digital signal, a) With EMI of 0% phase delay, b) With EMI of 50% phase delay.

Having introduced the previous results of this experiment, a comparison between simulation and real experiment is carried out to determine the differences and similarities between the results obtained. The following can be noticed from Figure 2.6 and Figure 2.7.

- A simulation will present ideal behaviour which can be difficult to replicate on a real laboratory demonstrator even including parasitic components. A good example of this can be appreciated by the

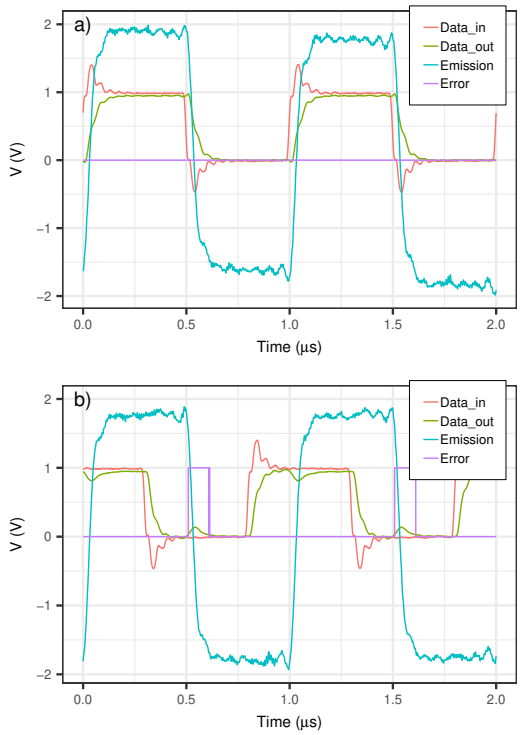

Figure 2.7: Experimental test: Crosstalk issue for a digital signal, a) With EMI of 0% phase delay, b) With EMI of 50% phase delay.

noise in the experimental test (Figure 2.7) which is not present in the simulation (Figure 2.6).

- The time response in the signals can be different due to the non ideal response of the equipment used as well as the signal delay.

2.2.4 Modulating Converters as EMI Sources

Nowadays, Switched Mode Power Supplies (SMPS) are widely used in common applications such as battery chargers, communications and, energy conversion. The most common EMI issues in microgrid are given by the nature of the switching frequency of the emission itself. Due to their switching behaviour, these devices can be considered as EMI sources if the proper mitigation procedures are not taken into consideration.

The main strategy followed by most of the electrical and electronic engineers all over the world to control these devices is the usage of Pulse Width

Modulation (PWM) with a constant switching frequency. This is termed in this thesis as Deterministic Modulation (DetM). DetM can contribute to a certain level of interference at the fundamental switching frequency and its higher order harmonics [27]. In some cases there will be hundreds of devices having the same or different switching frequencies which can be a difficult and demanding task to measure and understand. Individual or group effects can account for larger EMI.

In the following section, the main concepts needed for conducted EMI between electronic devices and its coupling will be reviewed and explained for the purposes of the thesis. Important considerations for the following chapters are considered such as the interference generated by SMPS and its possible mitigation.

Special focus discussed in this section about the coupling mechanisms due to the high importance for the generation of a Crosstalk environment. This information will be used to account for a time domain index in Chapter 5 to determine the impact of the mitigation technique developed and their advantages and disadvantages.

2.3 EMI Measurements

Generally, the recent research carried out for power converters with constant load are for switching frequencies below 200 kHz [28]. This usage of a single switching frequency can make a converter an adequate research subject, specially for uncovering aspects in the current standards such as that developed conventionally by International Special Committee on Radio Interference (CISPR).

The level of interference generated by a converter depends on the bandwidth used to measure it. In order to account for the propagation of interference there are established standard procedures that work over certain

bandwidths. In this research work, the use of CISPR-16 is considered for the analyses carried out for all the measurements and results. However a brief explanation of other important standards is discussed below.

- **CISPR 11.** This standard covers disturbances (in Radio Frequency) in the range of 9 kHz to 400 GHz. The limits in emissions apply to low voltage in AC and DC without considering the direction of the power flow. The current changes allow for example, the use of RF equipment used for measurement of Wireless Power Transfer (WPT), for instance for power supply and charging purposes [29].

- **CISPR 12.** This standard is designed to protect broadcast receivers in the frequency range from 30 MHz to 1000 MHz in the residential environment. The emissions can come from vehicles propelled by a combustion engine or electrical motor (or both), boats propelled by an combustion engine or electrical motor (or both) and, devices equipped with combustion engines [30].

- **CISPR 14.** This standard applies to the emissions in the frequency range from 9 kHz to 400 GHz from households, electric tools and similar apparatus. These appliances can be whether powered by AC or DC (including a batteries) [31].

- **CISPR 15.** This standard applies to conducted and radiated emissions in lighting equipment, Ultra Violet (UV) and Infra Read (IR) radiation, advertising signs, decorative lighting and emergency signs. The frequency range covered is 9 kHz to 400 GHz [32].

- **CISPR 16.** This standard provides a guidance of characteristics and performance for measuring equipment in the frequency range from 9 kHz to 18 GHz. The specifications in this standard apply to electromagnetic interference (EMI) receivers and spectrum analysers. The

whole information related to this standard is used for the measurement in this thesis [33] and the information is summarised in Appendix A.

- **CISPR 25.** This standard applies to vehicles, boats, internal combustion engines, trailers, devices and any electronic/electrical component on board vehicles, boats, trailers and devices. This standard is intended for the automotive sector. The frequency range is 150 kHz to 5925 MHz [34].

- **CISPR 32.** This publication provides requirements and protection for radio services to operate as intended in the frequency range 9 kHz to 400 GHz. It specifies procedures to ensure the reproducibility and repeatability of results [35].

2.3.1 EMI Standardised Measurements

There exists a specific setup to measure the interference generated by a given device according to a given standard. This ensures the repeatability and reproducibility of the results. To this end, the proposed setup measurement in CISPR-16 is considered. This standard covers 5 different bands (as can be seen in Table. 2.2). Since the focus of this work is in the low frequency, Band A of the standard is used to analyse the EMI generated by the converter as well for the whole analysis in the following chapters (Chapter IV). The other bands are out of the scope for the analyses carried out in this thesis work. The complete table considering all of the parameters used for the different bands can be found in Appendix A.

The setup to measure the emissions generated by a Device Under Test (DUT) is given by the EMI Receiver and the Line Impedance Stabilisation Network (LISN). The LISN provides stable impedance in the frequency range 9 - 150 kHz which covers the Band A of CISPR-16.

The block diagram according to the CISPR-16 standard is shown in

Table 2.2: CISPR 16 band limits.

CISPR Band	A	B	C	D	E
Frequency Range	9 kHz - 150 kHz	150 kHz - 30 MHz	30 MHz - 300 MHz	300 MHz - 1 GHz	1 GHz - 18 GHz

Figure 2.8. The explanation of all the blocks involved is given as follows.

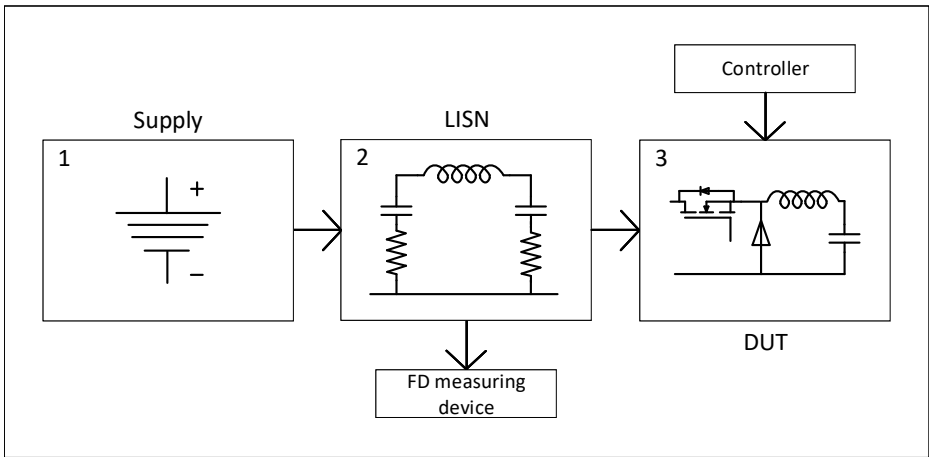

Figure 2.8: CISPR-16 Standard: Measurement Setup.

In block 1), the Supply is used to provide power to the DUT. In block 2), the LISN provides a fixed steady impedance between the supply and the DUT and prevents possible interference from the supply outside. The LISN allows for any measuring device or oscilloscope due to the signal conditioning according to the standard or an EMI Receiver, However it should be noted the impedance of the measuring device is assumed to be 50 ohms. When using a device with a high impedance such as an oscilloscope a 50 ohm impedance should be added in parallel to the connection to the LISN. The EMI Receiver is compliant to CISPR-16 as well as the LISN. Finally, block 3) shows the DUT the subject to the EMI analysis. The DUT for the purposes of this thesis is one DC-DC buck converter switching at different frequencies below 150 kHz (CISPR-16 Band A). The switching signals are generated by a microcontroller. Having to measure the EMI generated for an electrical device, a measurement using an oscilloscope is used to show

the time domain (TD) interference generated of one DC-DC converter that will be used for the experimental tests in the results. The measuring device can also be a spectrum analyser or an EMI receiver if necessary.

In order to provide initial measurement obtained from the previous set-up diagram (Figure 2.8), the Picoscope 5444D [36] which is a PC oscilloscope is used to measure the signal in the TD and through the use of Fourier transforms used to determine its frequency domain (FD) behaviour. The equipment diagram is shown in Figure 2.9 which includes the Power Supply, the LISN and the Power Converter. Important information with regards to the linearity and resolution of the Picoscope can be found in Table B.1 of Appendix B.

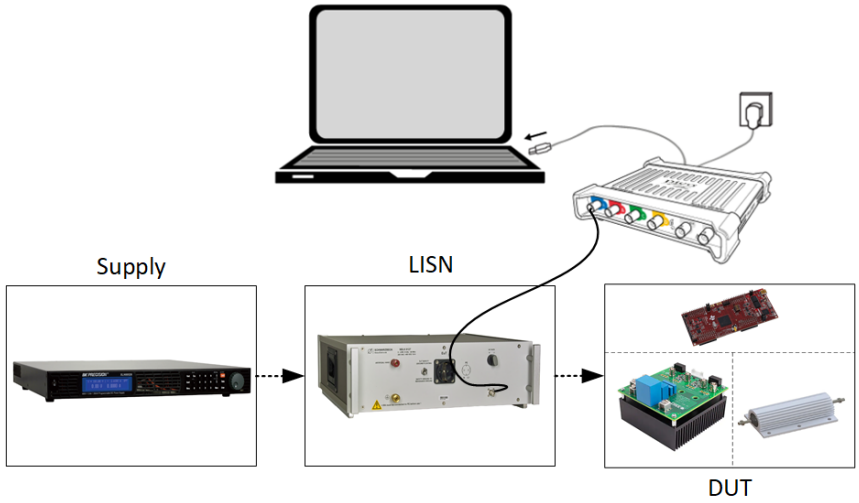

Figure 2.9: Measurement set-up with Picoscope including power supply, LISN and DUT.

The oscilloscope is used to measure in the TD (shown in Figure 2.10 with an amplitude of 0.5 V) with a fixed sampling frequency of 10 MHz. To obtain the spectra of the signal from the LISN (shown in Figure 2.11 demonstrating the Peak value of the switching frequency of 109 dBμV at 50 kHz). The use of an oscilloscope can provide a good understanding of EMI in particular applications, however these measurements can not be considered valid for the current standards from established bodies and organisations because the

framework used to assess different emissions at different frequencies rely on much complex procedures to decompose the interference.

The interference between 9 - 150 kHz for FD has been obtained by means of the FFT algorithm with the TD previous data stored from a file provided by the oscilloscope. The FFT algorithm focused on CISPR-16 standard is explained in detail in Chapter 4. The procedure to obtain the result in FD is discussed in the next chapter.

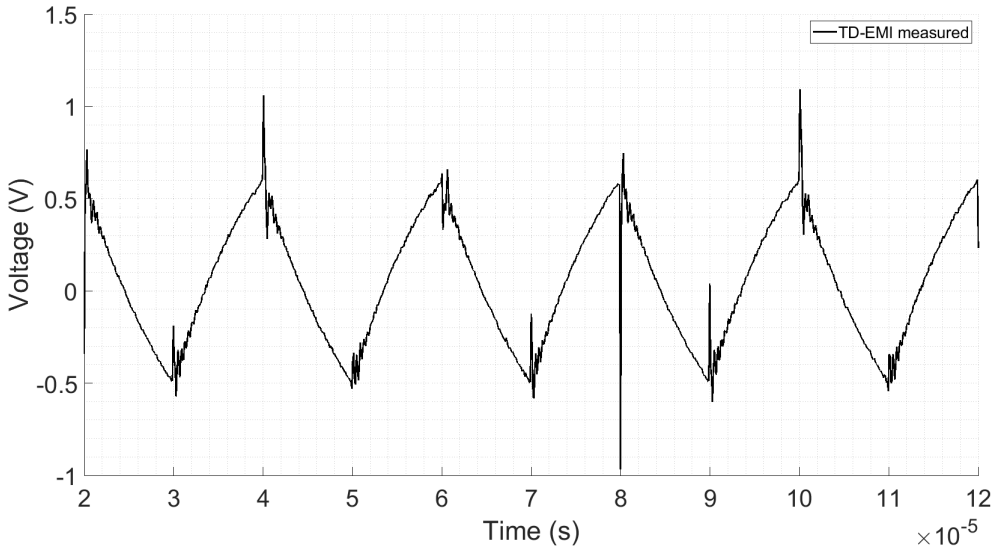

Figure 2.10: 50 kHz switching frequency DC converter TD signal from the LISN.

In real applications such as pre-compliance and compliance procedures for devices there are limits and measurement steps that must be met to determine if a system is suitable for using in certain applications. Since there is no agreement on how to deal with the electromagnetic interference generated by DC converters in low frequencies, this work will follow the standardised setup of CISPR-16 for the future experimental tests.

Having this initial standard is helpful to account for the indices used in the measurements. The steps for a measuring equipment compliant to CISPR-16 are shown in Figure 2.12 and explained as follows.

The explanation of the procedure is presented in [37] and considered in the EMI measuring steps as follows. The EMI signal is filtered according to the

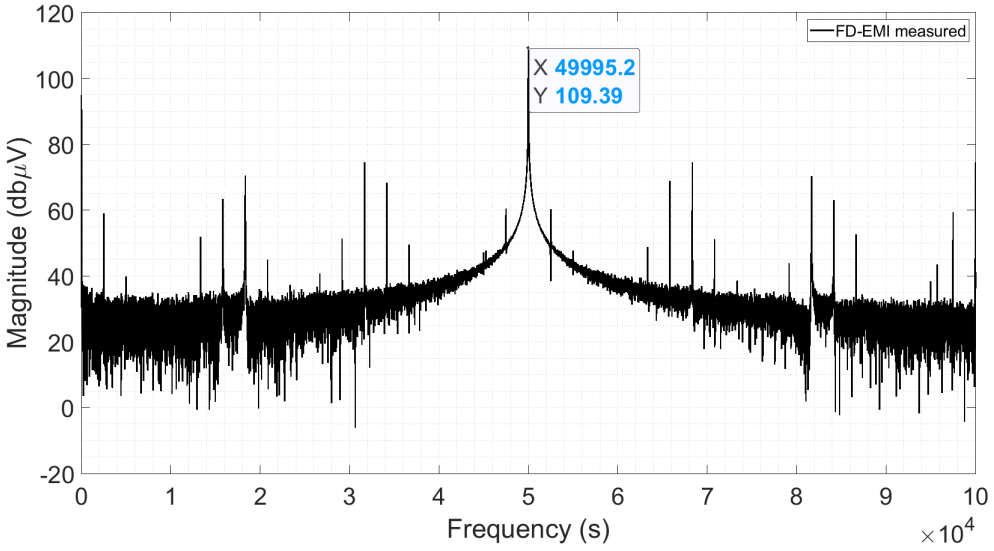

Figure 2.11: 50 kHz switching frequency DC converter FD signal from the LISN.

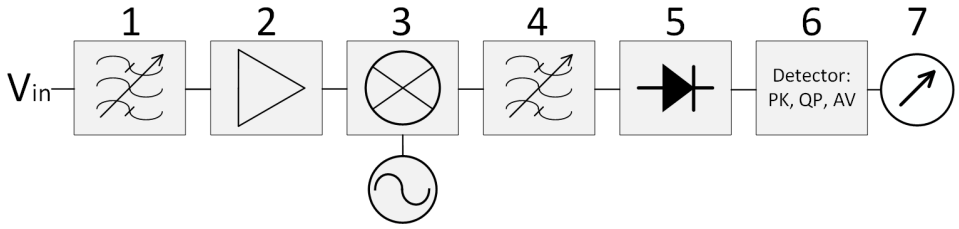

Figure 2.12: EMI Receiver measurement procedure according to CISPR-16.

RF pre-selection bandpass filter (1). The signal is then amplified for a low noise figure (2). The next step mixes the amplified signal and superimposes it to a signal from a Local Oscillator by means of the Intermediate Frequency (IF) (3). The next steps is the filter that determines the bandwidth and the characteristics of the EMI receiver (4). The result is then rectified and base-band limited to the half of the IF (5). Finally, the detectors are displayed (6) by including the critically damped delay of the mechanical instrument (7).

This standard has three main indices that should be taken into consideration. According to [38] and other authors [37], [39], [40], [41], the main idea behind the indices are explained as follows.

- Peak value (PK). The PK considers the maximum value of the peak

for a measured signal over a time constant. This means that in TD the PK works independently of the possible number of pulses repeated over a time period generated from the Electromagnetic source of noise. This effect is referred to as the Pulse Repetition Frequency (PRF).

- Quasi Peak value (QP) The main parameters for QP detector are given by the charge and discharge time of an envelope detector circuit (R_c, R_d and C). This circuit represents a demodulator circuit with dynamics given in Table. A.1. Therefore, the PRF will have a big influence in the measured QP value. The more pulses repeated over a certain time, the higher the QP value will be. The QP demodulator is shown in Figure 2.13

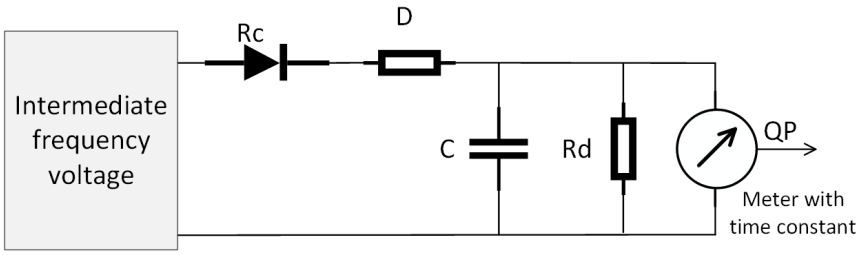

Figure 2.13: Quasi-peak demodulator circuit.

- Average value (AV). The AV index demonstrates the mean value of the demodulated intermediate filter over the time interval measured. Generally, the AV detector is not suitable for impulsive disturbances.

The behaviour in the time domain for the signals obtained from these detectors should follow the expected demodulation as shown in Figure 2.14.

In summary, a continuous signal will generate the same values for PK, QP and AV when measured by an EMI Receiver. However, when a modulated signal is measured, the results for the three main indices (PK, QP and AV) will generate different results when the Duty Cycle of the signal is different as shown in Figure 2.14. For a continuous signal the condition

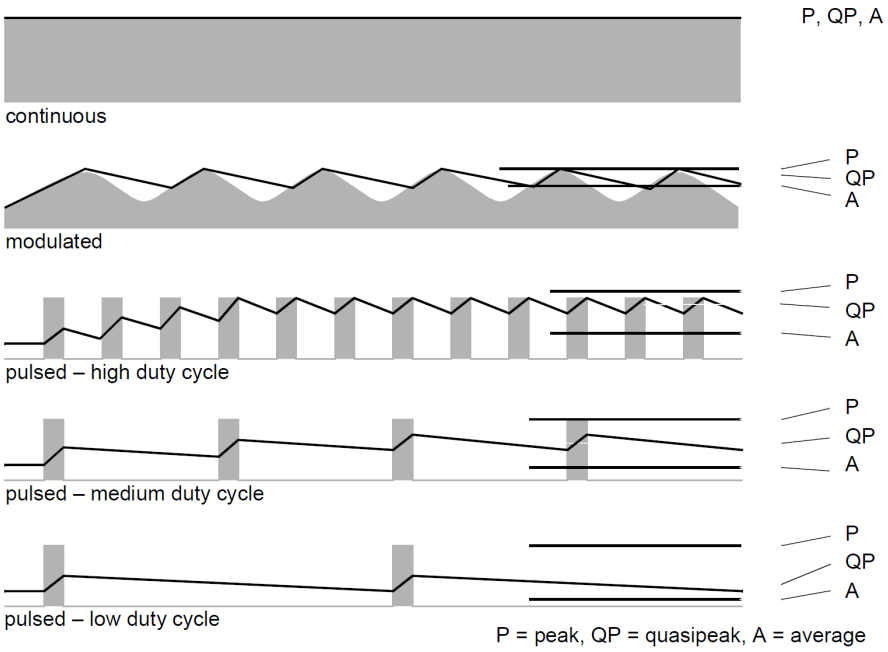

Figure 2.14: Example of a demodulation procedure as presented in [42].

$PK = QP = AV$ is true and a modulated signal presents the condition $PK > QP > AV$.

2.3.2 Standardised Measurement Compliant with CISPR-16

To account for an accurate and repeatable measurement in different environments that can be considered compliant to a standard (for future purposes), the CISPR-16 standard set-up is used. This standard includes equipment and instructions on the devices used to have a correct measurement. Due to the nature of noise generated on DC systems (either Differential or Common mode), the connection used is as follows in Figure 2.15. Notice the use of two branches for measuring the emissions coming from the positive side and the negative side. The schematic of the LISN used can be seen in Figure 2.15 and its main features will be explained in Chapter IV for the experimental measurements.

In the tests carried out in this thesis only the differential mode noise

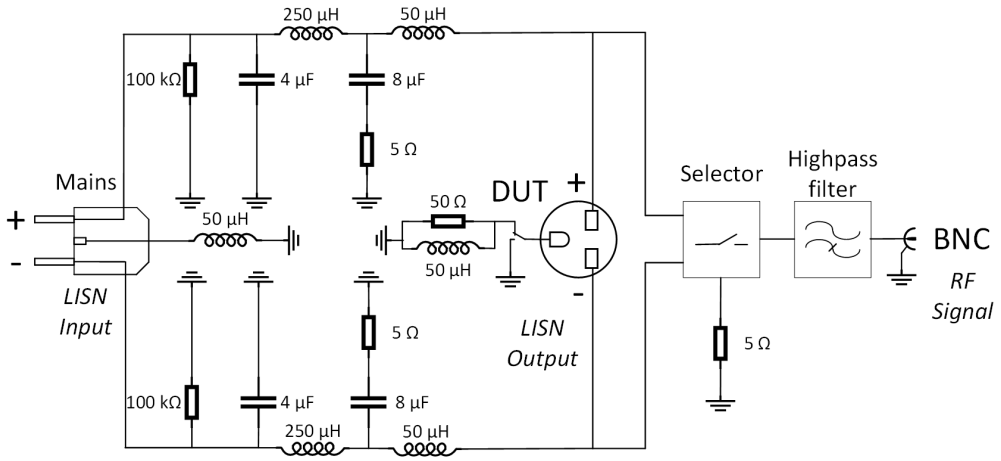

Figure 2.15: Typical connection of an AC LISN for DC devices.

is taken as the research subject due to the equipment and the laboratory facilities.

2.3.3 Crosstalk in Wired Communication Links

Crosstalk between two different conductors can be represented by the transmission line model as explained in Section 2.2. In [43], and [44] it has been demonstrated that a digital system using serial communication can be seriously compromised if a situation like this takes place. What is more, it has been concluded in both works that this is a highly non-linear effect even if the nature of the interference is somehow controlled periodically. The main cause of this is due to the effect of generating an error over a data bit. The voltage shape of the data signal is important to account for a reliable transmission of data.

To better explain this issue, the basic idea of a communication environment is considered. A complex communication system should consider different parameters. These parameters are taken into consideration by the Open Systems Interconnection (OSI) model and divided into different layers [45]. The layers and its explanation can be found in Table 2.3.

Crosstalk occurs when an EMI source generates compromises (wanted or

Table 2.3: OSI Model Layers.

Layer	**Description**	**Function**
7	Application Layer	Considers the interaction between the end user that controls the applications with network services.
6	Presentation Layer	Considers the encryption for the data exchange between network layer and application layer
5	Session Layer	Considers the communication channels between devices which are called sessions.
4	Transport Layer	Considers data transmission protocols, includes mechanisms to request data again if was not received.
3	Network Layer	Considers the routing of information usually using addresses for destination.
2	Data Link Layer	Considers the data framing. Error detection and correction mechanisms can be used.
1	Physical Layer	Considers the raw bit stream, based on the electrical medium and properties.

unwanted) to a signal. One example of this was analysed in [43], where the authors created two different environments to generate errors, one based on radiation and other based on conduction. The one that matters to the study carried out in this thesis is the one based on conduction. However, in their experimental setup, the authors used two cables and one ground plane (as was explained previously), and a Crosstalk situation takes place. The victim for this case is a TTL generated stream of bits transmitted and quantified by a Bit Error Rate Tester (BERT) while the aggressor is a signal with a controlled waveshape. The aggressor signal is based on the Square Series Fourier Wave (SSFW) (as can be seen in (2.11)) where n is the number of terms. This equation was proposed to generate the noise signal to measure the affect on the Bit Error Rate (BER) of a digital stream of data.

$$x(t) = \frac{4}{\pi} \sum_{n=1,3,5...}^{m} \frac{\sin(2\pi n t)}{n} \tag{2.11}$$

The authors found that, as the number of terms increases the BER

measured increases. The main explanation of this is because of the increase in the maximum value of $\frac{dv}{dt}$ contained in the interfering signal as the Fourier terms increase which then creates a larger interference magnetic field $L\frac{di}{dt}$. From a mathematical point of view, this is mainly caused by Gibbs phenomena, which represents a difficulty of Fourier series in approximating functions near their jump discontinuities, hence it manifests in overshoots and undershoots near such changes [46]. In this situation there is a moment in which adding more sinusoidal terms will lead to a discontinuity in the measured signal. An example of this effect with three different values for the number of terms can be seen in Figure 2.16.

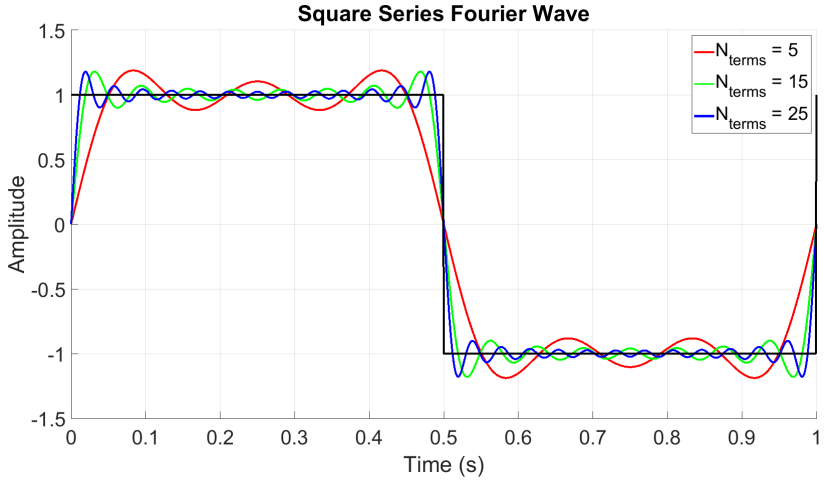

Figure 2.16: Gibbs phenomena caused by the increasing number of terms.

For the main purpose of the thesis, the simulated signal based on Fourier terms is changed to a power converter switching at different frequencies and with different schemes to investigate EMI and whether it can be reduced or mitigated.

2.3.4 Bit Error Rate in Communication Links

One useful measure of communication efficiency used in this work is the BER measurement. To measure BER specialised equipment is used, in this case a Bit Error Rate Tester (BERT). Unlike many other types of

measurement, examining the BER permits an understanding of the full end to end performance of a communication system including the transmitter and the receiver, all within a single parameter [47].

Fundamentally, a BERT provides the ratio of incorrectly transmitted bits to transmitted bits, as given by (2.12).

$$BER = \frac{N_{err}}{N_{bits}}, \tag{2.12}$$

where N_{err} is the number of incorrect bits whilst N_{bits} is the total number of bits sent in a time period. When data is transmitted over a data link, there is a possibility of bit errors being introduced to the system. If this occurs the system integrity may be compromised [48] with potentially severe repercussions. The likelihood of a given bit being incorrectly determined by a receiver, and therefore the value of the BER, is affected by many factors including the signal to noise ratio of the signal, distortion, and jitter [49].

Recently, Power Line Communications (PLC) has been widely studied due to the recent issues discovered in the low frequency band. The usage of the same cable as used for electrical appliances can be considered as an advantage from an infrastructure point of view, however there are important drawbacks due to the switching converters and the noise generated [50]. The main issue considered by the authors in this research is the inclusion of a 3 phase motor in combination with a transmission line that transfers power to it [50]. Coupled to this set-up a PLC communication link was placed to measure the effect of the BER. Interestingly, the BER increased when the emitted power of the motor decreased. Another conclusion given by the authors is the length of the cable which is one of the most problematic topics when analysing the EMC between devices.

This experimental test can be partially reproduced by the inclusion of a Power Line signal using the input voltage of a DC-DC converter, which is

the experimental test that will be explained in Chapter 4.

This section has explained the basic points for EMI measurements for electrical and electronic devices. It has introduced ideas for measuring in time and frequency domain as well as the standard needed for all the measurements. In addition a common problem in digital communications was introduced and the required equipment to measure this kind of interference.

2.4 EMI Mitigation Strategies

In real practice, there are many options to decrease the conducted interference generated by SMPS. In the review work carried out by Mainali et al. [51], the authors describe a list of different methods. These methods are divided into two different categories.

- Reducing the noise after its generation. This include the use of filters (either passive or active). Another important point here is the topology of the converter and the layout (shielding and similar techniques).

- Reducing the noise at the generation stage itself. This mitigation category includes considerations given by the circuit development and component selection, another consideration is usually the Switching Scheme (PWM techniques and Switching Frequency Modulation) and finally the Switching Transition which can be focused on the use of auxiliary circuits to decrease the slope of transitions (snubber circuits).

Considering the aims of this thesis a brief description of both methods will be explained. However, the focus of the research is in the mitigation of EMI using PWM techniques (second category).

2.4.1 Filtering

Historically, EMI filters and shielding have been a used as a practical and straightforward solution to comply with EMI standards and regulations of different countries, the main drawback of using passive components is the increase in volume and the addition of more components to the final designs which in some cases is translated into the change of design from the manufacturer side. According to [52], the filter value depends on the requirements and the impedance interaction to the supply which is connected. Hence, the dynamics of the converter and its operating conditions will be dependant on the other equipment connected, which at the very end can generate more uncertainties in the conducted emissions.

If a DC-DC converter is used for a particular application it will be required to generate the lowest EMI possible. The use of a simple LC filter can improve Differential Mode (DM) noise. However, the Common Mode (CM) noise might be considered as well (both Differential and Common were introduced in Section 2.1). The LC filter at the input of the DC converter is shown in Figure 2.17, this filter is used by the majority of converters to mitigate DM and to mitigate the noise from the source. On the other hand, a modification can be made to suppress Common Mode (CM) noise by using an inductor. The modification can be seen in Figure 2.18.

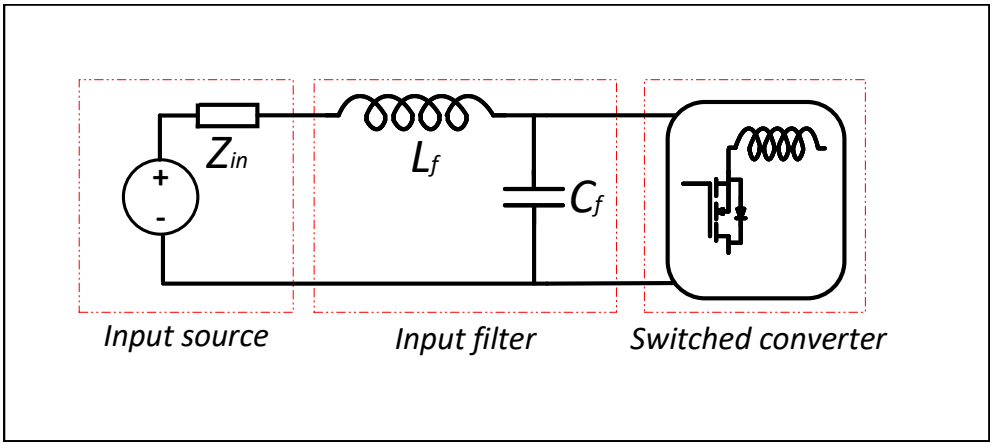

Figure 2.17: Differential mode filter for the input of a DC converter.

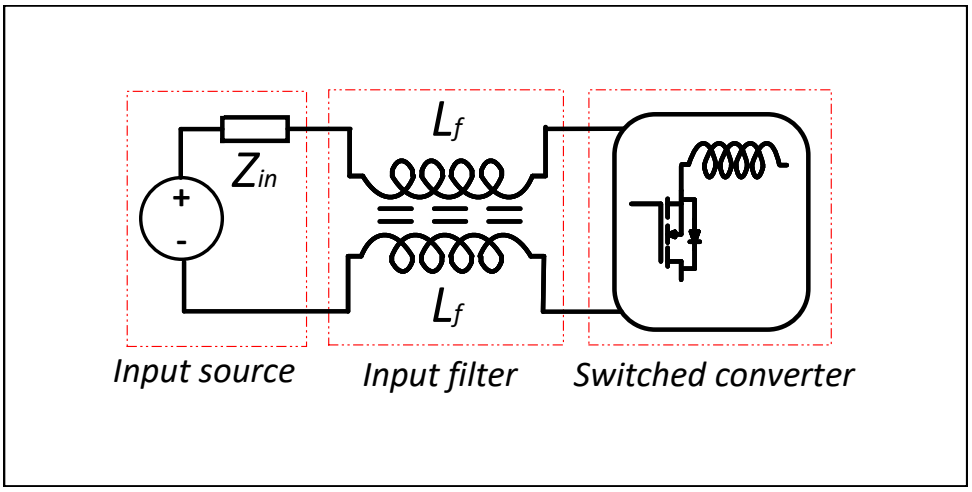

Figure 2.18: Common mode filter for the input of a DC converter.

The combination of both filter configurations (CM and DM) is called an EMI filter, this filter must comply with the following functional requirements [53],

- Stopband attenuation with a transfer function at the designed frequency.
- Low losses at line frequency (low passband attenuation).
- Low cost.

Considering the points mentioned before with regards to passive filter usage for EMC purposes, a list of disadvantages is presented according to [54], [55] [56], [57].

- Volume
- Heat generation/efficiency
- Potential resonances
- Reduction of robustness

For these reasons other mitigation techniques might need to be explored and analysed in more detail.

In addition, [58] and [59] suggest additional requirements for the successful design of EMI filters. In addition to the aforementioned points, filter

stability is also a requirement needed for more reliable systems along with the following.

- Knowledge of the noise impedance given by other parameters such as impedances and parasitics.
- Definition of the dominant components affecting the noise generation.
- Provide stability to the SMPS.

Stability and impedance are often related to Middlebrook's criterion ([60], [61]), which states that the filter should be comparable and able to handle the impedances in between the systems connected to provide stability. Consider two systems as shown in Figure 2.19, i.e. the source and the load subsystems both with a finite impedance (Figure 2.20). The ratio of these impedances is then referred to as the Middlebrook criterion. The condition that must be met is that the load subsystem's input impedance is larger than the magnitude of the source subsystem's output impedance.

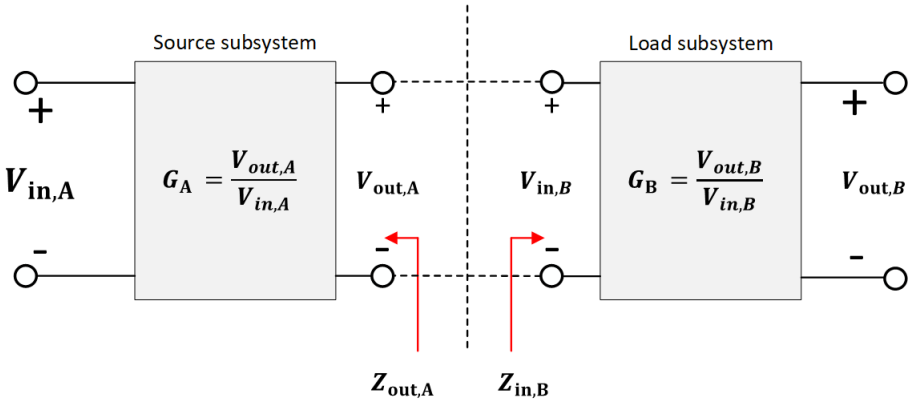

Figure 2.19: Middlebrook's Criterion explained as subsystems.

The mathematical description considers the two impedances with two different gains (G_A and G_B). Focusing on the transfer function given by the output voltage (V_{out}) and the input voltage (V_{in}).

$$\frac{V_{out,B}}{V_{in,A}} = G_A \cdot G_B \cdot \frac{Z_{in,B}}{Z_{in,B} + Z_{out,A}} = \frac{G_A \cdot G_B}{1 + T_M} \tag{2.13}$$

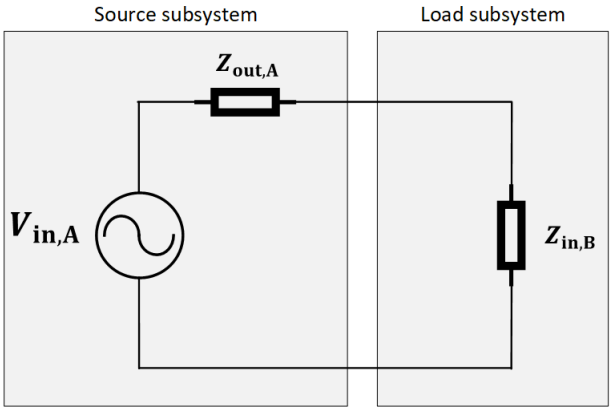

Figure 2.20: Middlebrook's Criterion explained as impedances.

The relation given by the ratio of the Source Impedance to the Load Impedance should have the following condition and is often referred to as the Minor Loop Gain (T_M),

$$T_M = \frac{Z_{out,A}}{Z_{in,B}} << 1 \tag{2.14}$$

In summary, the source impedance must be less than the load impedance for the system to be stable. This brings an interesting discussion on how to design a filter for a single converter. As mentioned many parameters and variables will play an important role and the usage of it should be designed according to particular needs.

2.4.2 Switching Frequency Modulation

To deal with the considerable disadvantages of filtering to mitigate EMI as presented before, the active frequency modulation approach can be considered. These techniques are referred to as Spread Spectrum Modulation (SSM). In Chapter III, the background of frequency modulations based on simulations are explored with a literature survey with regards to the main issues that can have a considerable impact in the generation of interference. The application of this technique to real measurements is presented in Chapter IV.

Recently, modulations of the switching frequency for DC-DC converters have been used to decrease the level of interference generated by a single and fixed frequency. There are several approaches to modulate a switching frequency, for example using a number of frequencies with a defined time change as presented in [62] or a dithering for a set number of predefined frequencies [63]. In most of the cases, frequency dithering or frequency hopping refer to the same nature of jumping between switching frequencies with the final aim of spreading the noise of a given undesired source by changing switching frequencies from one to another over a given time. These techniques can be applied to DC converters if the only aim is to improve the interference generated (in the frequency domain) by the switching frequency of the SMPS at the cost of slightly decreasing the steadiness of the output voltage and current of the converter.

In the work carried out in [27], the authors presented the application of Frequency Modulation Techniques to reduce EMI in Switched Power Converters by considering different modulating signals, the conclusion of this work states that the modulating signals depends on the target and all of them will behave differently according to the parameters chosen for the Spread Spectrum Modulation (SSM) technique. There exist different schemes with regards to the driving signal, but the most used are given by periodical and stochastic signals. Interestingly, both schemes can be combined to create hybrids that can decrease the EMI to lower limits when comparing them individually. These methods spread the interference across the frequency spectrum and even though there is a definition of the maximum and minimum limits for the bandwidth to spread.

Having explained briefly the Frequency Modulation for DC converters, the mathematical expression to account for it is shown in (2.15). This equation presents the complete background of Spread Spectrum that will be explained in Chapter III and Chapter IV focused exclusively on modulation

of the switching frequency [27].

$$f(t) = A \cdot \cos(2\pi f_C \cdot t + \theta(t)), \tag{2.15}$$

where, A is the amplitude of the original signal (modulating), f_C is the non-modulated frequency (carrier) and, $\theta(t)$ is the phase angle function.

The function $\theta(t)$ can be expanded to,

$$\theta(t) = \int_0^t k_w \cdot v_m(t) \cdot \, d\tau, \tag{2.16}$$

in which, k_w is the factor controlling the frequency deviation and $v_m(t)$ is the driving modulation function. The driving function $v_m(t)$ can be periodical or non periodical. A complete explanation of Frequency Modulation with regards to Spread Spectrum purposes is presented in Chapter III. It is worth mentioning that the use of a certain signal in the time domain will generate a particular shape in the frequency domain. The frequency modulation in the time domain for four different signals (Sine (b), Sawtooth (b) and Random (d)) can be seen in Figure 2.21. In this figure, the SSM graphs consider the factor in (2.16) as k_w, this is highlighted considering the symmetrical parts above and below the carrier frequency f_c. In fact, the parameter $\theta(t)$ in (2.15) is in reality the function of the generated signal.

The definition of the modulating signal in time domain is an important consideration for the application of this technique. As an introduction to the expected results, the different shapes generated in time domain are presented in the frequency domain by means of the FFT are shown in Figure 2.22 for a) Deterministic Modulation, b) Sine wave Spread Spectrum, c) Sawtooth wave Spread Spectrum and d) Random wave Spread Spectrum are shown in Figure. 2.22.

In this section the most common EMI mitigation strategies based on modifying the power converter switching frequency were introduced. The

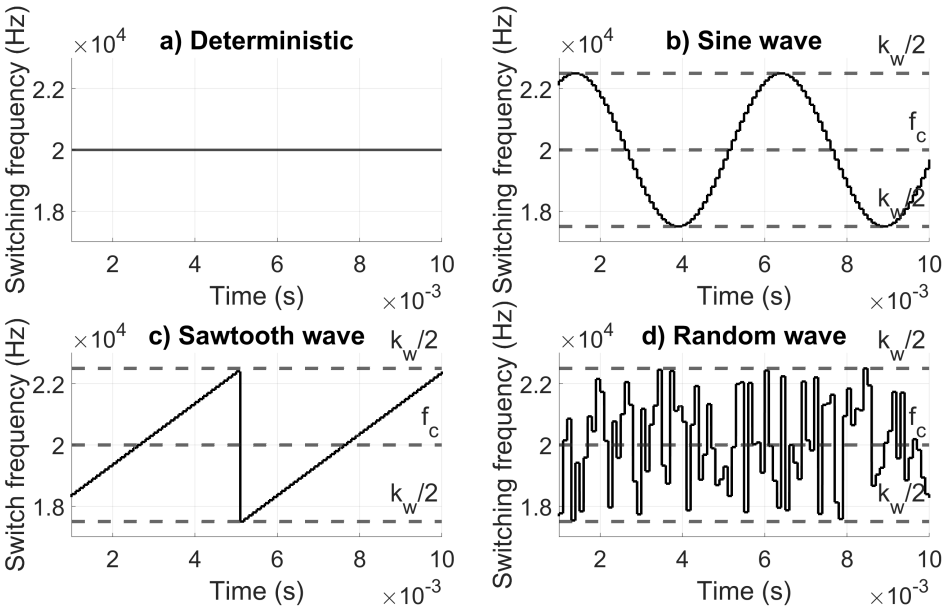

Figure 2.21: Time domain graphs of different driving signals for Spread Spectrum Modulation.

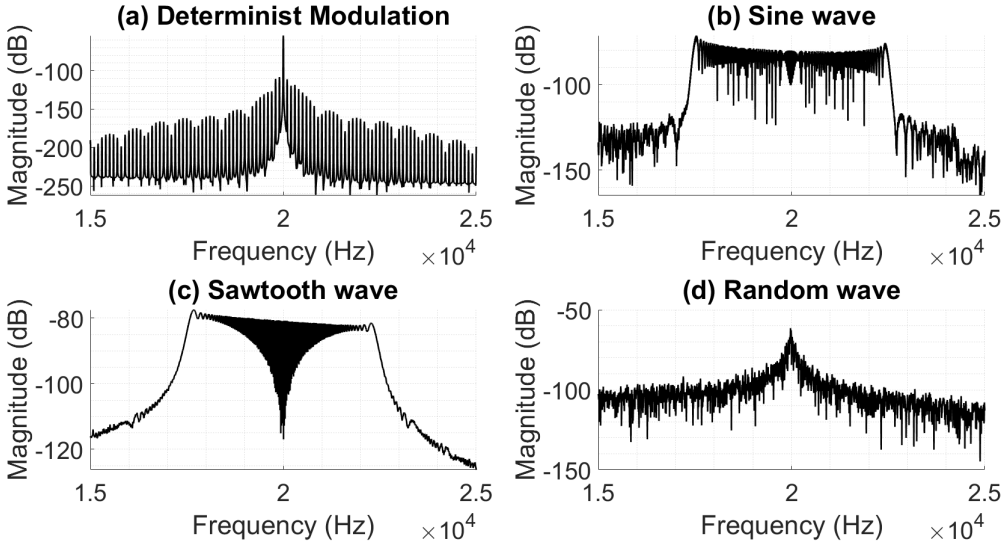

Figure 2.22: Frequency domain graphs of different driving signals for Spread Spectrum Modulation.

generation of the noise itself predominantly determines the method to apply, for instance two methods were highlighted in which one of them requires additional components and hardware and the other only requires a control of the switching frequency.

2.5 Chapter Conclusion

In this chapter the most important concepts for the analysis of mitigation of EMI have been introduced. Starting from the nature of the interference and coupling methods for measurements and standards. Several standards have been analysed to account for its bandwidths and the origin of disturbances, in particular the standard CISPR-16 has been considered mostly due to the equipment used for testing in the laboratory.

In addition, an explanation of Crosstalk as a part of a problem that can create EMI between communication devices and power grids was presented. Since a parameter must be used to determine a particular effect, the BER value is introduced as a way to determine the impact of different disturbances, what is more this value will be used to account for mitigation of EMI.

With regards to the main contributions mentioned in Chapter 1, the following bullet points are concluded:

- The re-distribution of noise when switching frequency modulation techniques were introduced. It can be concluded that different effects are obtained for different modulating signals in time and frequency domains.

- The Crosstalk theory and its effects have been demonstrated and it is concluded that the integrity of the signal is compromised when a potential noise (from a switching converter) can be used. For this

reason, the BER is introduced to measure as an auxiliar parameter.

- The propagation of interference has been presented (cable coupling) and it is concluded that a DC converter with a switching frequency modulation can be used as an EMI source.

Finally, this chapter presented the most common ways of EMI decrease by Filtering and Switching Frequency modulation. The requirements for filter design either for Common Mode or Differential Mode have been shown. Of particular interest for this research is the mitigation by Switching Frequency modulation which is the main topic that support this thesis.

Chapter 3

Spread Spectrum Modulation (SSM) for DC Converters

In this chapter, the use of SSM techniques is explored to show the performance of these EMI mitigation methods applied to a DC-DC power converter. The historical usage of Spread Spectrum will be discussed to develop ideas about the origins of this modulation technique. A literature survey of similar works is undertaken and analysed to support the application of SSM to this topic.

The chapter explains the mathematical background of frequency modulation used in SSM and the steps to program this technique for simulation software. There will be a discussion about the advantages and disadvantages when using different parameters to control the main properties of SSM. In addition, simulation results are introduced to understand the "ideal" performance of these modulation schemes when analysed using the Fast Fourier Transform (FFT) Decomposition and to provide the foundation of the CISPR-16 standard for measuring devices as employed by modern EMI receivers.

The aim of this chapter is to provide sufficient results and measurements to understand how frequency modulated DC converters can be considered as

EMI sources and the specific parameters which must be modified to decrease a given, undesired EMI behaviour to an acceptable level.

3.1 SSM Background

The Spread Spectrum technique was initially investigated as a communication procedure to optimise the bandwidth of a communication channel. In fact, there are many reports that it that was developed and practiced in World War II [64]. This was due to the battle for the electronic supremacy between combatants. Most of the the development of this theory took place during the same period in which Shannon's work started to be appreciated. Many people from well-known laboratories and universities worked on similar topics [65], and it is difficult to know exactly who invented Spread Spectrum and when.

It is during recent years that this technique has been brought to the attention of EMI research, mainly caused by the growing importance of microgrids as discussed in the first chapter. State-of-the-art microgrids make use of several switching power supplies to control the power flow. Communication systems are also part of these complex systems and will be affected by the behaviour of switching converters such as Switched Mode Power Supplies (SMPS). Spread Spectrum techniques are being used and developed for EMI mitigation for the automotive industry and other purposes, for example, Texas Instruments (TI) [66] has developed EMI mitigation SSM devices for SMPS which can help to reduce the effect of conducted emissions.

An interesting example of a device manufactured as an Integrated Circuit (IC) from TI which can have programmed modulation schemes for automotive drives mainly used in industrial transport, avionics and others is the device LM62460 [67]. The voltage range is from 3 to 36 V and this family of

devices is designed for low EMI and they incorporate pin-selectable spread spectrum modulation techniques.

On a similar application for EMI mitigation TI produces the LM25148-Q1 controller [68] that complies with automotive systems (CISPR-25). This is to deal with most of the interference generated by switching converters between 150 kHz to 30 MHz for 42 V systems.

Using a wide frequency range for a carrier signal. Spread Spectrum Modulation has the main objective of changing a narrowband interfering signal (green) of a considerable noise amplitude to a broad band signal (orange) that also decreases its magnitude of any individual harmonic with the condition of wider bandwidth occupied as can be seen in Figure 3.1.

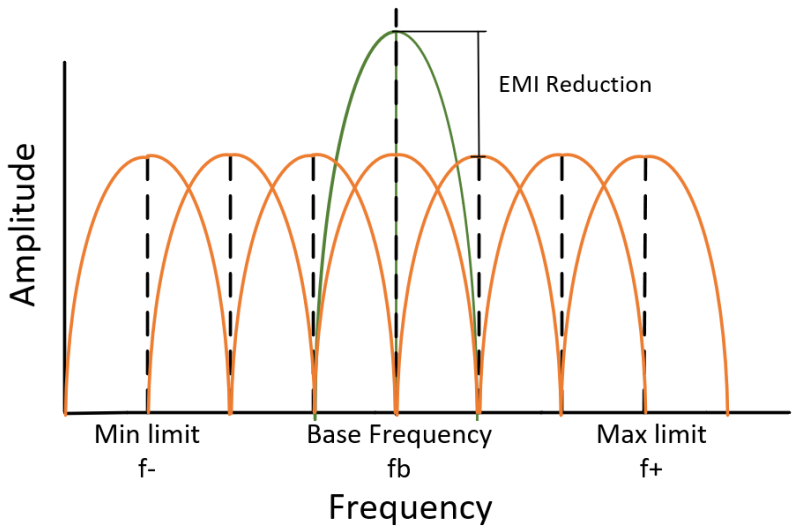

Figure 3.1: Basic spread Spectrum basic theory applied to an interfering signal to achieve an EMI reduction.

In the research review presented in [51], a survey of different methods for conducted EMI mitigation is carried out, in particular methods for SSM are analysed and it was concluded that SSM can provide an EMI Reduction of the switching frequency (as seen in Figure 3.1) of a SMPS by approximately 18 dBμV using common methods for switching frequency modulation. More complex methods are also presented in which the chaos generation of switching frequencies is adopted as a modulation pattern. This

review also concluded that the choice of a particular mitigation technique depends on various factors such as frequency bandwidth, magnitude to mitigate and the average noise spreading, hence the solution to a problem must be tailored in the sense that frequency limits have to be considered.

In [69], the authors present a random algorithm focused on Randomised Carrier Frequency Modulation with Fixed Duty Ratio (RCFMFD). In this strategy the randomisation is achieved by using a 12-bit Linear Feedback Shift Register (LFSR) programmed on a FPGA for a Boost converter. The authors state that Chaotic Modulation demonstrates interesting advantages over periodic PWM signals in most of the tests conducted. A similar study based on a Chaos generator has been analysed in [70]. In this work an analogue chaotic PWM was selected to generate the switching pattern. It was shown experimentally a reduction of the peak level of a switching frequency interference of 20 dBμV.

In other works, [71], [72] and the results from this thesis [73], the aim is to control the rate of change of the modulating signal (and therefore its associated EMI) by modifying the profile at the generation of the driving signal itself to modulate the DC converter.

What is important when using these frequency modulation methods is to understand how to modulate the driving signal and how this will be demodulated by the measuring equipment to achieve the best result when dealing with the mitigation of EMI. The intention of this chapter is to demonstrate what is the best possible way to reduce EMI considering the trade-offs seen from the converter point of view. To achieve the aforementioned intention, it should be noted that the analysis must consider two ends of the experimental tests, i.e. the converter control, and the behaviour of the EMI measuring process (Spectrum Analyser or EMI Receiver), so that a full understanding of their relationships can be achieved [74]. Measurements of EMI in the frequency domain alone might not present a full or true measure of the

effects of SSM on the electromagnetic emissions of the device [75]. Other measurement techniques should be considered and included when evaluating the EMI associated with SSM. Usually the most important parameters to be considered are given as follows:

- Time domain signal shape of the driving signal for the DUT.
- Rate of change of the driving signal, related to the sampling ratio for a periodical signal.
- Band of the standard to be measured.
- Resolution bandwidth (RBW) of the equipment or method to account for frequency domain.
- Dwell or measuring time.

3.1.1 Analogue Spread Spectrum Modulation

The usage of SSM is mainly based on analogue frequency modulation assumptions. The main idea behind frequency modulation is achieved with two main signals, the carrier and the modulating signal as given by:

$$f_{out}(t) = \cos(w_c t + \frac{\delta_f}{f_S(t)} \int dt S(t)), \tag{3.1}$$

where the term w_c is the carrier frequency, δ_f is the frequency deviation, $f_S(t)$ is the modulating signal frequency and $S(t)$ is the modulating signal function. This theory can be extended to account for a rule that defines the limits of the frequencies to be modulated. This rule is referred to as Carson's rule as can be seen in [76].

$$f_{out} = f_c \pm \frac{\Delta f}{2} \cdot \epsilon(t) \tag{3.2}$$

In (3.2), Δf is the frequency deviation (same as δ_f) based on the spreading range defined to the baseline frequency modulation to be mitigated (f_c). The value of $\epsilon(t)$ is the modulating signal and can be periodic (e.g. sine and triangular) or non-periodic (random and chaotic).

3.1.2 Bessel Function of its First Kind

The background of Spread Spectrum modulation can be explained by the representation of frequency modulated sinusoidal signals. Bessel functions are used to describe the propagation of physical phenomena [77] such as wave propagation in cylindrical coordinates. In this particular case, the propagation of electromagnetic waves is across a conductor (cable). Bessel functions of the first kind provide the introduction of the modulation index parameter for frequency modulation. This function provides a given magnitude of the wave of study according to a particular value of modulation index.

According to [78], the frequency modulation technique (shown in (3.1)) can be represented in two parts as shown in (3.3).

$$\begin{aligned} F(t) = A_c \cdot cos\left(w_c t + \frac{\Delta w_c}{w_m} sin w_m t\right) = A_c \cdot \Bigg\{ & J_0(\frac{\Delta w_c}{w_m}) \cdot cos w_c t \\ & + J_1(\frac{\Delta w_c}{w_m}) \cdot \left[cos(w_c + \frac{\Delta w_c}{w_m})t - cos(w_c - \frac{\Delta w_c}{w_m})t\right] \\ & - J_2(\frac{\Delta w_c}{w_m}) \cdot \left[cos(w_c + 2\frac{\Delta w_c}{w_m})t + cos(w_c - 2\frac{\Delta w_c}{w_m})t\right] \\ & + J_3(\frac{\Delta w_c}{w_m}) \cdot \left[cos(w_c + 3\frac{\Delta w_c}{w_m})t - cos(w_c - 3\frac{\Delta w_c}{w_m})t\right] \\ & - J_4(\frac{\Delta w_c}{w_m}) \cdot \left[cos(w_c + 4\frac{\Delta w_c}{w_m})t + cos(w_c - 4\frac{\Delta w_c}{w_m})t\right] \\ & + ... \Bigg\}, \end{aligned} \tag{3.3}$$

With the main values defined as:

A_c: amplitude of the carrier signal (switching central frequency).

w_c: angular frequency of the carrier signal.

w_m: angular frequency of the modulating signal.

J_x: corresponding Bessel functions of the first kind.

Δw_c: peak deviation of the carrier frequency.

A value that relates the effect of the frequency deviation and the modulating signal is the modulation index (m) and will be explained in the next subsection. The complete theory of Bessel functions as differential equations can be found in Appendix C. The first ten solutions for (3.3) can be seen in Figure.3.2.

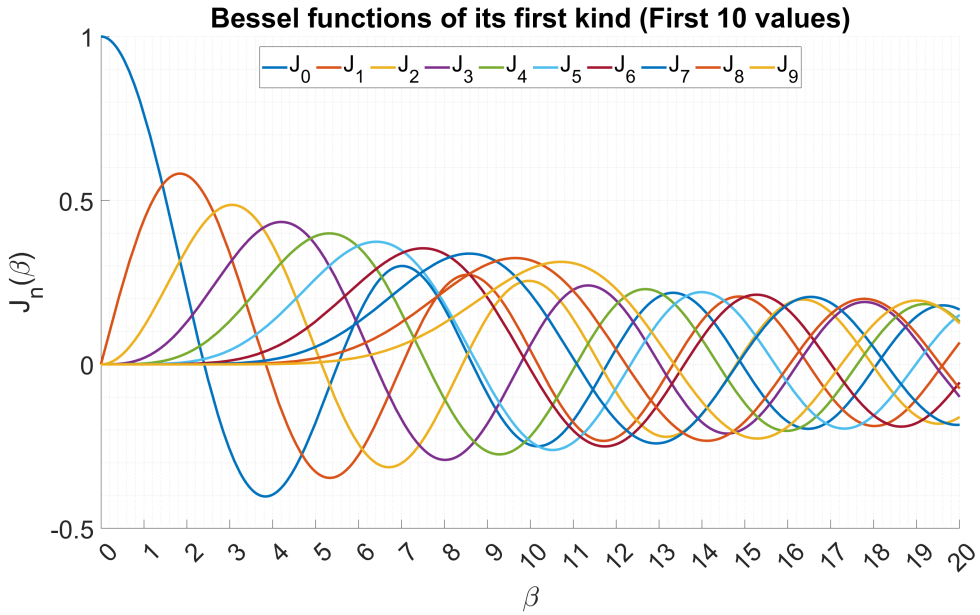

Figure 3.2: Bessel function of the first kind with the first ten values, β represents the modulation index.

The magnitude of the value calculated by the Bessel function of the first kind for every β is in reality the magnitude at a given modulation index that satisfies the function in (3.3) for a given value of $J_x(\frac{\Delta w_c}{w_m})$. This is an advantage and can be used to suppress a given component that could be a potential interference source by selecting the parameters that agree with that component as shown in [79].

3.1.3 Modulation Index

In the context of SSM, the modulation index (m) has a different meaning when compared to conventional Pulse width Modulation (PWM), where m is commonly used to define the ratio of the modulation wave peak, to the carrier peak. Here, the modulation index (m or β) is a variable related to two important parameters for frequency modulation, i.e., the sampling frequency (f_m) of the modulating signal and the frequency deviation (Δf), or δ_f in the analogue function. The value of Δf can be renamed the "spreading factor" (α) i.e. a percentage which deviates with regards to the baseline frequency (f_c) to be mitigated ($(\alpha \cdot f_c)/2$).

These parameters are then considered with the sampling frequency (f_m) of the modulating signal to obtain the modulation index (m). The modulation index relates the degree of modulation compared to a non-modulated case for a carrier frequency. This value is calculated as shown in (3.4).

$$m = \frac{(\alpha \cdot f_c)/2}{f_m} \tag{3.4}$$

The use of this modulation index applies as well for the implementation on a digital controller such as an FPGA or a microcontroller. In fact, the microcontroller can be programmed to provide different spreading factors for different carrier signals at different modulating frequencies. The relationship for the modulation index in the context of the analogue mathematical expression is then obtained as follows,

$$m = \frac{\delta_f}{f_{S(t)}}, \tag{3.5}$$

Which combined with (3.1) leads to,

$$f_{out}(t) = \cos(w_c t + m \int dt S(t)), \tag{3.6}$$

It is worth mentioning that for different values of α, the value of the modulating index will be different even if a similar value of f_m is used. For this reason the modulation index is a parameter that must be chosen carefully and can only be applied after a complete understanding of the advantages and disadvantages of a device or a group of devices. A better explanation of the effect of using SSM for power converters can be seen in Figure 3.3. In this figure additional considerations are shown with regards to Carson's rule. The complete Bandwidth covered is represented by B while the frequency deviation from the carrier frequency (f_c) is represented by Δf. This will have the exact same impact of decreasing an interfering signal (green) to a lower amplitude interfering signal (orange) for the carrier signal chosen (f_c) as shown previously in Figure 3.1.

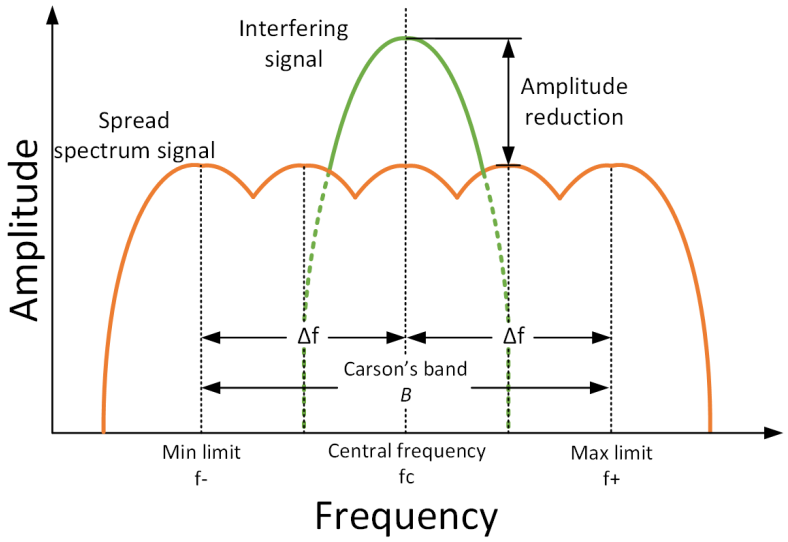

Figure 3.3: Extended Spread Spectrum theory applied to an interfering signal considering Carson's band (B).

An interesting measurement carried out at different sampling frequencies for a sine wave signal can be found in Appendix D. These measurements were obtained from a TD-EMI receiver at a Summer School in Zielona Gora, Poland. These graphs show how the sampling frequency variation for different cases is an important parameter for obtaining the different PK values and shapes of the spectrum measured for a DC converter using this

TD-EMI Receiver.

The theoretical background and use of SSM has been introduced in this section, and there are three important parameters (modulating signal, spreading factor and modulation index) that must be considered properly when using these techniques for a DC converter. In fact, the understanding of these parameters in the TD is important to determine the effects in the FD.

3.1.4 Measurements in Time and Frequency Domains

Depending on the modulation technique used for Spread Spectrum Modulation (SSM), the parameters to be used for driving a converter (such as modulating signal, sampling ratio and spreading factor) can provide different measurement results if the measuring instrument uses a different resolution. This happens even in the case with Deterministic Modulation, and is due to the time needed to demodulate a signal from the measuring equipment. It is important to account for a measurement Resolution Bandwidth (RBW) of the equipment in which the complete nature of a signal can be decomposed. In fact, all the SSM parameters can be kept the same and it can be possible to obtain different measurement results depending on the sampling frequency and window length of the measuring equipment. This approach can been seen in Figure 3.4 when comparing four values of period used for the exact same data measured at the input voltage of a DC converter when calculating the FFT of the converter driven by a DetM of 20 kHz. The sampling time of the algorithm was 1 μS. In this figure it can be seen how the peaks for periods of the FFT differ one from each other. For a period of 5 ms a value of -98.2402 dB was measured (Purple Signal), which is different when compared to a period of 20 ms (Yellow Signal) with a measured value of -85.5752 dB. If a higher period is considered such as 50 ms (Orange Signal) and 200 ms (Blue Signal), values

of -78.6788 dB and -65.6166 dB are measured, respectively. This test clearly shows the importance of the period chosen for calculating the FFT. It is worth noticing the slight difference between the Y axis values. Ideally, all of them must be equal to 20 kHz, however when the decomposition of the FFT is carried out (frequency points from time points) there are frequencies that can not be decomposed into the exact value and are rounded to the next possible value.

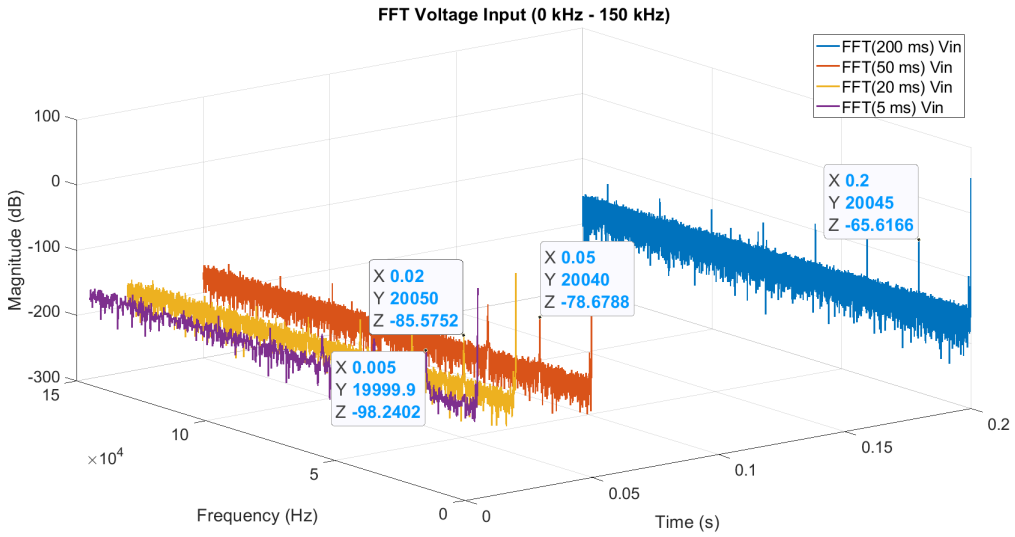

Figure 3.4: Frequency domain analysis for the buck converter as a DUT (0 - 150 kHz).

A similar task was performed by the EMI receiver employed for the experimental results in the next chapter, however additional filtering and signal processing is required which depends on the standard being used.

In this section, the main background of Spread Spectrum has been presented, an important literature review has been surveyed to determine the generation of the signals and how this is translated into a mitigation for EMI. The analogue representation has been explained along with important parameters such as the modulation index and the modulating frequency.

Finally, a simple example to demonstrate the importance of the measuring process has been introduced to understand the effects of the sample period

chosen for the FFT algorithm which is needed for future measurements and standards.

3.2 Design and Simulation of the SSM

When designing a Spread Spectrum modulator it should be noted that the complete modulator can be broken down in two blocks. The Frequency Modulator and the PWM Generator.

3.2.1 Spread Spectrum Modulator Block Design

The generation of the Spread Spectrum modulator is based on analogue frequency modulation as seen in (3.6), for simulation purposes the analogue blocks can be used to generate a straightforward method to modulate a converter, however when this technique is applied to a real modulator some considerations must be taken into account.

In (3.6) the frequency modulator equation was shown. The implementation of this is shown in Figure 3.5 for the purpose of simulation using Matlab as well for the experimental implementation. The complete modulator block relies on the theory and formulas presented previously in Section 3.1.

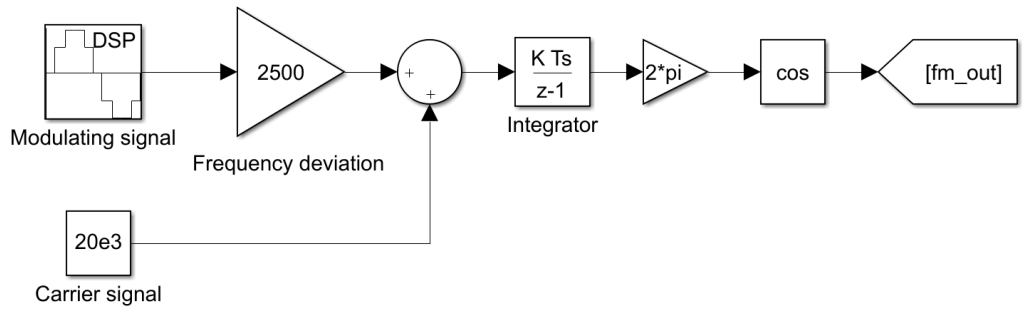

Figure 3.5: Simulation blocks for frequency modulation.

A brief explanation of the blocks involved is presented as follows.

- The use of a “Modulating signal” which generates a signal in the

time domain with the considerations of sampling frequency and signal frequency.

- The "Carrier signal" is the central (or baseline) frequency of the frequency modulator.
- The block "Frequency deviation" represents the deviation from the carrier signal to be used. In Figure. 3.5, a value of 2500 Hz was used because of the representation of a deviation greater than the 10%.
- The use of the block "Integrator" calculates the integral of the signal with the previous operations added in the previous operation point.
- Finally, after the operation of integration, the calculation of the cosine wave with the results provided (in radians) is calculated to generate the output modulated frequency.

The block diagram shown in Figure 3.5 generates at the output a modulated sine wave signal. In order to convert this to be used as a carrier signal and to be compared, a conversion is needed. A convenient way to convert a sine wave to a triangle is by using the inverse sine wave (arc sin). The triangle relation to a Square wave is then as follows,

$$x(t) = \int_0^t sign(\sin\frac{u}{p})\,du, \tag{3.7}$$

A triangle wave with period P and amplitude A can be expressed in terms of sine and arcsine as follows:

$$s(x) = \frac{2A}{\pi} arcsin(sin\frac{2\pi}{p}x), \tag{3.8}$$

Having considered this it is only required to apply the arcsin function to the modulated frequency.

$$s(x) = \frac{A}{\pi} arcsin(sinx), \tag{3.9}$$

This equation is then represented by the block diagram show in Figure 3.6.

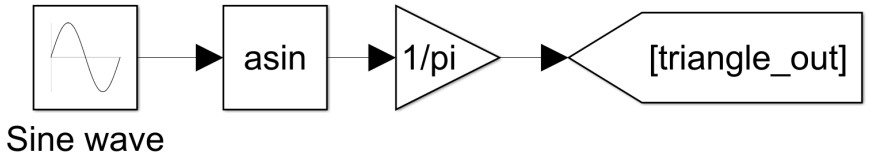

Figure 3.6: Conversion to a sine wave.

The demonstration for the modulation in frequency process and how to convert the sine wave into a triangle wave has been shown, however the PWM modulator must be explained in a simple mathematical equation. Considering a deterministic PWM, A Constant Frequency (CF) signal can be produced by comparing a reference signal $r(t)$ with a carrier signal ($c(t)$). The binary PWM output can be mathematically written as,

$$s_{pwm} = sign(r(t) - c(t)), \tag{3.10}$$

where, $sign$ is represents the sign (positive or negative) of the function. The carrier signal in the Spread Spectrum modulation is then modulated with a defined Duty cycle as shown in Figure 3.7.

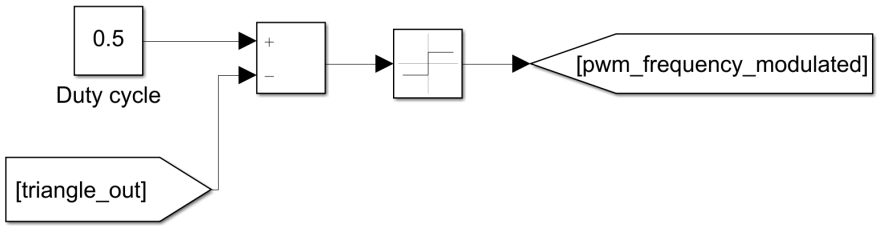

Figure 3.7: Conversion to a square modulated signal.

The complete modulator considering the analogue background is then shown in Figure. 3.8.

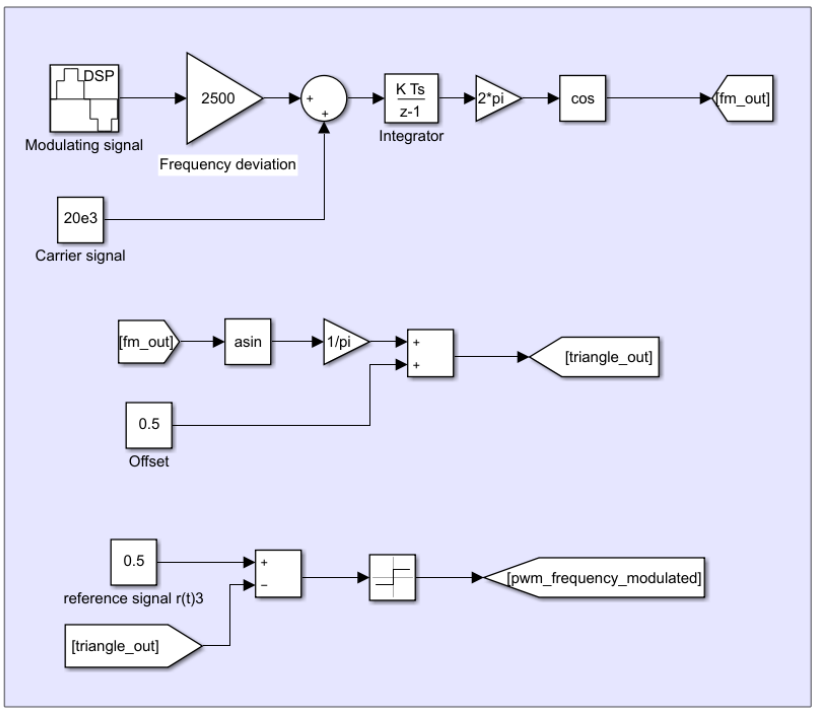

Figure 3.8: Simulated SSM block for driving a converter.

3.2.2 Pulse Width Modulator Block Design

The PWM works with a Carrier Signal and a Modulating Signal that are compared at every clock cycle to generate the output pulse. The PWM is an important block. Common techniques for PWM are explained in [80], and shown in Figure 3.9. These can be with a) Sawtooth Carrier, b) Inverted Sawtooth Carrier and c) Triangle Carrier . For the frequency modulation block diagram designed, the triangle carrier was chosen due to the conversion carried out previously.

3.2.3 Simulation Results Using Matlab/Simulink

The implementation of the modulator for simulation purposes is discussed in this section by employing Simulink blocks. The solver configuration uses a fixed sampling frequency of 10 MHz using a discrete solver. This value for the solver is high enough to provide accurate measurements for the frequency band under analysis. In order to demonstrate a practi-

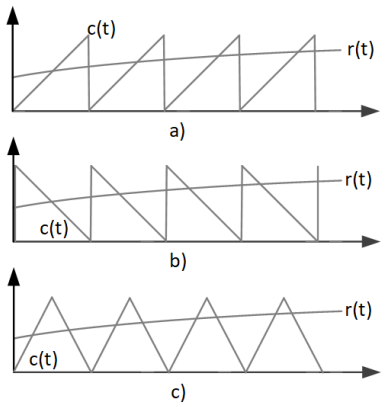

Figure 3.9: Different PWM carrier signals for Power Converters.

cal procedure for understanding SSM with regards to switching frequency PEAK mitigation before any laboratory measurement some considerations are explained as follows,

- The simulation parameters are given by:

  The spreading factor of $\alpha = 0.25$,

  The carrier frequency is set at $f_c = 20$ kHz,

  The sampling frequency of the system/solver is configured as $f_{sam} = 200$ kHz,

  The bandwidth covered is given by, $\Delta \text{f} = f_b * \alpha = 20000 * 0.25 = 5000$ Hz.

  All the values have been selected to demonstrate in a clear and simple way the effects of Spread Spread Modulation.

- The relation between the frequency of the modulating signal (f_{sig}) to the value of Δf is considered to be a factor using β as follows:

$$f_{sig} = \frac{\Delta f}{\beta}, \tag{3.11}$$

  where the resulting values are shown in Table 3.1 to generate a sweep analysis from low to high signal frequencies to test.

- The results based on simulation rely on a FFT resolution of 200 ms (5 Hz) similar as the band used for Power Quality analyses suggested in [81].

Table 3.1: Modulating signal division by the factor β.

β	**Signal Frequency (Hz)**
5000	1 Hz
1000	5 Hz
500	10 Hz
100	50 Hz
50	100 Hz
10	500 Hz
5	1000 Hz
1	5000 Hz

- The measurements as stated by standards (employing a LISN) are considered when possible.

- The results obtained in this section are not focused on matching experimental measurements in future chapters since it is not possible to have all the required equipment at the laboratory and most of the measurements were carried out at different times and different places over the course of the three year PhD.

- The procedure that was followed in this section provided the framework for the experimental tests in Chapter 4.

- The comparison of the noise mitigation is with the ideal simulated case when the converter uses DetM.

The results from the simulation have the only aim to provide an interesting introduction for understanding the parameters used for SSM in a real laboratory application. This is due to the difficult task of replicating the environment in a real experimental measurement. The step size and the solver of the simulation are important to obtain accurate results, however these are not a guarantee for having similar results in a real application provided by a laboratory measurement.

The schematic of the buck converter used can be seen in Figure 3.10, while the list of parameters of the buck converter used can be found in

Table 3.2.

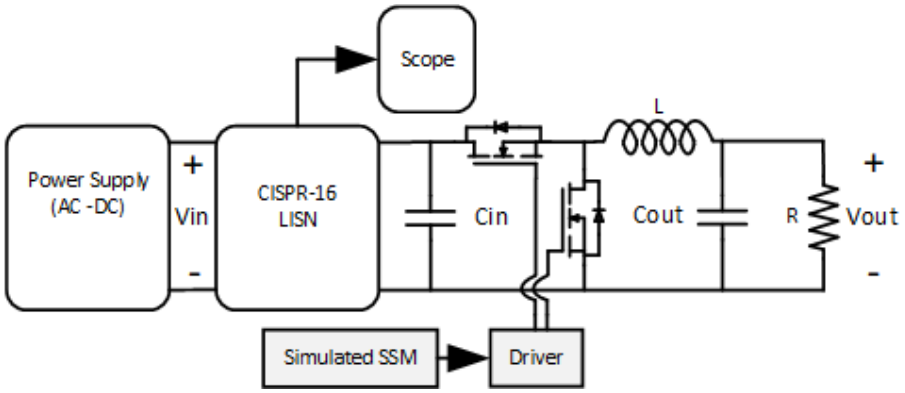

Figure 3.10: Buck converter used for the simulation.

Table 3.2: Buck converter main parameters for the analysis.

Parameter	**Value**
Input voltage (V_{in})	48 V
Output voltage (V_{out})	24 V
Switching frequency	20 kHz
Duty Cycle	50%
Inductor (L)	1 mH
Input capacitor (C_{in})	5.1 μF
Output capacitor (C_{out})	470 μF
Output load (R)	47 Ω

In the next part of this section the different factors of β are shown. Two pair of β are considered for every graph presented to better explain the changes.

SSM Simulation for $\beta = 5000$ and $\beta = 1000$

Considering the values of β introduced in Table 3.1, these pair of results rely on the usage of a slow modulating signal. The modulating frequency is 1 Hz and 5 Hz. Hence a steady signal can not be expected from the FFT algorithm.

The results obtained when β is used for 5000 and 1000 can be seen in Figure. 3.11. When β is 5000 (top panel) the resolution of the FFT can not decompose the signal, because of the low frequency for the modulating

signal of 1 Hz (lower than the 5 Hz of the FFT). When β is 1000 or 5 Hz (bottom panel) the FFT algorithm is able to decompose the signal and the characteristic shape of a time domain sine wave modulated signal in the frequency domain is clearly seen as introduced in Section 2.4.

The main reason behind the correct decomposition is due to use a modulating signal frequency similar as the FFT resolution which is in fact 5 Hz (200 ms), for this case a value of -42.1895 dB has been obtained in comparison to the ideal value of -21.9858 dB for the DetM case.

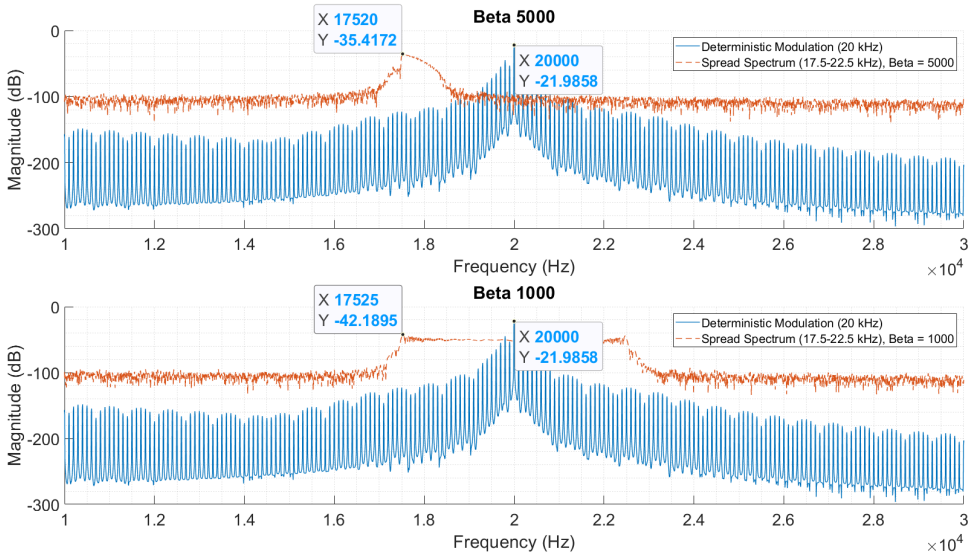

Figure 3.11: SSM simulation for $\beta = 5000$ and $\beta = 1000$.

SSM simulation for $\beta = 500$ and $\beta = 100$

When the value of β is then changed to 500 (top panel) and 100 (bottom panel) the results can be seen in Figure. 3.12. Along with a decreasing value β the frequency of the modulating signal will increase as seen in Table 3.1. This effect of frequency increase can be noticed with the increase of peaks for the following Spread Spectrum cases in which additional peaks are generated within the whole band under analysis. The main reason behind it is for the high frequency used that the resolution of the FFT method is not able to handle. When β is 500 (10 Hz) a value of -40.3881 dB was measured when

compared to a value of -34.7934 dB for β equal to 100 (50 Hz).

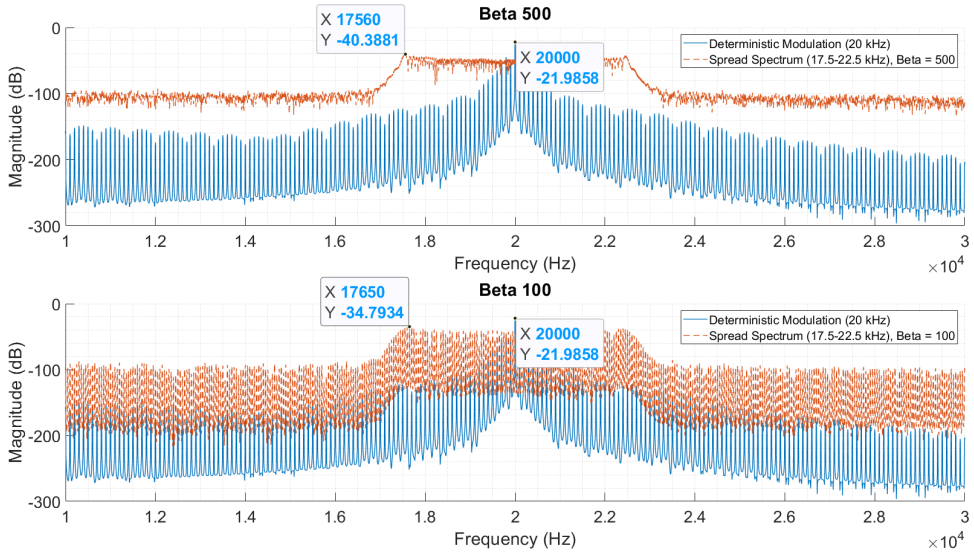

Figure 3.12: SSM simulation for $\beta = 500$ and $\beta = 100$.

SSM simulation for $\beta = 50$ and $\beta = 10$

Figure 3.13 shows what happens if the value of β is further decreased to 50 and 10, top and bottom panels respectively. The FFT starts to develop peaks in the whole range of frequencies measured. When $\beta = 50$ (100 Hz), the peak value obtained is -35.4375 dB and when $\beta = 10$ (500 Hz) the location of a peak value is difficult to define given the fast change of the signal. However three points are highlighted for the Spread Spectrum signal in the bottom panel (-29.1344 dB, -29.982 dB and -21.9858 dB to determine which one could be the lowest).

SSM simulation for $\beta = 5$ and $\beta = 1$

For the lowest values of $\beta = 5$ (top) and 1 (bottom) in Figure.3.14 the results do not agree with the expected results of peak decrease. For $\beta = 5$ (1000 Hz), there exist two highest peaks, -27.9564 dB and -27.5365 dB. In these, the peak difference is very low when compared to some of the cases presented before. For $\beta = 1$ (5000 Hz), the signal generates two peaks, one

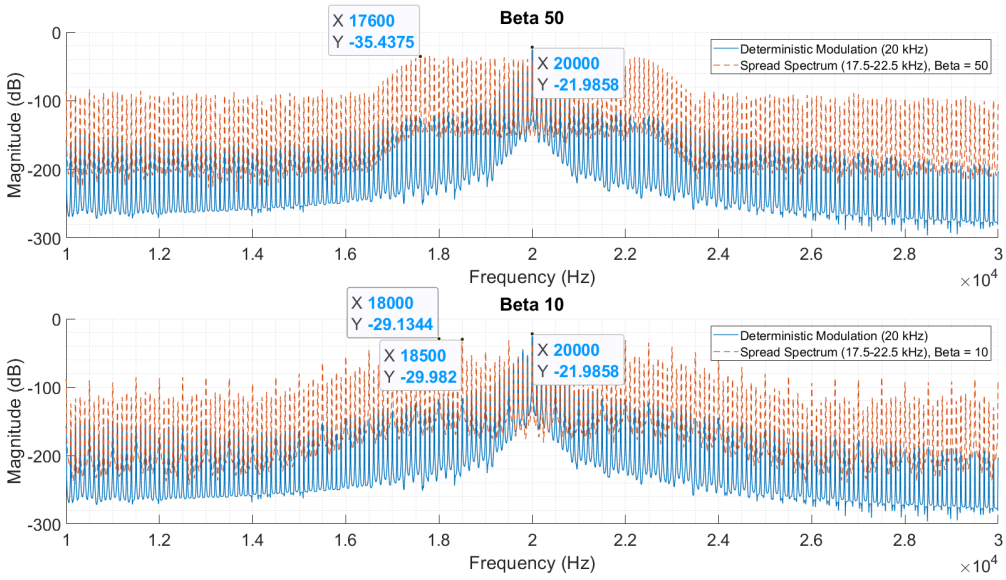

Figure 3.13: SSM simulation for $\beta = 50$ and $\beta = 10$.

lower peak of -31.5955 dB when compared to the DetM case of -22.5553 dB and one peak of -22.5553 dB at the same frequency (20 k Hz) of a DetM case.

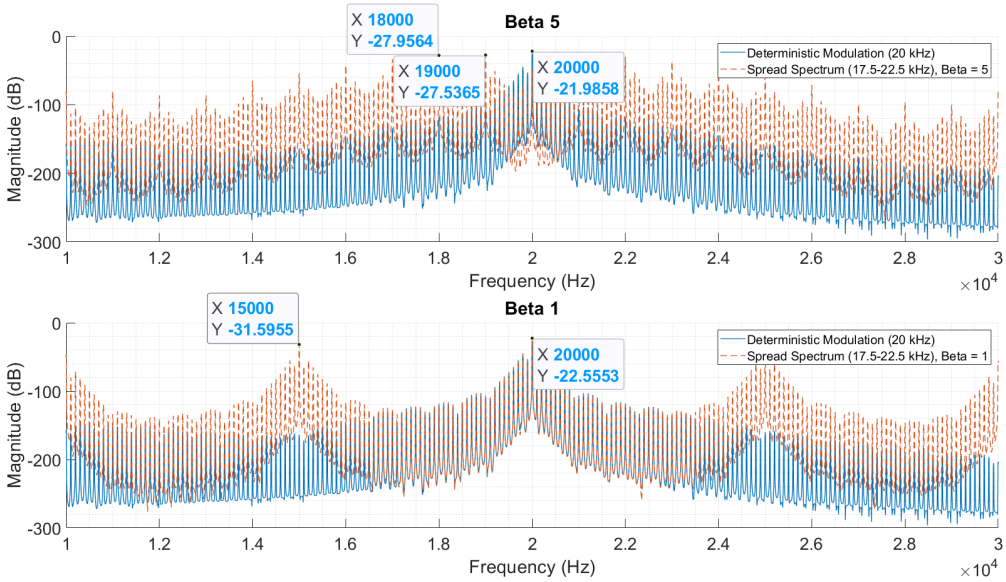

Figure 3.14: SSM simulation for $\beta = 5$ and $\beta = 1$.

3.2.4 SSM: Discussion of the Simulation Results

With all the results obtained previously it is clear that there is one point at which the peak decrease obtained can be considerable whilst also being steady in the frequency domain signal, by the appropriate choice of the time domain parameters. The results for every value of β are shown in Table 3.3 along with the respective PK value and the additional column of relative peak decrease when compared to the value obtained for DetM.

Table 3.3: Peak value relative decrease for β.

β	**PEAK value dB**	**Relative reduction dB**
1	-31.5955*	9.0402
5	-27.9564	5.9706
10	-29.9820	7.9962
50	-35.4375	13.4517
100	-34.7934	12.8076
500	-40.3881	18.4023
1000	-42.1895	20.2037
5000	-35.4172	13.4314

It is worth mentioning that these results rely on the resolution of the FFT algorithm which is 200 ms (or 5 Hz). Interestingly, the FFT develops a good agreement at this point ($\beta = 1000$) due to the equal value of FTT resolution and sampling frequency of the modulating signal. This is the main reason for obtaining a reduction of approximately 20 dB, with 5 Hz. This brings the conclusion that the results of a peak decrease must be analysed according to the instrument or algorithm used to measure the interference. In an effort to determine the point at which the signal improves the most, a graphical conceptualisation is shown in Figure 3.15. The spectral components are shown by green triangles. Along with these values the equivalent value of β and frequency of modulation (FM) can be seen below. Two values are highlighted with a circle, $\beta = 500$ and $\beta = 1000$ which are the best results measured when the FFT is used with a sample period of 200 ms.

Considering the measurement procedure carried out in this section, the

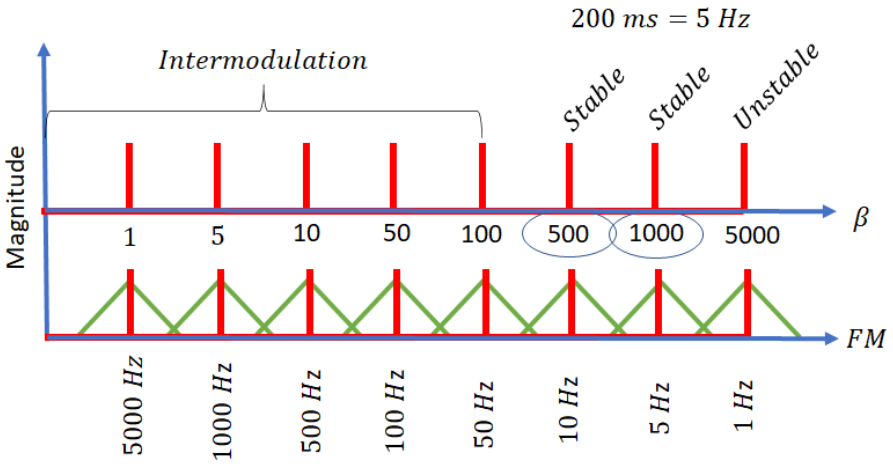

Figure 3.15: Relation between β, frequency of the modulating signal (FM) and Resolution Bandwidth of the FFT.

following can be concluded.

- If the intention of SSM is to find the best peak decrease, then the idea is to be as close to the resolution of the FFT or the resolution of the EMI instrument in use.

This section has provided the implementation of a simulation for a DC converter using Spread Spectrum modulation. The fundamentals of frequency modulation were included in the simulation. In addition, a starting framework for future laboratory measurements was presented. In the next chapter one of the main tasks is to find a similar point when measuring according to a certain established standard (with a defined resolution bandwidth).

3.3 Chapter Conclusion

This chapter has presented the background theory and the main effects in the frequency domain when Spread Spectrum Modulation is used for EMI mitigation for a DC buck converter. Important considerations for time and frequency domains were discussed as well as the generation of the signal.

Important parameters were highlighted to understand better the usage of SSM such as the modulation index. The simulations carried out in this chapter shown that there is a point at which a good peak decrease can be achieved just by controlling the frequency of the sine modulating signal. The points in which steady measurements can be found are when the modulating signal used 10 Hz and 5 Hz. This was due to the value of the resolution for the FFT used. To assess a future analysis, the simulation with a sine wave modulating signal was developed as an introduction for the laboratory measurements with real devices. An important point to comment on is the that the mitigation is dependant on the resolution bandwidth of the FFT algorithm used for measurement.

Chapter 4

SSM According to CISPR-16 Band A

This chapter provides the measurements carried at the laboratory for a DC buck converter driven by SSM. For the first part of the analysis in this chapter, the generation of the driving signal is explained in Section 4.1 and Section 4.2 due to its important role. The second part of the analysis (Section 4.3 and Section 4.4) relies on the understanding of the Standard used to measure as well as the usage of the SSM parameters to generate an agreement of the results obtained.

4.1 SSM Generation of Signals

The generation of the modulating signal should be introduced since a digital system uses a fixed master clock to generate the driving signal. This means that inherently the driving signal (either random or sinusoidal), will have fixed steps at every point of the switching frequency generated to modulate the DC converter. A graphical explanation of this behaviour can be seen in Figure 4.1, the given steps in both cases, a) and b) show the same duration for both signals, sine and random. The parameter F_c refers to the frequency

of the carrier signal while the parameters (F_{s-}) and (F_{s+}) are the minimum and maximum frequency allowed by Carson's rule considering the spreading factor used.

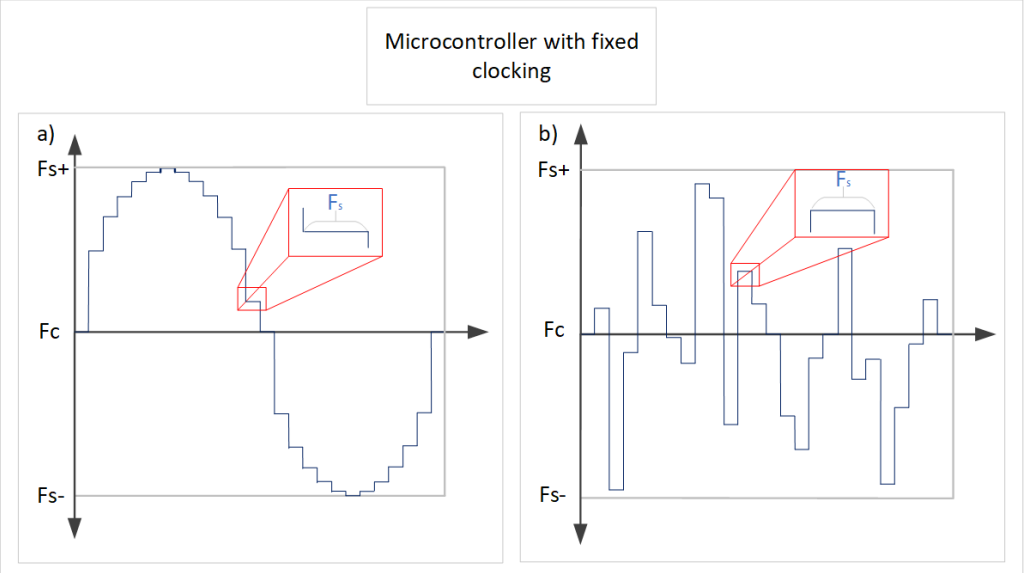

Figure 4.1: Master clock for a fixed clocking generation, a) for a periodical sinusoidal driving signal, b) for a random driving signal.

In the analysis presented in Chapter VI, a different approach for the generation of a random signal with a random clocking generator is used. To achieve this behaviour in the Spread Spectrum Modulation technique, a FPGA is used to control every step of the clock generator randomly. By doing this it is possible to achieve better mitigation objectives. An example is presented in Figure 4.2 to show how a change in the instantaneous sampling frequency can be understood. In this figure it can be seen that there is no fixed sampling frequency for the given signal. In fact three different points have been considered which all show a different instantaneous sampling frequency (F_{s1}, F_{s2}, and F_{sn}). When having a generator like this, there will be n values of instantaneous values for F_{sn}.

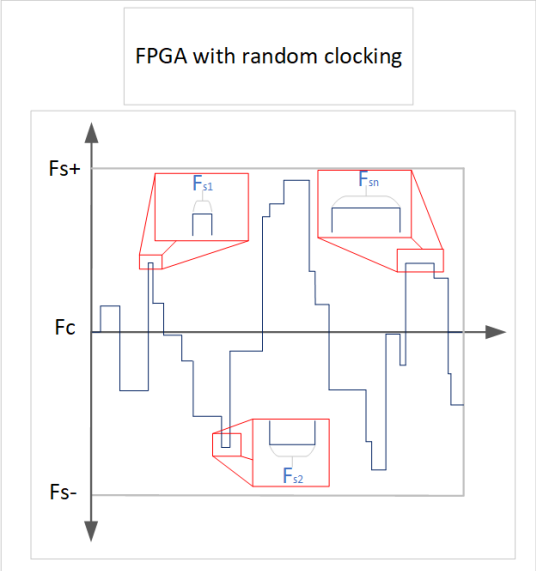

Figure 4.2: Master clock for a random clocking generation.

4.1.1 Time Domain (TD) Effects of SSM

In the TD, the effects of a fixed RBW or dwell time will provide stable and repeatable results for a given signal. In order to demonstrate a practical explanation of how important the TD effect is, a signal that changes quickly can lead to the wrong idea that it will cover more points if it is compared to a signal that changes slowly. It is because of this assumption that design engineers might have to rethink how to modulate a converter with SSM to comply with different standards and consequently different resolution bandwidths. A graphical explanation of these effects with regards to RBW can be seen in Figure 4.3. In this graph a sine wave is specifically changing from f_{b1} =40 kHz to f_{b2} = 10 kHz, then to f_{b3} =20 kHz and finally to f_{b4} =30 kHz. The dwell times (or RBW) are equal to: (a) 25 ms, (b) 125 ms, (c) 200 ms and (d) 1000 ms. In the case of (a), the dwell time is not long enough compared to the frequencies to be measured, hence the demodulation can not be achieved steadily. In (b) the dwell time has been increased and allows more time for the signals to be demodulated. The same holds for the remaining cases in which the dwell time is changed to 200 ms and 1000 ms. It is clear that there is one point at which a good

demodulation can be achieved, even measuring with a low dwell time.

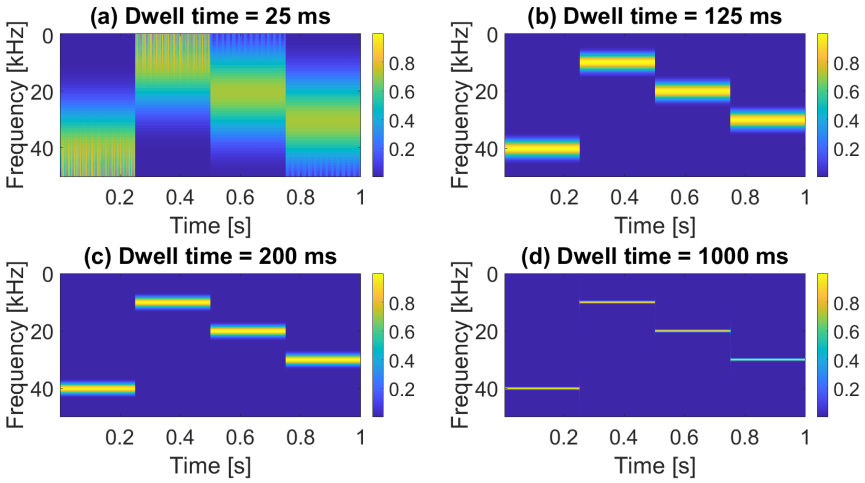

Figure 4.3: MATLAB simulation of Short Time Fourier Transform (STFT) for a sinusoidal signal .

This section has shown the importance of the frequency domain effects for SSM. The most straightforward method to calculate the FD spectra from the TD signal is the FFT method as shown in Chapter II and Chapter III. In this method a signal is decomposed into several sinusoidal components according to the frequency recorded for a given time window at a given sampling frequency. Hence, one of the important parameters is the recording time window which can be referred to as the resolution bandwidth of the measurement equipment in combination with the sampling frequency. However, these do not directly relate to the Bandwidth of the signal to be measured since there can be other considerations e.g. measurement filters.

4.2 Importance of Driving Signals

The generation of the signal used in this thesis chapter is based on simple waveforms generated by a microcontroller. It is worth noting that in digital and discrete systems an important parameter is the Sampling Time (T_s) or Sampling Frequency (F_s) of the signal to be generated. As stated by Nyquist (4.1), the Sampling Frequency must be at least two times the frequency to

be measured or as a simple mathematical expression,

$$f_{sampling} >= 2 \cdot fsignal, \tag{4.1}$$

The signals used for this chapter are based on a simple sine and random wave modulation considering the important assumptions with regards to the fixed clocking signal, which means the use of a fixed sampling signal that is based on the analogue modulation techniques that were developed initially for communications as presented in Section 4.1.

4.2.1 Periodic Driving Signals

Most of the common periodic signals can be used to drive a converter as suggested in [76]. The most common signals used are Sine and Triangular/Sawtooth waveforms. The effect of such TD signals in the FD will have a different impact in the frequency domain analysis as shown in Chapter II.

An interesting example of a periodical driving signal is stated in [73]. The algorithm designed considers a ramp profile with frequencies close to 20 kHz. The ramp profile has 4 different frequencies with a separation of 1 kHz. Figure 4.4 shows the output signal that drives the converter.

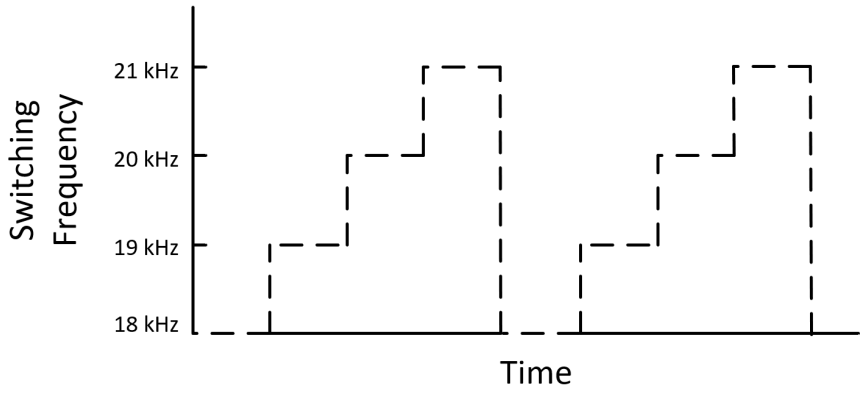

Figure 4.4: Proposed ramp profile for the frequency modulation.

What can be concluded from [73] is that the main advantage of using a certain profile or driving signal for SSM is the ability to set fixed frequency

steps for the frequencies used in the modulation scheme. The full controllabity at every PWM period keeps the energy changes between switching frequencies defined, resulting in the energy from one switching frequency to another being kept the same.

4.2.2 Non-periodic Driving Signals

The stochastic generation of non-periodical signals for SSM (often called Random Modulation (RanM)) is one of the most interesting topics when considering modulating a given DC-DC converter focused on EMI issues and their mitigation[82], [83] and [84].

[82] shows a method to generate random switching frequencies considering Carson's rule for a Buck converter. This research mentions that it is very important to account for the total impact of these strategies when designing measurement by an EMI Receiver. It also compared different modulation schemes and the number of the switching actions over a long time period when a FPGA is used as a switching frequency generator, concluding that the maximum Peak level of interference does not reduce the aggregated measurement of noise power.

When addressing the effect of modulation based on Random distributions it can be difficult to decide which method is the best when measuring or understanding the effect of EMI. A method of spectrum aggregation is proposed in [83], which simulates a similar procedure to the windowing techniques of state-of-the-art EMI receivers to account for the impact of Random Modulation. It uses a cosinusoidal window (EMI receivers use Gaussian windows) to aggregate the spectrum. The authors state that this method can make the measurement accurate and reliable. From this research work it can be concluded that the evaluation of the mitigation of EMI using random modulation depends entirely on the measurement pro-

cedure employed. This is achieved by comparing the effect of the resolution bandwidth to aggregate the spectrum.

The aggregation of conducted emissions mentioned in [83] is also analysed in [85] to account for the effect of converters using random modulation with identical converters. In this research work it is concluded that the statistical parameters of the Random Modulation can lead to misleading conclusions due to the limitations of EMI receivers to demodulate a signal.

Considering previous research work based on random generation of switching frequencies it appears that the statistical aspect is important to mitigate the EMI generated by a DC converter. This generation of random values for a switching frequency introduces a discussion to produce the best shape with the lowest energy located at the fundamental frequency. To demonstrate these effects two different distributions are analysed. These distributions are normalised between -0.5 to 0.5 as the lowest and the highest values representing the limits of the frequency deviation, respectively. The value of 0 represents the location of the carrier frequency (F_c). For comparison, a value of $\alpha = 15$ % has been chosen along with a Sampling Frequency (F_s) of 10 kHz to demonstrate two possible outcomes. The generation of the graphs to analyse the random distributions consider 1000 bins for an entire data measured for 1 second with a sampling ratio of 1 MHz. This can be seen as an average of 1000 samples for the complete data. A Gaussian distribution (red line) in both graphs has been plotted to highlight the differences of the distributions obtained. If the distribution of switching frequencies is analysed to generate random patterns two possible cases are considered,

- Normal Gaussian distribution.

  In this generation of random switching frequencies the main parameter to control the distribution is given by the variance which has been chosen as 0.0225 to cover the limits from -0.5 to 0.5 for the normal

distribution. The distribution of the Gaussian stream of switching frequencies can be seen in Figure 4.5.

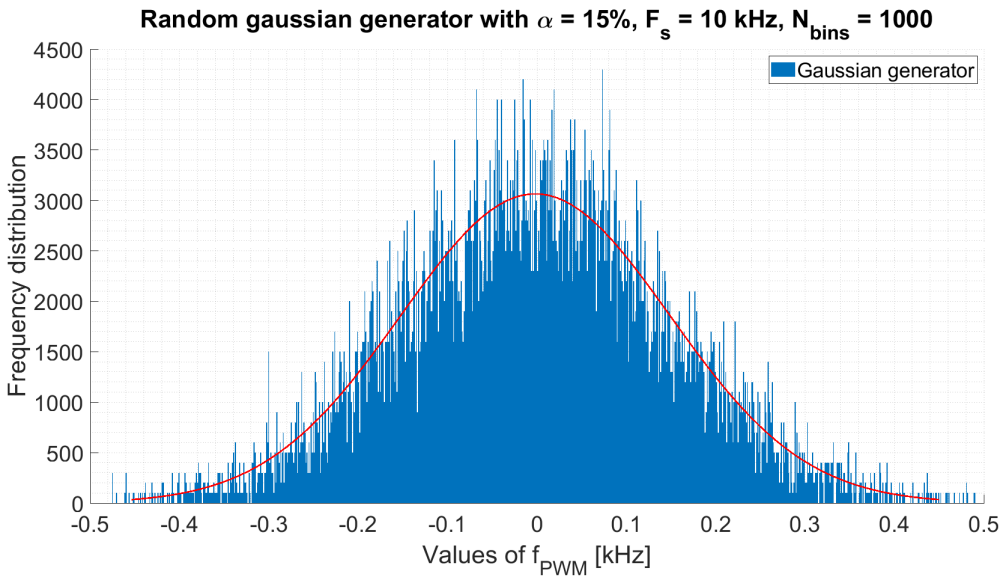

Figure 4.5: Random normal distribution for the switching frequencies in the Spread Spectrum mitigation technique.

- Linear random distribution.

  In this way of creating random switching frequencies all of the possible options will have exactly the same probability to appear in the random switching frequency generation. There is no variance parameter because of this reason. The distribution for this case is shown in Figure 4.6.

Considering the shapes and maximum values obtained for the Frequency distribution in Figure 4.5 and Figure 4.6, it seems that the magnitude for frequency distribution presents a lower value for a Random Linear distribution of approximately 1500 while a Random Gaussian distribution has a maximum value of Frequency distribution of 4000. This shows an interesting form to generate the best shape for mitigation EMI at the point of generation i.e. the switching frequency. A different and more complex approach for generating random modulating signals is explained in Section VI.

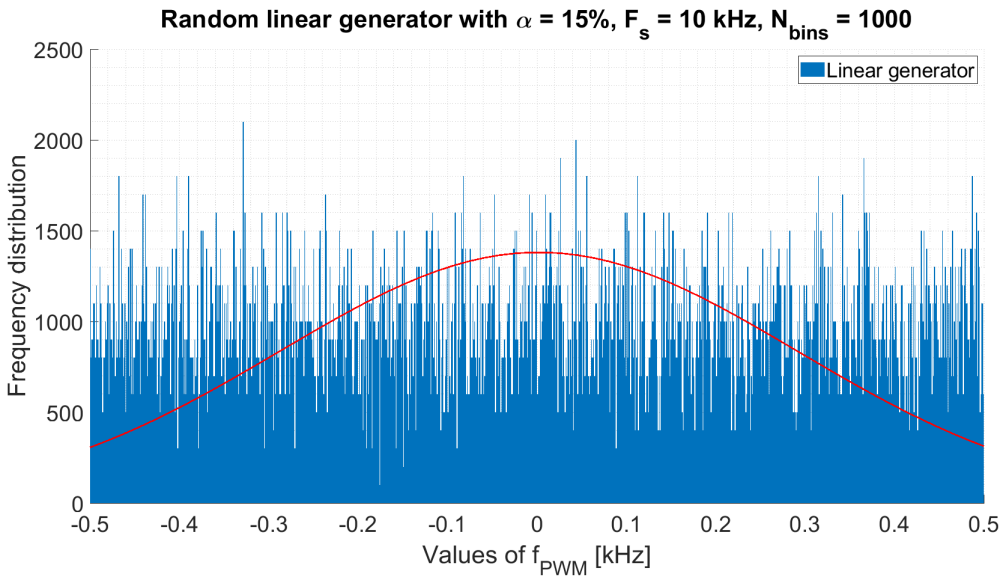

Figure 4.6: Random linear distribution for the switching frequencies in the Spread Spectrum mitigation technique.

In this section an important point to be stated is the interesting differences that can be found when using different strategies applied to SSM. In fact, the distribution of random variables can also affect the mitigation objectives if these are not carefully chosen. In the next section, the measurements carried out considering SSM with a Sine wave and Linear Random distribution are shown to discuss what are the main differences between both testing cases.

4.3 CISPR-16 Measuring Background

In order to provide a brief explanation of the functioning of the state-of-the-art EMI receivers the FFT decomposition algorithm for EMI receivers is considered in [37] for the standard CISPR-16.

The modern digital EMI receivers use a Fourier Analysis, which requires sampling in the time domain by the Analogue to Digital Converter ADC. The sampling period of the instrument is important to define the maximum frequency possible. This follows the Nyquist-Shannon theorem, which states

that to measure a certain frequency, we need to sample at more than twice the signal frequency. The FFT algorithm can be summarised using the Discrete Fourier Transform (DFT). The DFT is defined as follows in (4.2).

$$X[k] = \sum_{n=0}^{N-1} x[n] \cdot e^{-j2\pi kn/N} \tag{4.2}$$

where, $x[n]$ is the sampled signal in time domain, $X[k]$ is the discretised amplitude spectrum, n is the integer value starting at the measure 0 to N-1 in the time domain. Finally, k is the starting integer at the measure 0 to N-1 of the signal in frequency domain.

However, the measurement should not only consider steady state signals as it is possible to improve the measurement of transients and noise in real scenarios. This is why the Short Time Fourier Transform (STFT) is used with a bandpass filter. The STFT formula is as follows:

$$Z[m,k] = \sum_{n=0}^{N-1} x[n-m] \cdot w[n] \cdot e^{-j2\pi kn/N} \tag{4.3}$$

Based on (4.3), the parameters given by $x[n-m]$ are the sampled signal measured in time domain, $w[n]$ is the discretised window, N is the length of a DFT signal calculation, n is an integer ranging from 0 to N-1. Finally, k is an integer from 0 to N-1 that stores the element number of the spectrogram $Z[m,k]$ in the frequency domain and m is the integer value of the element number for the spectrogram.

4.3.1 EMI Receiver Bandpass Filter

The bandpass filter of the EMI receiver is described in terms of the window function. This measurement step considers the sampled window function $w[n]$ to the sampled input signal $x[n]$, in which n is the integer representing the number of the data measured. This can be explained by the expression,

$z[n] = x[n] \times w[n]$.

Thus, considering that the input signal is measured according to a certain sample interval T_s, a Gaussian window is obtained. The window function can be seen in (4.4).

$$w[n] = \frac{1}{G_c N} \exp\left[-\frac{1}{2}\left(\frac{\pi}{\sqrt{2\ln 2} B_{IF} T_0 n}\right)^2\right] \tag{4.4}$$

where, B_{IF} is equivalent to the bandwidth of the Intermediate Frequency (IF) filter of a Heterodyne Receiver for the CISPR A frequency band, T_0 is the sampling ratio of the discrete samples, and n is the current number of the sample. The parameter G_c is a scaling factor to compensate the energy loss because of the window used. It is calculated as follows:

$$G_c = \sum_{n=0}^{N-1} w[n] \tag{4.5}$$

The IF bandpass filter parameters are necessary for the EMI measurements obtained when driving frequency modulation techniques with any signal. In Table 4.1, the main parameters are shown for the CISPR-16 frequency band A.

Table 4.1: CISPR 16 Band A parameters.

Parameter	**Value**
Frequency range	9 kHz - 150 kHz
IF Bandwidth	200 Hz

The EMI receiver generates a sweep of windows over the frequency band to be measured by computing several FFTs at the same time. These operations are carried out with a small shift percentage to keep steadiness between one FFT and the next one. According to information of Rhode and Schwarz in [86] the scanning procedure carried out by the EMI receiver is shown in Figure 4.7. Considering this procedure, the signals are measured correctly along the desired bandwidth under test.

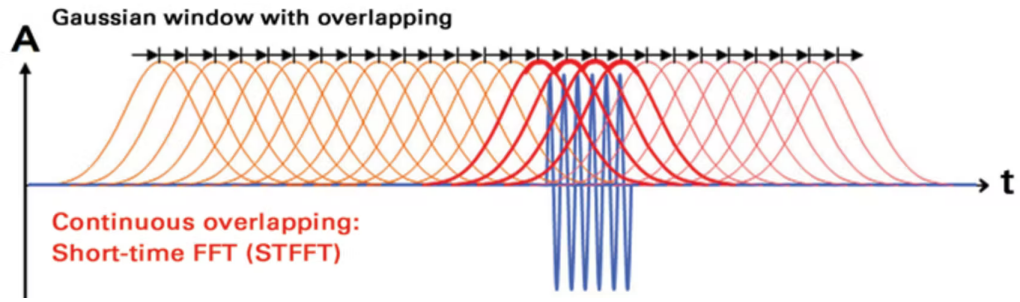

Figure 4.7: EMI Receiver demodulation process [86].

Having considering the discussion in this section regarding the generation of a signal to be analysed, the important points to account for are the capabilities of the measuring equipment such as resolution bandwidth and sampling frequency, with the understanding of these parameters a mitigation technique might be used to avoid undesired results. For this reason the CISPR-16 standard has been chosen to analyse a signal due to its frequency range as it is similar to the switching frequency of typical power converters.

4.3.2 EMI Experimental Test Set-up for FD

The main goal of this thesis chapter is based on the mitigation of EMI by analysing a low frequency band (below 150 kHz). Therefore the standard CISPR-16 has been considered for different spreading factors (α). In order to analyse these effects there are two main pieces of measurement equipment,

- The EMI Receiver
- The LISN

According to [37], the main set-up proposed is presented in Figure 4.8. This set-up was briefly explained in Chapter II but is repeated here for convenience.

The description of the equipment involved is as follows,

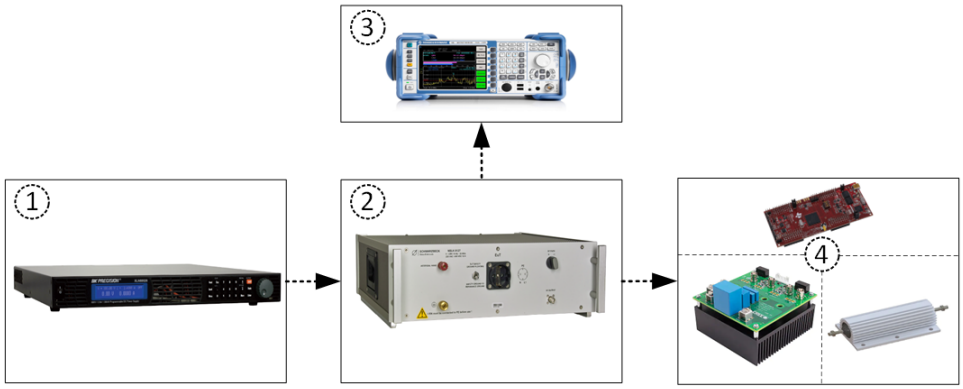

Figure 4.8: Frequency domain test set-up.

1. **Power Supply.** The Power Supply provides 100 V with a maximum current of 14 A. The power supply can be controlled remotely in order to generate sweeps of different voltages. The complete information of the Power Supply can be found in its datasheet [87].

2. **LISN.** The LISN used is the Schwarzbeck NSLK 8127. This LISN is CISPR-16 compliant with a frequency range from 9 kHz to 30 MHz, the schematic was shown in Chapter II. More information can be found in [88].

3. **EMI Receiver.** The EMI Receiver is the R&S ESL3 with a frequency range of 9 kHz to 3 GHz (CISPR-16 compliant), more information can be found in [89]. This EMI Receiver covers the most important bands (A,B,C and D) of the CISPR-16 Standard for the main three indices, PK, QP and AV (detailed in [89]). The theoretical background of these indices was explained in Chapter II and more information can be found in the manual.

4. **DC Converter.** The DC-DC converter development board, the model is KIT8020-CRD-8FF1217P-1 and is a half bridge converter with SiC-based Mosfet transistors (manufactured by Cred/Wolfspeed) [90]. This board allows the user to configure several topologies for DC and even AC converters under specific circumstances. The converter

topology is a Synchronous Buck Converter with a base switching frequency of 50 kHz. More information about the Mosfet and the Diode can be found in Table E.1 and in Appendix E. The converter uses an input capacitor of 5.1 uF and the output capacitor is 470 uF to decrease the ripple generated and to provide a steady voltage at the output. A TI C2000 board is used to generate the SSM patterns: for all the cases, a 50 % of Duty Cycle is used. The output load of the converter is 10 Ω.

4.3.3 Experimental Test Measurements

Considering the main points discussed from Section 4.1 to this Section, the aim here is to choose modulation indices with sufficient separation between values to understand how a wide range of different frequencies can adversely generate an important effect for the measurement assessment of EMI. Initially, the measurement procedure must consider the signals without the use of Spread Spectrum. This is the case for Deterministic Modulation (DetM) which is briefly explained as the starting point to have values to compare. After measuring the Deterministic Modulation cases the modulating frequency is divided by a common factor for all the different spreading factors. The RBW of the EMI Receiver is kept at 200 Hz to analyse the effect of the low frequency band (9 kHz - 150 kHz). The laboratory test set-up used is shown in Figure 4.9. This is based on the block diagram presented in Figure 4.8.

A selection of various modulation indices will be used to analyse the effect of modulating the switching frequency applied to the DC-DC converter. The baseline case to be shown is when the converter uses DetM, this is when the DC converter is considered as the DUT as presented in the CISPR 16 standard set-up. In this procedure, a Peak (PK) of 109.74 dBμV has been

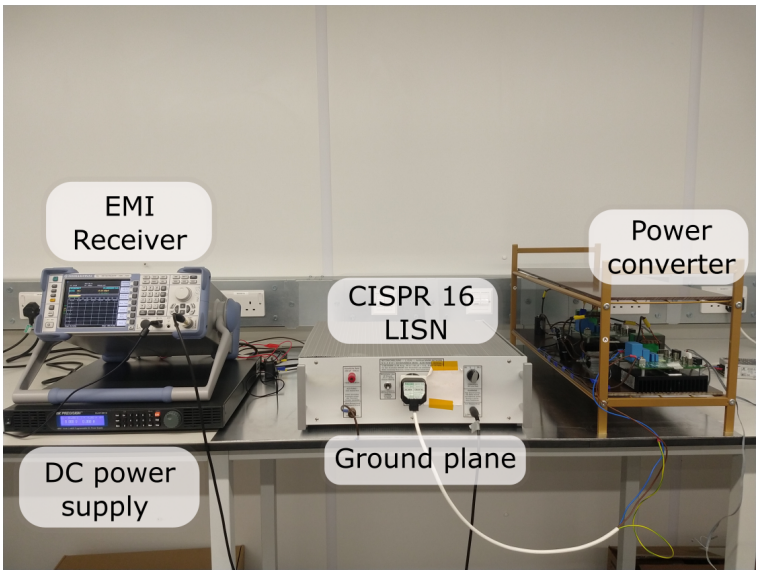

Figure 4.9: Experimental test set-up used for the FD analysis: EMI Receiver, DC power supply, CISPR-16 Lisn over a ground plane and the Power converter.

obtained for the switching frequency of 50 kHz. The complete spectrum (obtained from the EMI receiver) between 9 kHz to 150 kHz can be seen in Figure 4.10a in which the second and third harmonics of the switching frequency are also measured, while the zoomed version considers only the peak of the first harmonic (shown in Figure 4.10b). Interestingly there is a Peak of low amplitude (approximately 40 dBμV) which could be caused by the cabling between devices and the layout in the laboratory test set-up and the auxiliary power supply used.

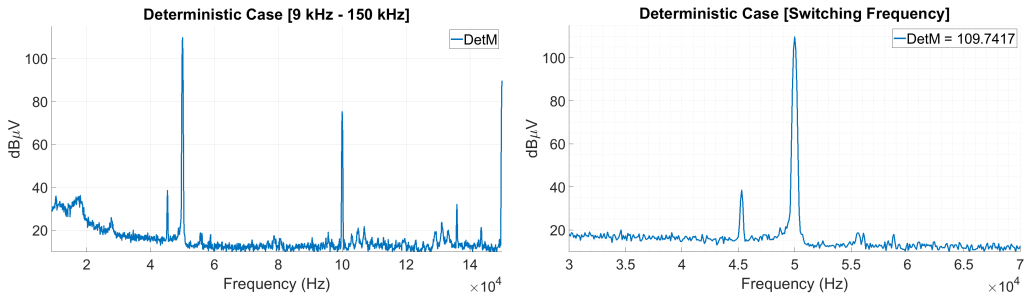

(a) DetM - 9 kHz to 150 kHz. (b) DetM - 50 kHz Switching frequency.

Figure 4.10: Deterministic modulation results from the EMI Receiver for the DC converter.

In an effort to present graphically the effect of SSM for the low frequency

band and its effect over the entire CISPR-16 Band A bandwidth, a graph of every modulation case is shown and compared to the main DetM result in the following sections.

4.3.4 SSM Measurement Procedure Key Points

In this part, a sine and a random wave modulating signals have been chosen for the different values used for the frequency deviation and the Frequency of the Modulating signals (F_m). There will be a different impact on the measured conducted EMI. For the measurement procedure three important points are considered for sine and random modulating signals to provide stability to the converter.

- The lower limit of the percentage given by the spreading factor should be significant to avoid scenarios close to Deterministic Modulation. This is greater or equal to a 5 % of the carrier frequency.
- The higher limit of the percentage given by the spreading factor must be lower than 45 +% since high values can cause more problems than benefits to the voltage and current of the converter.
- The frequency of the modulating signal should be varied according to the different spreading factors used.

Having considered these important points, Table 4.2 presents the results of the modulation indices used for all the cases measured. These modulation indices are based on (3.4) and they describe the behaviour of the signal according to the important parameters. In this table it can be seen the value of F_m in the left column and the value of α in the top row, considering these values a unique value of m is obtained for all the different cases.

Table 4.2: Different modulation indices for different spreading factors (α) and modulating frequencies (F_m).

		α				
		5%	15%	25%	35%	45%
F_m	1,000,000	0.0025	0.00775	0.0125	0.0175	0.0225
	200,000	0.0125	0.0375	0.0625	0.0875	0.1125
	100,000	0.025	0.075	0.125	0.175	0.225
	20,000	0.125	0.375	0.625	0.875	1.125
	10,000	0.25	0.75	1.25	1.75	2.25
	2,000	1.25	3.75	6.25	8.75	11.25
	1,000	2.5	7.5	12.5	17.5	22.5
	200	12.5	37.5	62.5	87.5	112.5
	100	25	75	125	175	225

4.3.5 SSM Sine Modulating Wave Signal

For every spreading factor (α) from 5% to 45% the graphs obtained are shown in the next group of figures. Figure 4.11 shows the spectra for each test using SSM with a Sine wave modulating signal with $\alpha = 5\%$, the modulation indices used are given in Table 4.2. The use of 5% for a central frequency of 50 kHz will generate a lower limit at 48,750 Hz while the higher limit 51,250 Hz. Each graph shows a spectrum for a specific test, together with the measurement of the dBμV of the peak component in the spectrum at the top right.

In Figure 4.11, it can be seen that from Figure 4.11a to Figure 4.11c there is a noticeable generation of peaks and the mitigation achieved is very low compared to the DetM case (i.e. there is little difference between the peak value measured for DetM, and the peak value measured for the SSM case).

If the values of Figure 4.11d and Figure 4.11e are analysed, the values of the PK are lower and steady with values of 102 dBμV to 103 dBμV approximately. In fact, Figure 4.11e presents the lowest PK value of all the graphs. Finally, for the graphs from Figure 4.11f to Figure 4.11g, the Peak value measured is close to the DetM case which shows that a correct demodulation can not be achieved.

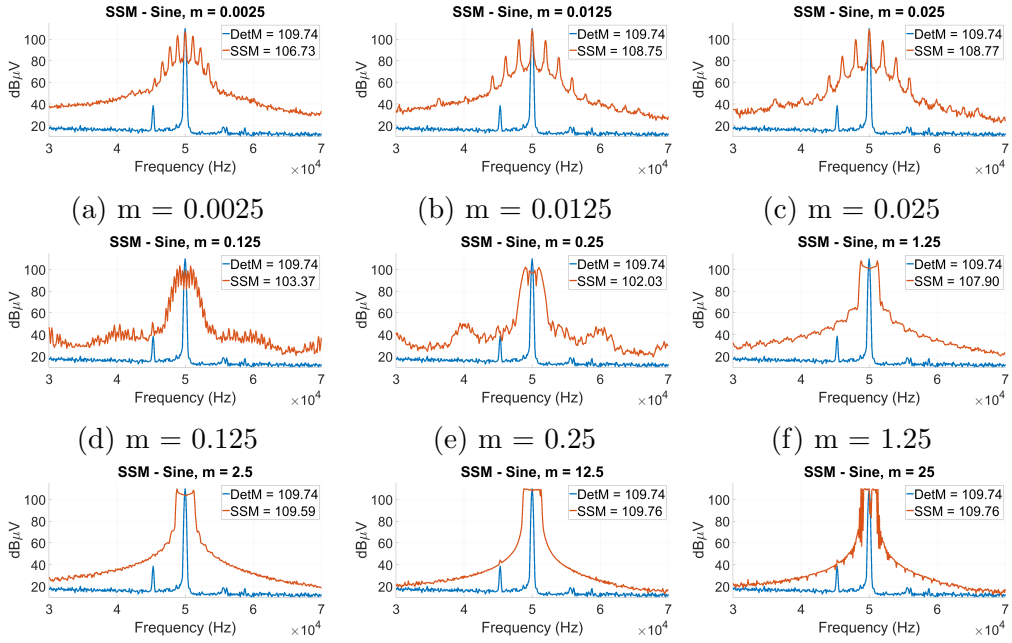

(a) m = 0.0025 (b) m = 0.0125 (c) m = 0.025

(d) m = 0.125 (e) m = 0.25 (f) m = 1.25

(g) m = 2.5 (h) m = 12.5 (i) m = 25

Figure 4.11: Spread spectrum Sine wave modulating for $\alpha = 5\%$.

For a spreading factor of $\alpha = 15\%$, the results obtained are shown in Figure 4.12. The minimum and maximum limits with regards the spreading factor are 46,250 Hz and 53,750 Hz, respectively. From Figure 4.12a to Figure 4.12c the graphs show that there is a small decrease in the PK magnitude (105-107 dBμV) and the generation of peaks are noticeable. The lowest values obtained are found in Figure 4.12d and Figure 4.12e, in fact the latter shows the best mitigation case with a value of 99.23 dBμV. For the cases shown in Figure 4.12f and Figure 4.12g the shapes look smooth, however the EMI Peak reduction is not considerable with PK values of 106.91 dBμV and 108.54 dBμV. The remaining cases in Figure 4.12h and Figure 4.12i actually increase the PK value over 109 dBμV, i.e. no mitigation is achieved with these values of m.

As for the results when $\alpha = 25\%$ the results are shown in Figure 4.13. The limits covered for this spreading factor are between 43,750 Hz to 56,250 Hz. In these graphs, the cases from Figure 4.13a to Figure 4.13c show a good performance with a PK decrease of 102.06 dBμV, 103.96 dBμV and 104.15 dBμV

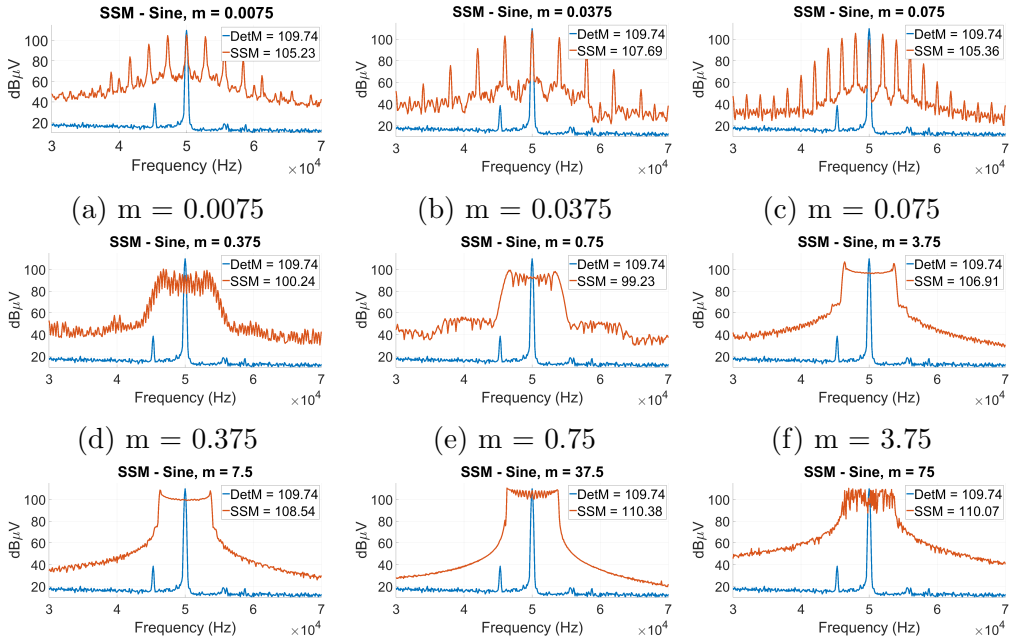

(a) m = 0.0075 (b) m = 0.0375 (c) m = 0.075

(d) m = 0.375 (e) m = 0.75 (f) m = 3.75

(g) m = 7.5 (h) m = 37.5 (i) m = 75

Figure 4.12: Spread spectrum Sine wave results for $\alpha = 15\%$.

respectively. It is in this value of α in which the mitigation effect is clearly seen even with lower values of m. The lowest PK values obtained can be seen in Figure 4.13d and Figure 4.13e. In fact, the value measured in Figure 4.13e represents the best reduction with a PK of 98.31 dBμV. Considering the remaining cases in Figure 4.13f, Figure 4.13g, Figure 4.13h and Figure 4.13i, it seems that using these modulation indices the effect of mitigation does not provide good results with values from 106.16 to 110.70 dBμV.

If the value of α is increased to 35%, the effect of mitigation can be seen in Figure 4.14 for all the modulation indices used, the frequency limits in this particular case are from 41,250 Hz to 58,750 Hz. In a similar way, the graphs from Figure 4.14a to Figure 4.14c, start to develop interesting values of PK mitigation but can not be considered as the best ones. The values obtained are 101.47 dBμV, 103.29 dBμV and 103.23 dBμV, respectively. The lowest values are shown in Figure 4.14d with a PK of 98.95 dBμV and Figure 4.14e 97.89 dBμV being the better optimisation cases. Considering the other values in Figure 4.14f and Figure 4.14g there is an interesting

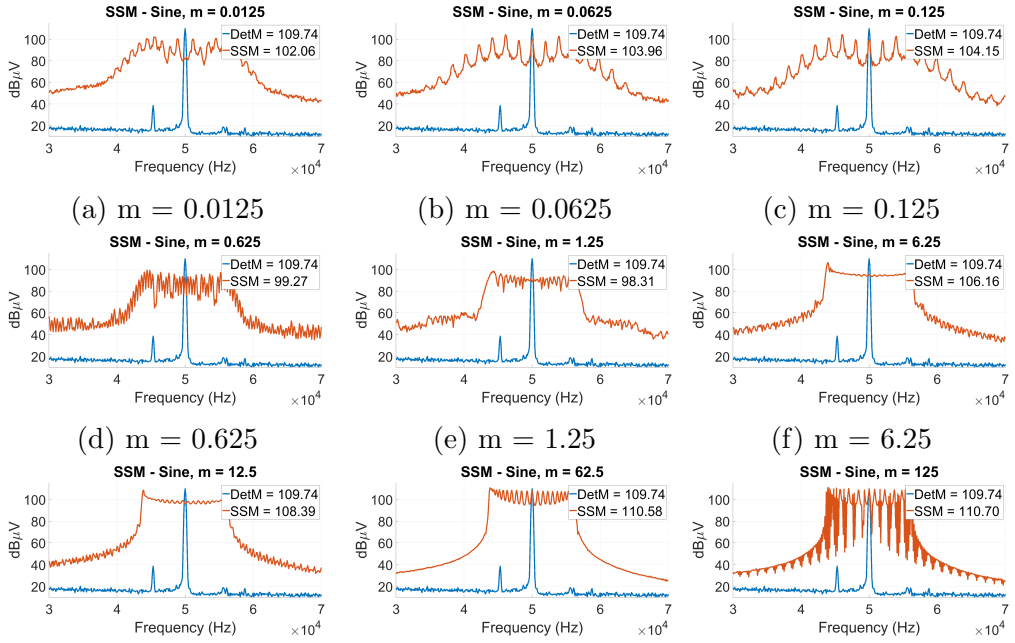

(a) m = 0.0125 (b) m = 0.0625 (c) m = 0.125

(d) m = 0.625 (e) m = 1.25 (f) m = 6.25

(g) m = 12.5 (h) m = 62.5 (i) m = 125

Figure 4.13: Spread spectrum Sine wave results for $\alpha = 25\%$.

mitigation of the PK magnitude but the limit of the demodulation from the EMI receiver point of view has been reduced with values of 105.88 dBμV and 108.75 dBμV.

Finally, the remaining cases that perform worse with regards to mitigation purposes are the ones with values of 111.27 dBμV and 111.07 dBμV for Figure 4.14h and Figure 4.14i.

The results obtained for $\alpha = 45\%$ are shown in Figure 4.15. There are interesting points to mention in this group of graphs. The limits for this experimental tests are 38,750 Hz to 61,250 Hz. The analysis of the results demonstrates that Figure 4.15a presents a good value for mitigation with a PK of 100.87 dBμV. The other cases shown from Figure 4.15b to Figure 4.15d present values between 98.79 dBμV and 102.81 dBμV. The best case for the Peak reduction can be seen in Figure 4.15e with a PK of 97.75 dBμV. Considering, Figure 4.15f and Figure 4.15g the peak change is going towards an increasing trend with values of 106.05 dBμV and 109.00 dBμV. The remaining cases shown in Figure 4.15h and Figure 4.15i

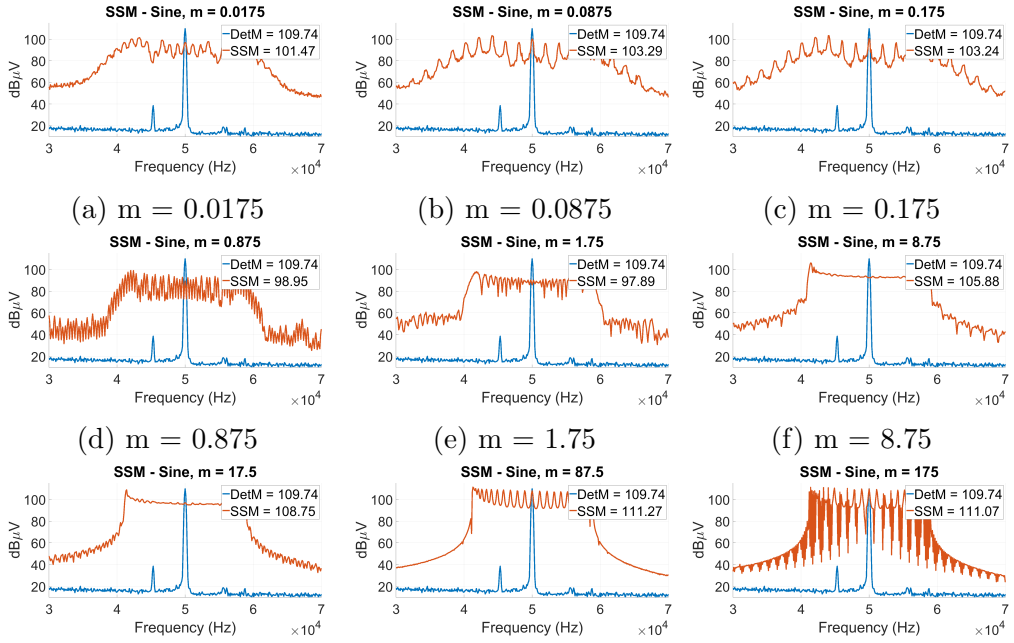

(a) m = 0.0175 (b) m = 0.0875 (c) m = 0.175

(d) m = 0.875 (e) m = 1.75 (f) m = 8.75

(g) m = 17.5 (h) m = 87.5 (i) m = 175

Figure 4.14: Spread spectrum Sine wave results for $\alpha = 35\%$.

develop worse scenarios for mitigation with PK values of 111.83 dBμV and 111.33 dBμV. In all of these pictures it can be seen how the spreading factor (α) affects the measured EMI peak value generated by the switching converter as well as the characteristic shape.

4.3.6 SSM Random Modulating Wave Signal

In this section the measured results for SSM driven by a linear random modulation signal are presented. In these graphs the different spreading factors of Table 4.2 are gathered for the effect of switching frequency harmonic mitigation. As was presented in the previous case for sine wave results, these graphs show the different results of changing the value α. What is interesting is the different shape generated with the exact same parameters.

The results when $\alpha = 5\%$ are shown in Figure 4.16. The limit considerations are the same as per the parameters used in the previous section when a sine wave was used. The bandwidth limits for this group of graphs are 48,750 Hz to 51,250 Hz. The cases from Figure 4.16a to Figure 4.16d

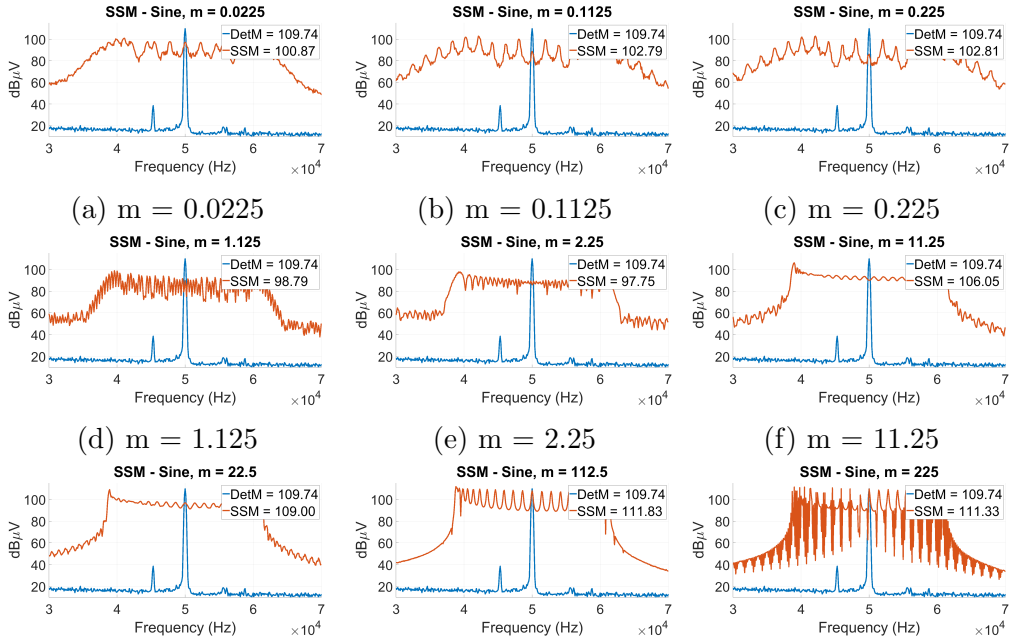

(a) m = 0.0225 (b) m = 0.1125 (c) m = 0.225

(d) m = 1.125 (e) m = 2.25 (f) m = 11.25

(g) m = 22.5 (h) m = 112.5 (i) m = 225

Figure 4.15: Spread spectrum Sine wave results for $\alpha = 45\%$.

show a very low value with regards to peak reduction, in fact all of these results present values close to 109 dBμV i.e. the DetM peak value used as a reference. For the graphs of Figure 4.16e and Figure 4.16f, it is difficult for the EMI receiver to demodulate the signal because small peaks appear in the signal obtained, the measured values are 108.40 dBμV and 107.42 dBμV, respectively. The best case for peak reduction purposes is when $m = 2.5$ shown in Figure 4.16g with a value of 107.03 dBμV. The remaining cases shown in Figure 4.16h and Figure 4.16i show very small values of mitigation but interestingly the shape looks squared due to the linear random distribution used.

The graphs measured when the value of α is then changed to 15% are shown in Figure 4.17. The limits are 46,250 Hz to 53,750 Hz. In these graphs Figure 4.17a, Figure 4.17b, and Figure 4.17c show PK values close to 107 dBμV. The cases presented in Figure 4.17d and Figure 4.17e show changes in the PK with a trend of flattening the peak shape. It is worth noting the lowest value of peak reduction when $m = 3.75$ presented in

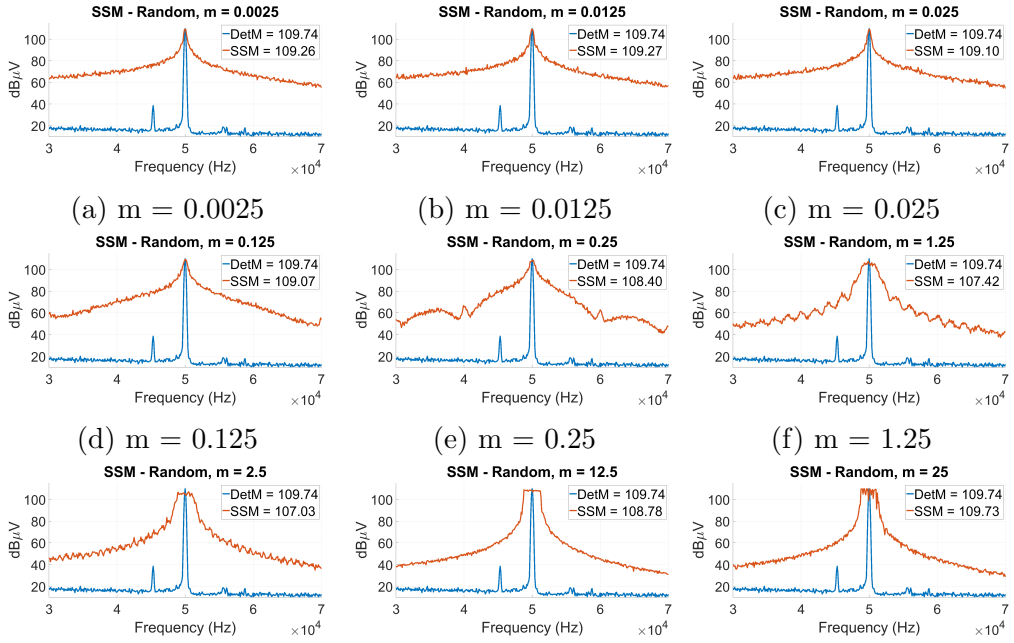

(a) m = 0.0025 (b) m = 0.0125 (c) m = 0.025

(d) m = 0.125 (e) m = 0.25 (f) m = 1.25

(g) m = 2.5 (h) m = 12.5 (i) m = 25

Figure 4.16: Spread spectrum Random wave results for $\alpha = 5\%$.

Figure 4.17f. The remaining values shown in Figure 4.17g, Figure 4.17h and Figure 4.17i develop a squared shaped (due to the linear distribution chosen) with almost no mitigation and the latter even increases the magnitude of interference with a value of 110.20 dBμV.

For a spreading factor of 25%, the graphs obtained are shown in Figure 4.18. There is a low peak reduction effect for Figure 4.18a, Figure 4.18b, and Figure 4.18c with PK values of 104.44 dBμV, 104.66 dBμV and 105.31 dBμV. The best modulation cases are presented in Figure 4.18d and Figure 4.18e when the PK values are 101.60 dBμV and 101.32 dBμV. After using these values of m the trend of mitigation develops higher PK values such as 103.75 dBμV and 104.52 dBμV for the cases presented in Figure 4.18f and Figure 4.18g. Finally, the cases with poor mitigation and even worse performance are show in Figure 4.18h and Figure 4.18i.

When the value of alpha is 35%, the mitigation effects are clearly seen. For Figure 4.19a, Figure 4.19b and Figure 4.19c, the values of PK measured are 103.58 dBμV for $m = 0.0125$, 103.80 dBμV for $m = 0.0125$ and 103.64 dBμV

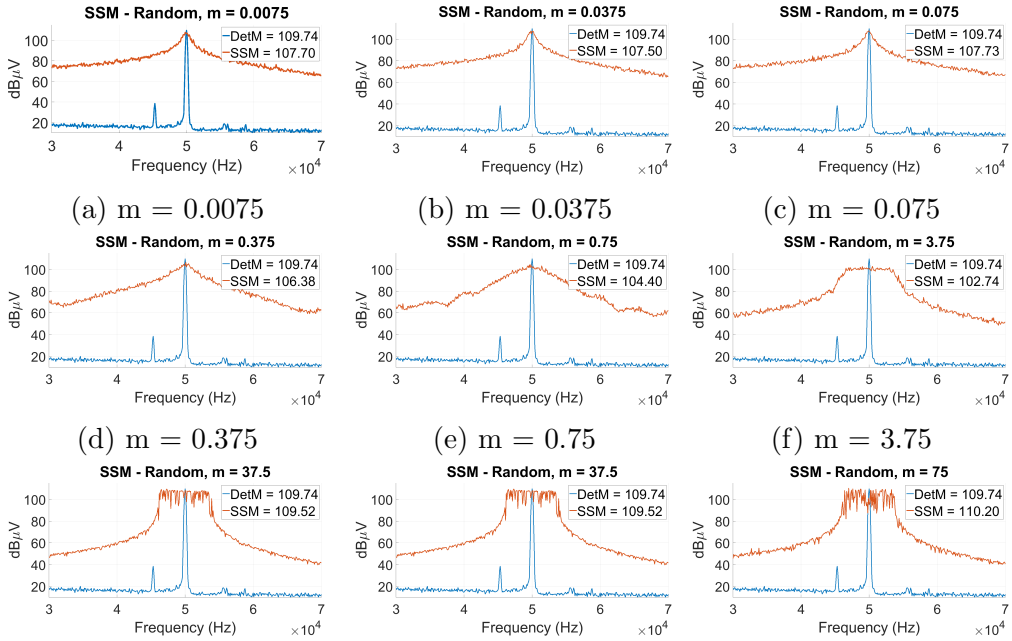

(a) m = 0.0075 (b) m = 0.0375 (c) m = 0.075

(d) m = 0.375 (e) m = 0.75 (f) m = 3.75

(g) m = 7.5 (h) m = 37.5 (i) m = 75

Figure 4.17: Spread spectrum Random wave results for $\alpha = 15\%$.

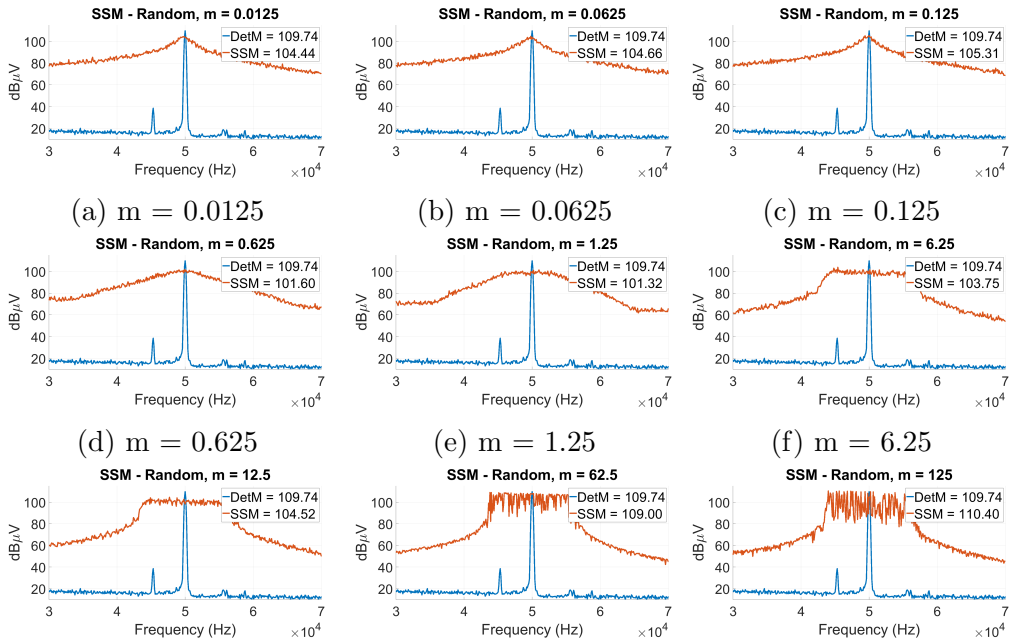

(a) m = 0.0125 (b) m = 0.0625 (c) m = 0.125

(d) m = 0.625 (e) m = 1.25 (f) m = 6.25

(g) m = 12.5 (h) m = 62.5 (i) m = 125

Figure 4.18: Spread spectrum Random wave results for $\alpha = 25\%$.

for $m = 0.175$. The graphs in Figure 4.19d and Figure 4.19e show the best options for peak reduction. In fact the latter develops a mitigation PK value of 99.85 dBμV. As for the other cases shown in Figure 4.19f and Figure 4.19g the values between them are 103 dBμV with a peak square shaped. The remaining cases in Figure 4.19h and Figure 4.19i increase the PK value close to the DetM case, which presents a problem for the mitigation purposes.

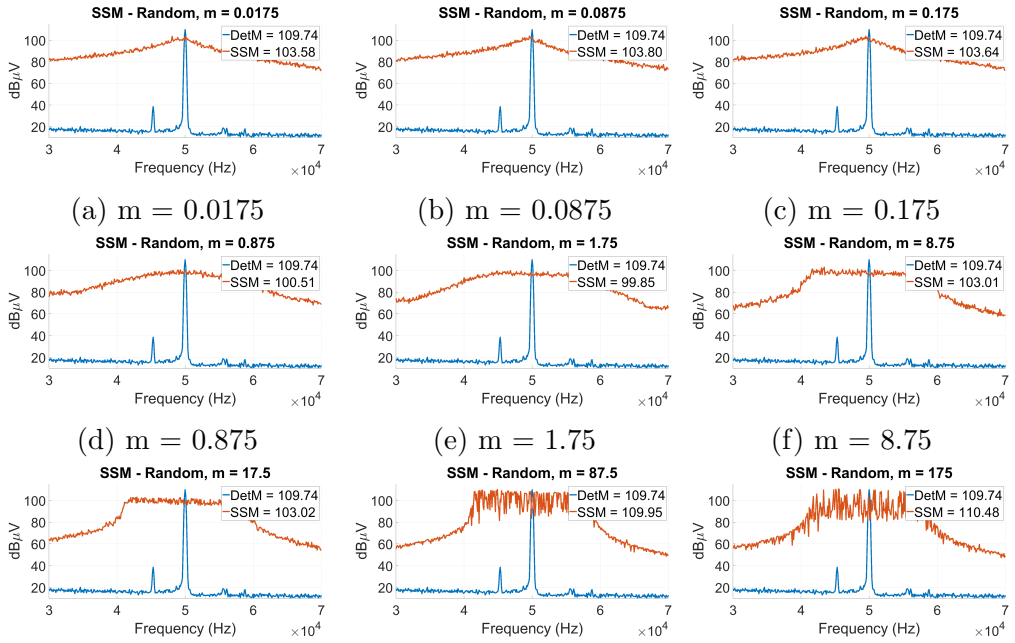

(a) m = 0.0175 (b) m = 0.0875 (c) m = 0.175

(d) m = 0.875 (e) m = 1.75 (f) m = 8.75

(g) m = 17.5 (h) m = 87.5 (i) m = 175

Figure 4.19: Spread spectrum Random wave results for $\alpha = 35\%$.

The highest value of α used is 45%, the graphs obtained are shown in Figure 4.20, in similar manner as presented in the previous cases with a lower value of α. For Figure 4.20a, Figure 4.20b and Figure 4.20c, the mitigation achieved is considerable with values of 101.34 dBμV, 101.58 dBμV and 102.03 dBμV. The best cases to mitigate the effect of the switching frequency are in Figure 4.20d when m = 1.125, and Figure 4.20e when m = 2.25. The PK value increases again in Figure 4.20f and Figure 4.20g with values of 102.40 dBμV and 104.35 dBμV. Finally, in Figure 4.20h and Figure 4.20i the peak reductions are not effective with even worse values of 110.05 dBμV and 111.44 dBμV for the PK values measured.

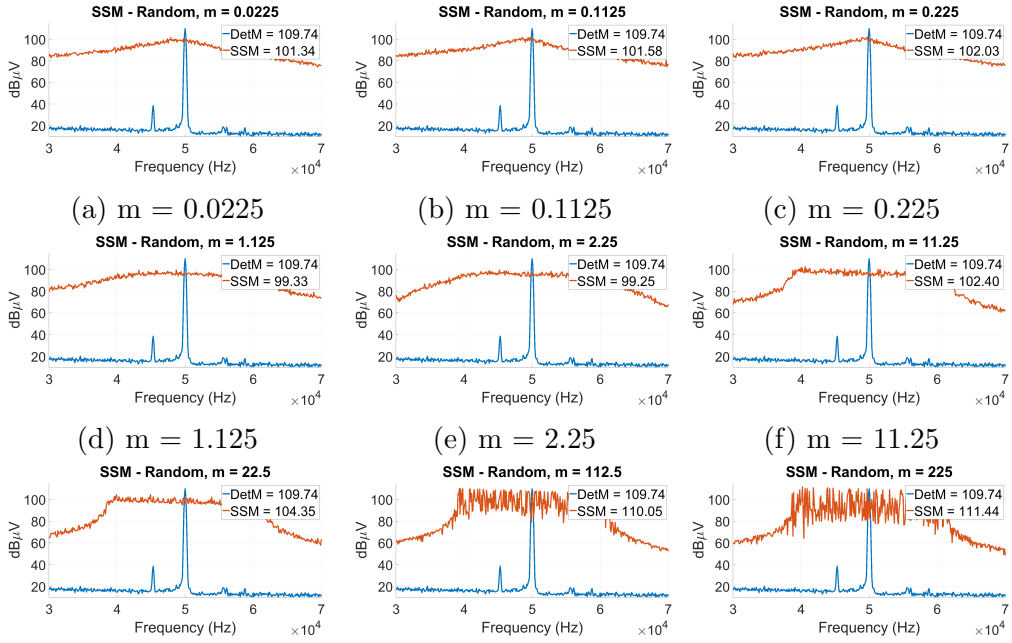

(a) m = 0.0225 (b) m = 0.1125 (c) m = 0.225

(d) m = 1.125 (e) m = 2.25 (f) m = 11.25

(g) m = 22.5 (h) m = 112.5 (i) m = 225

Figure 4.20: Spread spectrum Random wave results for $\alpha = 45\%$.

From the results obtained when the two different signals are used, the Sine wave and Linear Random modulating signals. It can be concluded that, when peaks are generated close to the carrier frequency the signal may not be able to be demodulated by the measurement device. In addition, a clean and steady signal might not be the best in terms of reducing peak values. Another important point to mention is the modulation indices that are close to one ($m = 1$) as shown in the graphs presented, lower or higher values appear to be good choices to achieve a reduction of the peak. Considering the comparison of both signals analysed (sine and random), the two of them perform in a similar way in many cases. In the case of a random signal, the higher the modulation index value the more square the shape of the signal in FD. This means that the spectrum can be shaped accordingly to the random distribution used along with the change in the modulation index.

4.4 Importance of the Modulating Signal and the Spreading Factor

In order to gather all the measurements carried out to determine the best possible operating point to reduce the effect of the switching frequency of the DC-DC converter driven by SSM, a multivariable graph considering the important parameters (α, F_m and PK value) has been plotted for both cases, the Sine and the Random wave modulating signals. After considering the parameters used, a heatmap seems to sum up all the information of the measurements obtained from the EMI Receiver. This graph, provides a two dimensional and interesting way to find similarities and differences when analysing Sine and Random modulating signals.

This graph is generated with the help of two main algorithms. Initially an algorithm was developed to find the peaks located in the Carson's band for the first switching harmonic.

Secondly, with the peaks obtained at the different modulation indices a cubic interpolation algorithm is used to interpolated between these values. With the complete values (α and F_s) the heatmap is generated considering all the data. These considerations can be seen in the Flowchart in Figure 4.21.

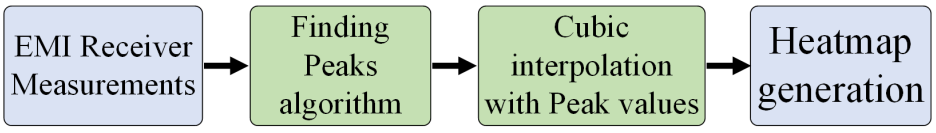

Figure 4.21: Heatmap generation flowchart for the driving signals used, green blocks show functions while blue blocks show input/output.

With the heatmaps generated as shown in Figure 4.22 and Figure 4.22, the analysis to find the best mitigation points is carried out. By a simple observation, the lowest PK values of mitigation are obtained when the colour bar at the right develops to dark blue. This happens when the Sampling

Time is 10^{-4} s, however this zone shows two main limits as highlighted by the red dots which are $Ts = 203$ μs and $Ts = 102$ μS (in Figure 4.22 and Figure 4.22).

The calculation of the modulation index (if needed) for this band will rely on the same Equation in 4.6, however the Sampling Frequency must be used instead of the Sampling Time. The equation showing this can be seen in (4.6), as follows.

$$m = \frac{(\alpha \cdot F_c)/2}{(1/T_s)}, \tag{4.6}$$

The use of these heatmaps will provide an understanding about the best points to obtain a good mitigation of EMI with regards to the Sampling Time (or Sampling Frequency) according to different Modulation Indices.

Sine Wave Modulating Signal

The heatmap for the Sine wave modulating signal is shown in Figure 4.22.

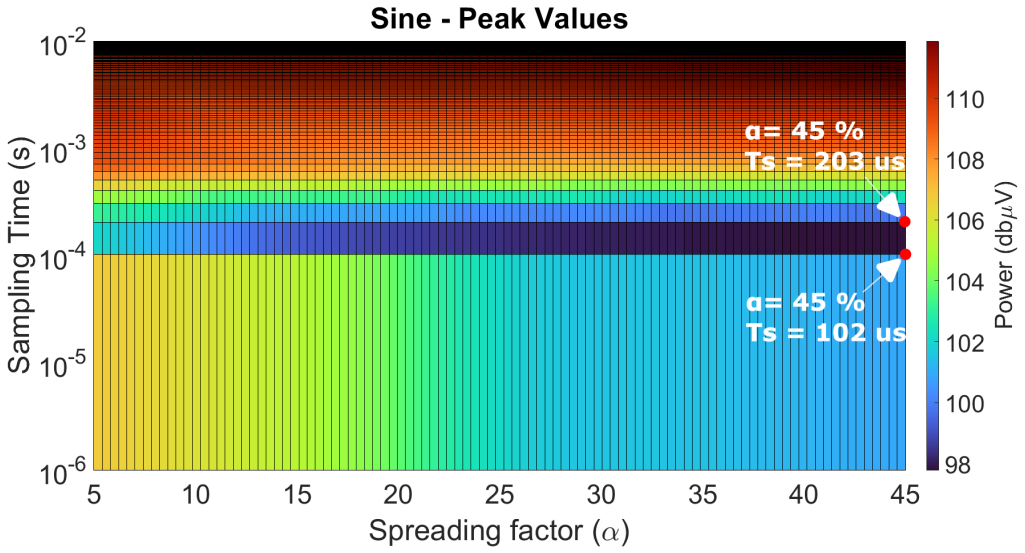

Figure 4.22: Spread Spectrum heatmap for a sine wave signal highlighting the best mitigation zone of Sampling Time.

Random Wave Modulating Signal

The heatmap for the Random wave modulating signal can be seen in Figure 4.23.

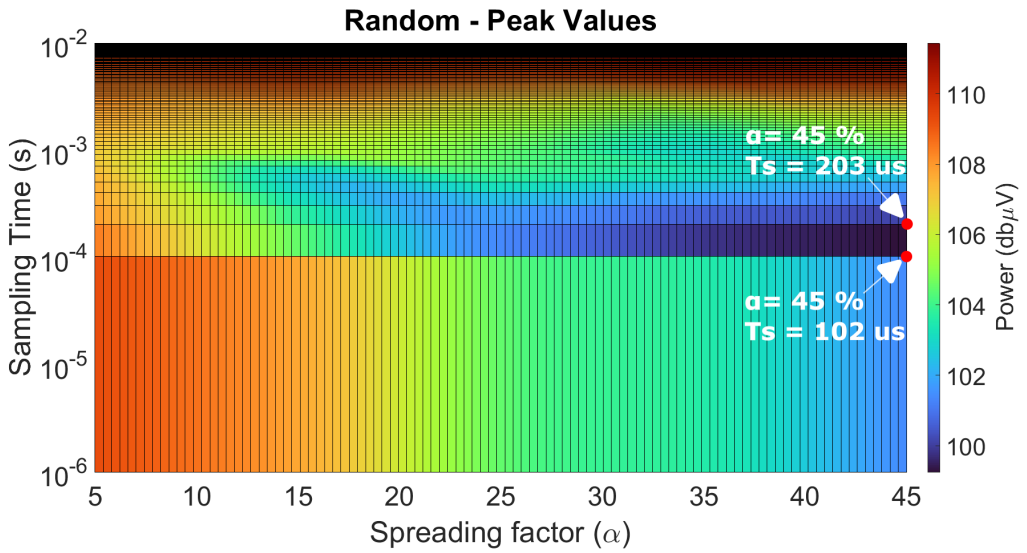

Figure 4.23: Spread Spectrum heatmap for a random wave signal highlighting the best mitigation zone of Sampling Time.

Having considered the highlighted points in both heatmaps, Table 4.3 shows the obtained lowest and highest modulation indices with the value of the PK decrease. With the help of this graphical resource, it seems that the modulation indices have to increase according to the spreading factor used, however the Sampling Time can be kept close to 10^{-4} s or 10 kHz (Sampling Frequency).

Table 4.3: Heatmap Sine/Random wave points of interest for best EMI mitigation.

α (%)	**m: Low Limit (102 μs)**	**m: High limit (203 μs)**	**Sine Low** PK **(dBμV)**	**Sine High** PK **(dBμV)**	**Random Low** PK **(dBμV)**	**Random High** PK **(dBμV)**
5	0.1275	0.25375	102.044	103.166	108.376	107.864
15	0.3825	0.76125	99.2316	101.037	104.348	103.698
25	0.6375	1.26875	98.3269	100.234	101.297	101.688
35	0.8925	1.77625	97.9238	99.842	99.8607	100.603
45	1.1475	2.28375	97.786	99.9357	99.2547	100.106

Important observations can be discussed in the generation of the heatmaps for different spreading factors as well considering Table 4.3 as a supporting resource.

- For modulation indices when the Sampling Time is 102 μs better mitigation PK values are obtained when compared to the higher limit of Sampling Time given by 203 μs. This provides the best mitigation zone for the Switching Frequency used as well as the modulation indices related to it. An example of this is the extreme case of $\alpha = 45\%$ which decreases the PK interference to a value of 97.78 dBμV for a Sine wave and to 99.2547 dBμV for a Random wave.

- The use of a Sine wave as a modulating signal shows consistent and smooth behaviour in the Sampling Ratio region approximately between 10^{-4} s to 20^{-4} s, this applies for most of the points from $\alpha = 5\%$ to 45 %. On the other hand, the Random modulating signal starts to decrease the value close to 10^{-4} s with spreading factor between 15 % and 20 %.

- The Random modulating profile seems to work better over a limited range of spreading factors (from 35 % to 45 %) with a Sampling Ratio between (10^{-4} s to 20^{-4} s) when the dark blue colour remains consistently. The mitigation is very low if the same zone is considered at lower values of spreading factor (from 5 % to 25 %).

4.4.1 EMI Modulation Index Graphs

Finally, to demonstrate the complete effect for the SSM mitigation technique, a study based only on the modulation index has been carried out considering the graph and results in Section 4.3.5 and 4.3.6.

The modulation index indicates how close a signal is modulated close to the non-modulated case i.e. how steady a signal is according to the carrier signal. To support the usage of SSM to find the best mitigation point, a graph is plotted comparing both modulating signals with the exact same parameters. The results obtained from all of the different spreading factors

and different modulation indices are shown in Figure 4.24.

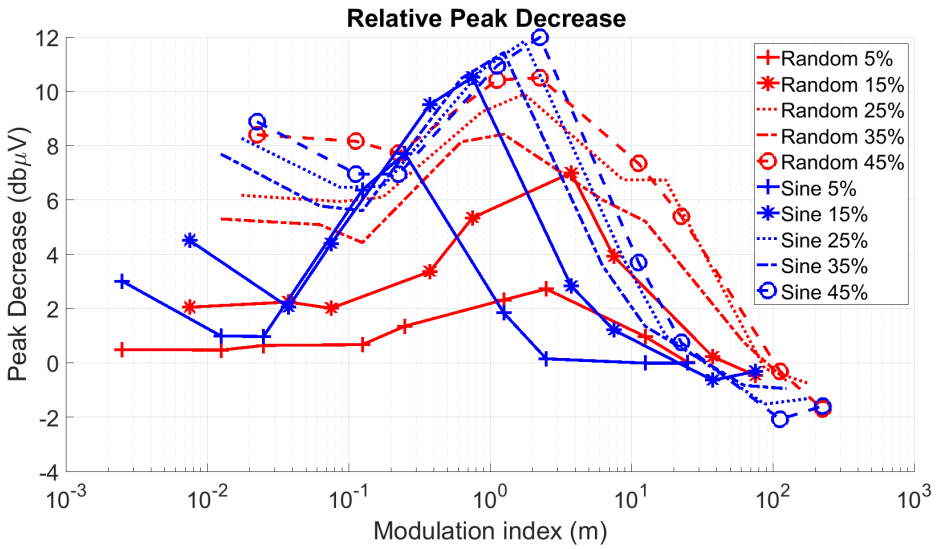

Figure 4.24: Relative Peak Decrease for different spreading factors and different modulation indices (higher is better).

In Figure 4.24, the expected results of increasing the spreading factor will decrease the PK value measured. However, there are interesting cases in which Random and Sine driving signals will perform in a similar manner, when the modulation index is near one (or 10^0 in Figure 4.24). This applies slightly differently for the five cases of α presented but it does happen, especially for higher spreading factors.

It should be mentioned that the lower the modulation index the lower the best mitigation is. This presents a good challenge for designers and EMC compatibility researchers to find the best mitigation point for a particular application.

This section has presented a comprehensive procedure for analysing two different Spread Spectrum modulating signals in order to understand the nature of the EMI generated. This process was carried out by employing the heatmaps which are an interesting graphical resource to demonstrate the regions in which SSM will create the best peak reduction compared to DetM. In addition, the importance of the modulation index has been highlighted and it can be concluded that there exists an optimum point for

peak reduction with regards to the frequency domain measurements.

4.5 Chapter Conclusion

This chapter has provided the technical and theoretical background of CISPR-16 band A for measuring and accounting for the effects of SSM for a buck converter.

The measured results from the EMI Receiver have shown that there exists one point (values close to $m = 1$) where the best optimisation point can be achieved in the low frequency band of CISPR-16. However this point tends to change with the spreading factor as seen in Table 4.2. This conclusion is helpful for EMI design engineers to account for the modulation cases that do not impact the performance of the converter in the frequency domain for the CISPR Band A under test.

An important point worth noting is given by the similarities in the demodulating process of the signals used and compared against. For the higher modulation indices both signals generated some undesired spikes, this is mainly caused by the frequency used of the modulating signal.

Another important point is given by the similarities in the measured results when both signals are compared (sine and random). However they tend to develop in a similar manner: this is mainly caused by the use of a fixed clocked generator which is inherently to the microcontroller used.

An interesting conclusion that can be considered is that when a random clocking method is used to generate random switching frequencies for the Spread Spectrum modulation technique, it performs similar to a sine wave approach as the clocking circuit used for the SSM generation is the same for both approaches. However the floor noise is increased between the minimum and maximum limits given by α.

Chapter 5

BER Measurements in the Presence of a Spread Spectrum Modulated Converter

In this chapter an analysis of a communication link under the interference of a DC converter controlled using the SSM modulation techniques is presented. The important task is to determine experimentally the effects of using SSM as a mitigation technique when the noise is superimposed on a digital communication signal to determine the Bit Error Rate (BER) created.

5.1 SSM Interference and its Relation to BER

To support the experimental work carried out in this chapter similar research has been surveyed. In work presented in [91] and [92] a communication channel is interfered by a controlled noise in a Crosstalk environment. The communication channels are tested using similar interference sources demonstrating that DC converters which use SSM techniques can be harmful for the devices close it.

In [91], the BER measured for a communication system in the presence of the interference generated by a converter is analysed. The coupling method uses a two-layer Printed Circuit Board (PCB) in which the traces are close to each other to generate interference between both lines. This configuration presents a Crosstalk case from which the experimental tests in this research work are based. As was explained in Chapter 2, Crosstalk takes places when two conductors are close together and one conductor has the capability to interfere with the second conductor. Similar effects are found in automotive grids and smarts grids considering the amount of cables without shielding and even in PCB routes.

In [92], the research focus was based on a standardised communication (I2C) link to determine the effect of Spread Spectrum modulation. This research demonstrated the increase of the BER for different spreading factors for the switching frequency of the DC converter.

The topic of interference in communication is considered in [93]. In this research an analysis is made of the PLC channel performance when a converter with Spread Spectrum modulation is used with a carrier frequency of 63 kHz. The coupling method is based on a capacitive link which can be considered as Intentional Electromagnetic Interference (IEMI). This work showed a decrease of the EMI generated from the converter side whilst at the same time it increased the BER on the PLC communication link

This chapter shows experimentally what is the real effect of the two SSM modulation techniques developed from Chapter 3 to Chapter 4. The analysis considers the same theoretical background and values with regards to the main parameters of SSM such as Spreading Factor, Modulating Signal Frequency and Modulation Index. To determine these effects a Crosstalk-based experimental set-up is proposed to investigate these effects and statistical analyses are made to determine the advantages and disadvantages of SSM under different circumstances. The first study provides a simple

but interesting statistical test to measure the BER for different spreading factors by using Boxplots. The relationship of BER and PK measurements obtained in Chapter 4 are considered to calculate Relative Values (with DetM as the reference case) to investigate the correlation of variables. This chapter then proposes a time domain analysis using BER as the main value of interest in order to analyse when these SSM techniques are used to improve the frequency domain characteristics and, the consequences for the time domain measurements. Having considering this important point, the combined effort is then focused on generating a rule of thumb to address both domains when SSM is applied to a power converter.

5.2 Figure of Merit: BER

The reliability of a communication channel, for digital purposes is often tested by measuring the BER. This parameter is a good indicator of the susceptibility of a communication link against external interference and undesired effects generated by different devices.

The device used to measure BER is often called the Bit Error Rate Tester (BERT), which transmits bits from its output and receives data bits at its input for comparison. The bits are generated with the use of Linear Feedback Shift Registers (LFSR). The voltage levels can be different from one system to another but the main idea of the comparison remains the same. Fundamentally, Bit Error Rate is calculated as (5.1),

$$BER = \frac{N_{err}}{N_{bits}} \tag{5.1}$$

Considering that the equipment is capable of handling high frequency bit counting, one important parameter is the measurement period. This value will provide reliability for the BER measurement in case of reproducing the results in similar conditions with similar equipment. In addition, it helps

to align measuring devices and protocols. To account for a reproducible Bit Error Rate measurement, the Confidence Level (CL) index can be implemented. This index should consider the period for a measurement and what BER value can be tolerated by the communication system.

In [94], different communication channels are shown with regards to the allowable limits of the BER, Table 5.1 shows these parameters and information about each communication channel. Different values of CL are presented for five different communication protocols to define a common time to determine the BER.

Table 5.1: Standard confidence levels at 95% for different communication protocols.

CL	**PCI Express 5 Gb/s NRZ**	**PCI Express 16 Gb/s NRZ**	**IEEE 802.3 j25.78125 Gb/s NRZ**	**IEEE 802.3 bs 26.5625 Gbd PAM4**	**IEEE 802.3 bs 26.5625 Gbd PAM4**
1.0E-15	$\sim$ 165 hrs	$\sim$ 51 hrs	$\sim$ 32 hrs	$\sim$ 31 hrs	$\sim$ 16 hrs
1.0E-12	$\sim$ 10 min	$\sim$ 3.1 min	$\sim$ 1.9 min	$\sim$ 1.9 min	$\sim$ 1 min
1.0E-09	$\sim$ 59 secs	$\sim$ 19 secs	$\sim$ 12 secs	$\sim$ 11 secs	$\sim$ 6 secs
1.0E-06	$\sim$ 2 µsec	$\sim$ 0.7 µsec	$\sim$ 0.4 µsec	$\sim$ 0.4 µsec	$\sim$ 0.2 µsec

By defining the CL value, a comparison of different tests for protocols can be achieved with a common point for understanding the Bit Error Rate created by frequency modulated DC converters acting as EMI sources. The equation for the Confidence Level (CL) is given in (5.2),

$$CL = 1 - e^{-N_{bits} x BER_s} \tag{5.2}$$

where, N_{bits} is the total bits transmitted, and BER_s is the maximum allowed BER for the test (usually provided as one standard value). N_{bits} can be calculated as,

$$N_{bits} = \frac{-\ln(1 - CL)}{BER} \tag{5.3}$$

and the time period needed to achieve a given CL, can be derived as:

$$Time(s) = \frac{-\ln(1 - CL)}{BER * BitRate} \tag{5.4}$$

These expressions are used to consider the maximum value of BER allowed on a system with a desired maximum Bit Error Rate over a certain time period.

The parameters for the BER experimental tests described in this thesis are given in Table 5.2. A value of 95 % has been used in this test for the Confidence Level as it is an industry standard rule of thumb [94].

Table 5.2: BER Confidence Level for 500 kHz.

Parameter	**Value**
Ber_{max}	1e-10
Bit Ratio	1e9
CL	95 %

With these parameters a time period of 30 seconds has been obtained, the frequency of the BER tester has been set at 500 kHz which is then translated into a value of 1 Mbit/s. This Sampling Rate for the BER is sufficient for the 50 kHz used for the Switching Frequency of the converter considering the sampling theorem for signal analysis.

In this section a brief introduction to the Confidence Level parameter as a rule for measuring the quality of a communication channel was explained. It is important to account for a value that provides a good agreement in the measuring process as was suggested in Chapter III and Chapter IV with regards to the recorded time (resolution time) to calculate the spectra of a signal from a time domain signal. It has also been shown about other standardised communications protocols with regards to the allowed number of errors and their most common confidence levels to have an initial idea of the experiment in this chapter.

5.3 BER Measurement Set-up

The measurement test set-up aims to measure Crosstalk, as was mentioned in previous section. This is a basic concept used in EMI theory. It is mainly based on the situation when two conductors interfere each other. For the purpose of the thesis, three conductors are used.

For this set-up, the EMI receiver and the LISN are not required since the analysis is purely focused on the time domain effect seen in the communication channel generated by the Crosstalk between lines. The equipment is based on the power supply, the cable bundle, the Bit Error Rate tester and the DC-DC converter. This set-up is based on a Crosstalk environment in which the cable bundle includes an EMI Source cable and one EMI Victim cable. The block diagram of the set-up is shown in Figure 5.1. The same bundle structure has been used in [43] to demonstrate the adverse effect of a Square Fourier Series wave and the BER effect.

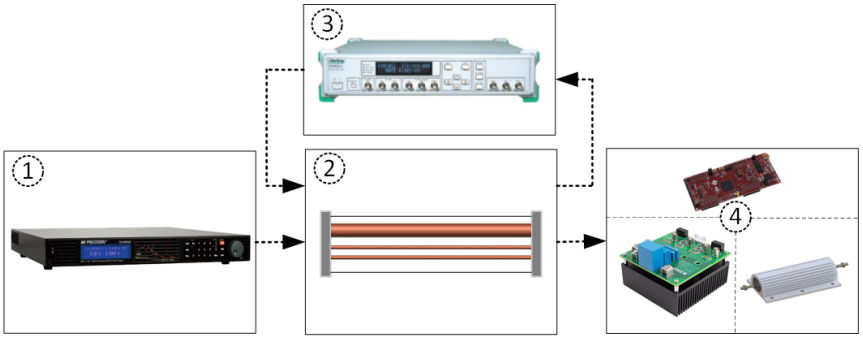

Figure 5.1: Experimental setup for the Bit Error Rate measurements.

A brief explanation of the equipment involved is now given:

1. **Power Supply.** The Power Supply is the same as used in the Frequency Domain experimental test set-up.

2. **Cable bundle.** The cable bundle generates a Crosstalk effect between the cables involved. The cable bundle has 3 conductors: two are AWG-36 and they are used for the BER tester data transmission (Data and

Data Ground). The other is AWG-14: this is used for the input voltage of the DC-DC converter. By having this cable arrangement, the switching behaviour of the converter modulation will have an interfering effect in the Data Lines, and errors will be generated. The main parameters of the cable bundle can be found in Table 5.3. These parameters were chosen because this research follows previous research carried out in the laboratory. For convenience, it was then decided to continue with the same set-up.

Table 5.3: Cable Bundle Parameters.

Parameter	**Value**
Distance between cables	1 cm
Height of cables	3 cm
Length of bundle	1.5 m
Cable connections	SMA

The termination of the cable bundle (input of the BER tester), includes a 50 Ω load to match the impedances of the BER tester input by providing signal stability.

3. **BER Tester** The Bit Error Rate Tester (BERT) is an Anritsu BERT MP8302A [95]. This equipment can generate data with a bit ratio from 1 kHz to 155 MHz. The waveform used is a TTL signal modulated as a Non-Return to Zero (NRZ). For the purposes of this work, the frequency has been set at 500 kHz (10 times the switching frequency to comply with Nyquist Shannon theorem). The BERT is programmed as an automated device to get measurements at every desired time. A program routine created in LabView is in charge of sending the control signals over a Serial Communication protocol to get accurate measurements without human intervention.

4. **DC Converter.** The DC-DC converter is the same as that used previously, with the same components and the same switching frequency

parameters. However, the output load has been changed to 4.7 Ω to generate a higher load current which is directly translated into an stronger electromagnetic field in the power cable.

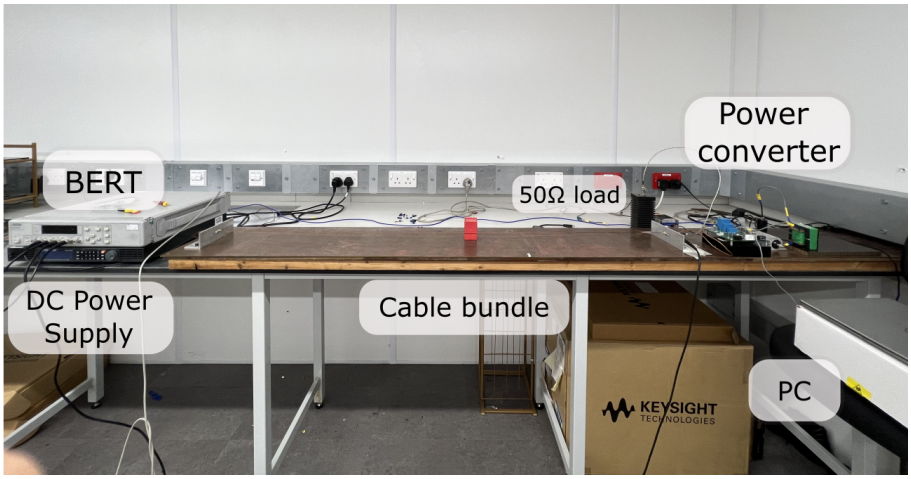

Figure 5.2: BER experimental test set-up.

5.3.1 Automated BER Measurements

To control every step of the measuring procedure for the BERT a repetitive but programmable routine was developed in Labview [96]. This program requires input parameters to generate the measurements of the BER. In addition, it can control the voltage of the power supply but this has been kept fixed for the purposes of this chapter. A flowchart with the three important tasks of the program is shown in Figure 5.3 followed by a complete explanation of the signals. The Labview block diagram can be found in Appendix F.

- a) Number of voltages (No_Volt). This defines the number of voltages to measure. This parameter controls the maximum count to be reached for directly controlling the power supply. For this specific case it is not used.

- b) Input voltage (Input_voltage). This defines the starting value of the voltage for the power supply. For the measurements carried out in this

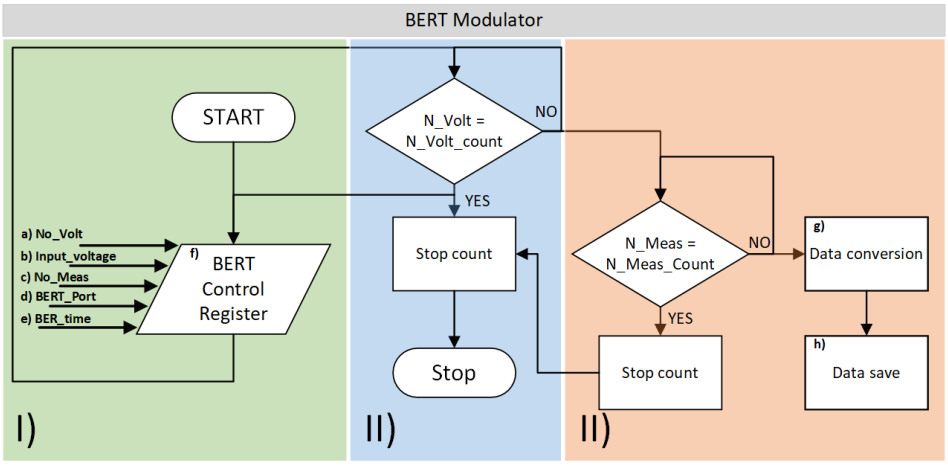

Figure 5.3: Programmed flowchart block in Labview for the control of the BERT.

chapter a value of 60 V has been programmed as can be considered a standard value used in DC grids.

- c) Number of measurements (No_Meas). This value defines the number of times a measurement with the same voltage has to be obtained. For the measurement purposes in this chapter a value of 100 has been used. This value was decided to provide a good statistical agreement while getting the average of the total measurements.

- d) Anritsu MP8320A Port (BERT_Port). This parameter defines the Serial Port to be used by the BERT and allows the Labview interface to control the equipment.

- e) Time for BER (BER_Time). An important parameter to determine the effect of the interference over a desired time. The BERT program is ready to measure any time in a minute time base, for the following tests a value of 0.5 min (30 seconds) is used. After several experimental tests this value provided stability in the parameter measured from the BER tester.

- f) BERT Control Register. In this block all the registers to control

the main parameters of the BERT are programmed. In this block it is possible to change the data type, frequency of data, etc.

- g) Data conversion. The measured values from the BERT are obtained and converted from text to decimal.

- h) Data save. In this part the data converted is transferred to the txt file generated.

Having considered the inputs and outputs of the program in Labview, the front panel is shown in Figure 5.4.

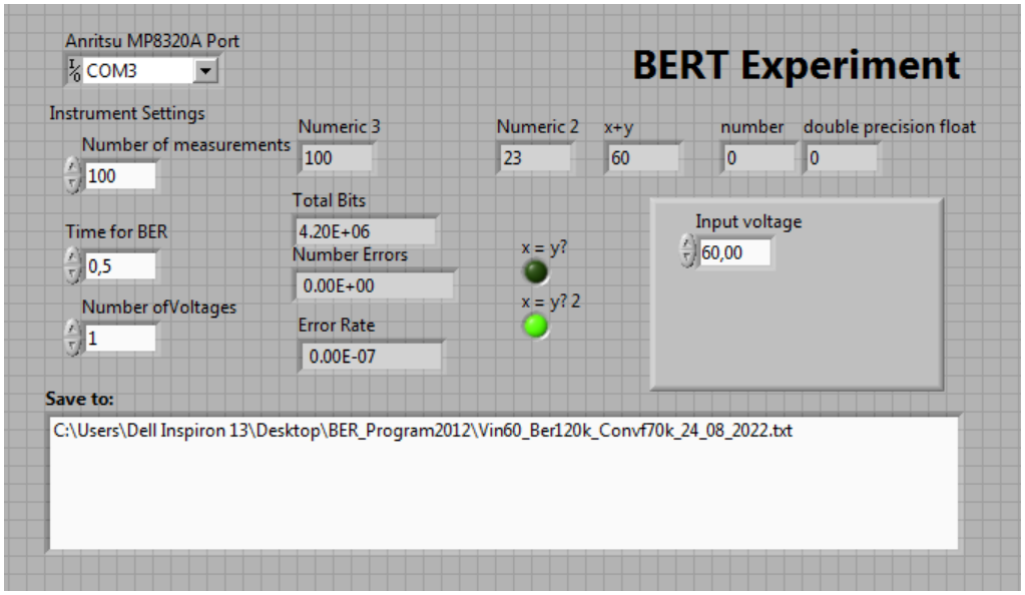

Figure 5.4: Labview front panel for controlling the BERT over a serial communication link.

This section has provided the explanation of the equipment under use. It is important to notice the parameters used that refer to the Confidence Level that defined the required time for measurement. Due to the large time to be used for the measurements, an automated process was carried out to measure and save at the same time using Labview.

5.4 BER Analysis for Driving Signals

In this section the results for a Sine and a Random wave modulating signal are shown. Five different spreading factors are considered, 5 %, 15 %, 25 %, 35 % and 45 % for the nine values of modulating signal frequency as was presented in Table 4.2. It is worth mentioning the BER value obtained for a Deterministic Modulation case which was $6.148 * 10^{-4}$ as a comparison point. Due to the nature of the BER (adimensional) there are no units in this measurement. All the graphs have been plotted by using the free downloadable plotting toolbox "Gramm" which can be found in [97]

The graphs given are based on Boxplots. This graphical resource is a good way to demonstrate a good number of statistical values of a sample under analysis. The Boxplots show the average value of the measurement at the centre of the box as a line, the quantile extremes limiting the box upper and lower sides. The values that represent statistical inconsistencies are shown by dots and are referred to as outliers. These values are indeed part of the data, but they do not take part of useful data since they can distort the overall distribution.

1. BER with $\alpha = 5$ %. In Figure 5.5 it can be seen that increasing the modulation index (m) has a very low impact for the Random signal (red) and the Sine signal (green). It can also be seen that when the modulation indices are less than 1 the difference is noticeable. This trend changes when the modulation index is increased to values bigger than 1. The two modulating signals perform almost identically with a BER value close to the deterministic modulation case from $4.0 * 10^{-4}$ to $6.7 * 10^{-4}$.

   In this first case of $\alpha = 5\%$ it can be concluded that the percentage of spreading is very low and will create similar values of BER as the deterministic case. Moreover, it seems that a considerable level of

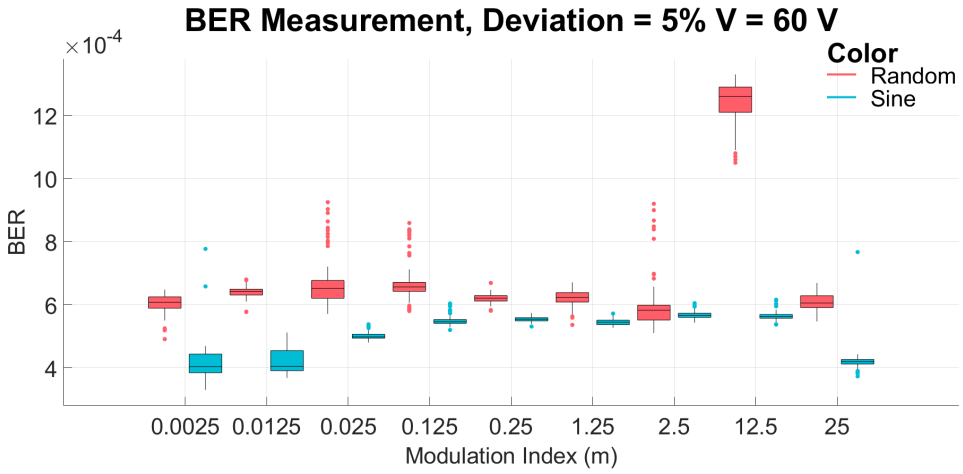

Figure 5.5: BER values for $\alpha = 5\%$ and different modulation indices.

outliers have been obtained in the Random results when compared to the Sine results.

2. BER with $\alpha = 15\ \%$. It can be seen in Figure 5.6 that the modulation index does not have a considerable impact when the two modulating signals are compared. However, the change from $\alpha = 5\%$ to $\alpha = 15\%$ is considerable. The BER values change almost one order of magnitude which is a big difference from the BER obtained in the previous case.

   The comparison of the performance for both signals is close to $1 * 10^{-3}$ and decreases with higher values for the modulation index. The BER value seems to be steady over the whole modulating index range proposed within the limits from $0.5 * 10^{-3}$ to $1 * 10^{-3}$.

3. BER with $\alpha = 25\ \%$, in Figure 5.7 is where the effect of the spreading factor with regards to the BER value starts to change when different modulating signals are used. It can be seen that the modulation index values below 1.25 generate a large difference in the BER measurement when the Random signal is used compared to the Sine wave modulating values that remain steady for the whole test with a BER between $1*10^{-3}$ to $2*10^{-3}$. In this graph it can be concluded that random and

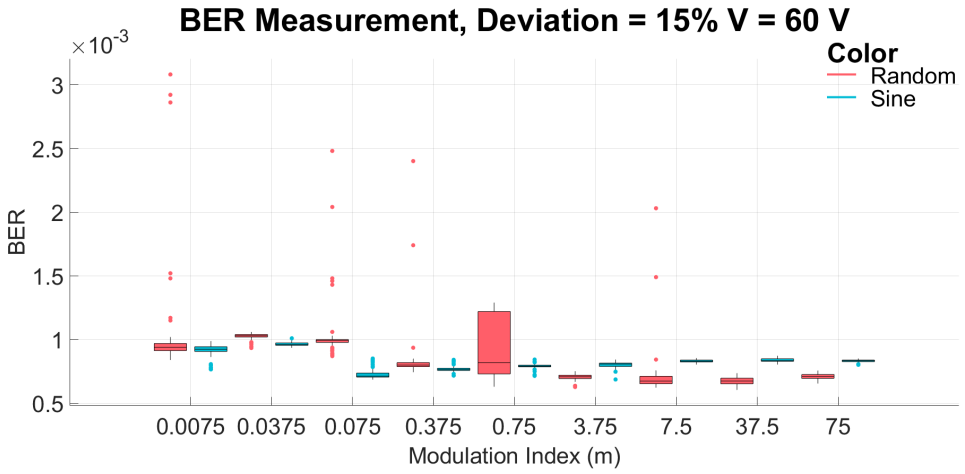

Figure 5.6: BER values for $\alpha = 15\%$ and different modulation indices.

sine wave modulating signals start to perform differently according to the chosen parameters.

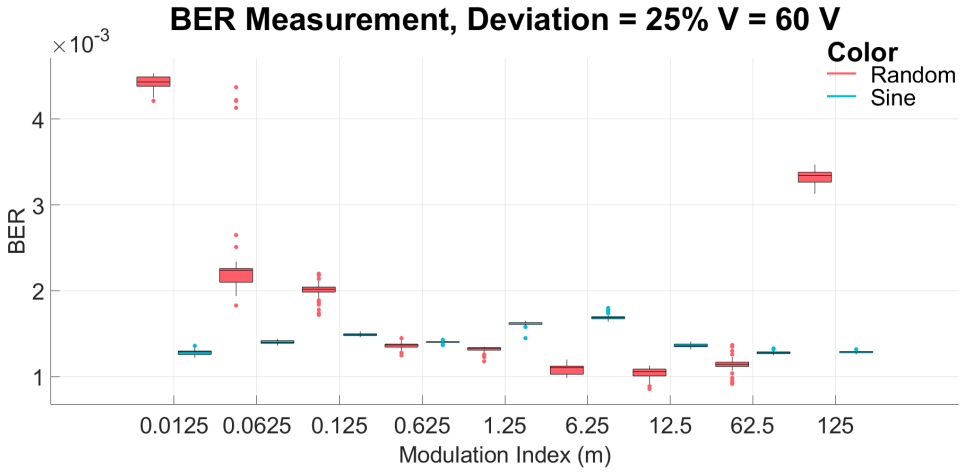

Figure 5.7: BER values for $\alpha = 25\%$ and different modulation indices.

4. BER with $\alpha = 35$ %. The measured results for $\alpha = 35\%$ are shown in Figure 5.8. For this specific case, the performance of the two modulating signals show a completely different behaviour when the modulation index is below 1.75. In fact, the random modulating signal generates higher BER when compared to the Sine modulating signal. However, there is a point at which both signals will perform in a similar way, i.e. when reaching values higher than 8.75 with BER of

approximately to $3.5 * 10^{-3}$.

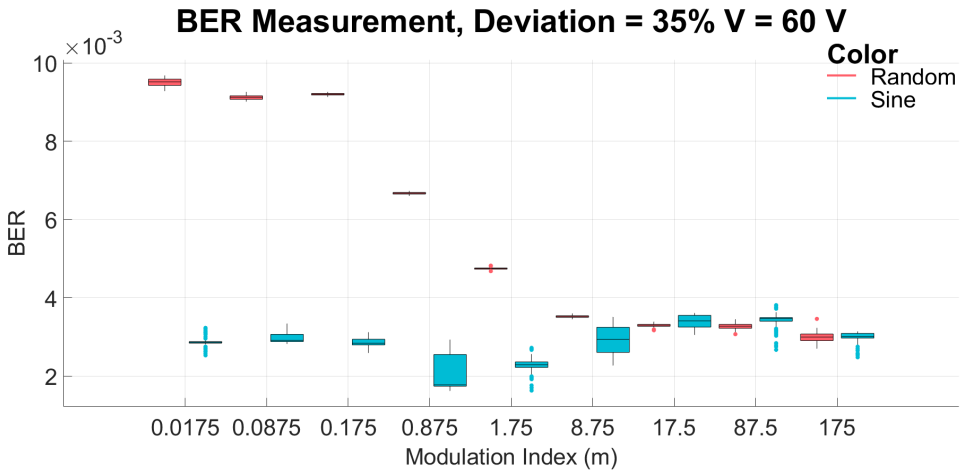

Figure 5.8: BER values for $\alpha = 35\%$ and different modulation indices.

5. BER with $\alpha = 45$ %. Finally, the results obtained for the highest case measured in this thesis are shown in Figure 5.9. For this specific graph the behaviour of both signals should be analysed. Both signals generate the highest BER. This is to be expected due to the increasing trend given by the spreading factor.

   The comparison of both signals provides interesting points to discuss. Firstly, the random modulation has a considerable change for modulation indices from the initial modulation index value of 0.0225 to 2.25, in fact there is an increasing trend that goes to a decreasing trend for a value slightly greater than 2.25.

5.4.1 Discussion of BER Results

From the results obtained the following can be concluded,

- Considering the cases from $\alpha = 5\%$ and $\alpha = 15\%$, it is worth noting that both signals (sine and random) perform similarly with a BER value close to $6 * 10^{-4}$ ($\alpha = 5\%$) and $1 * 10^{-3}$ ($\alpha = 15\%$). These are low values but the the modulations approaches do not present a

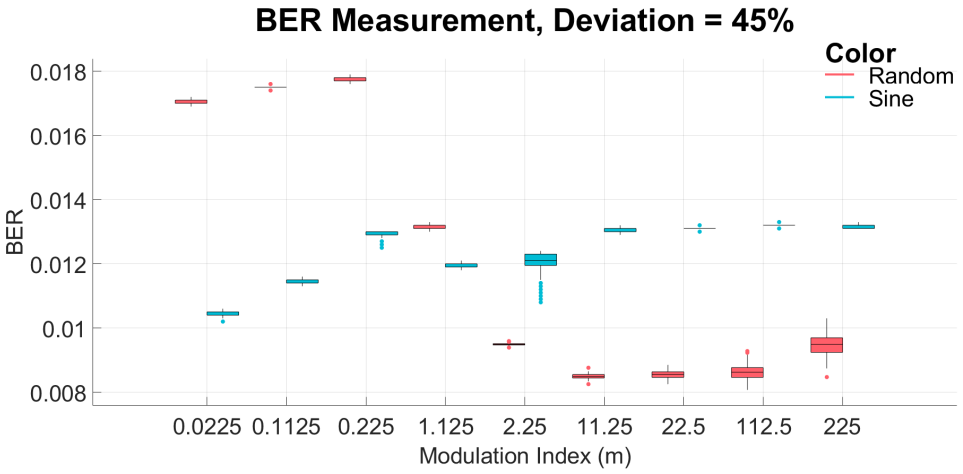

Figure 5.9: BER values for $\alpha = 45\%$ and different modulation indices.

remarkable difference. However, a considerable number of outliers are obtained. This is mainly caused by the short distribution and the slow modulating frequency cannot be tracked by the BER.

- When the value of α is increased to 25%, the differences between the Sine and Random signal start to be noticeable. This happens for modulation indices that are lower than $m = 1.25$. In fact it seems that the BER measured can be almost four times bigger for random than sine. This happens because the modulation index does not give steady measurements below $m = 1$ for the random signal.

- For the remaining cases of $\alpha = 35\%$ and $\alpha = 45\%$, the behaviour of the random graph in both cases presents a change of trend when $m < 1$. This is slightly different for the sine graph. It appears to be that the random distribution has a considerably higher impact at modulation frequencies lower than one.

5.5 BER and its Relationship to EMI Peak Decrease

The results from the previous chapters are considered to provide more information to generate an understanding when both values (EMI PK and BER) are measured for the same modulation index (m). This information will be helpful to relate these important values into a single statistical parameter to correlate them. The results are gathered in tables for a better analysis: the tables will consider the modulation index and the BER and Peak measurements. In addition, the quantile values are also calculated (Q1, Q2, Q3) to determine possible inconsistencies. For practical and structural purposes with regards to the thesis, these tables can be found in Appendix G.

5.5.1 Experimental Test Results

The tables (Appendix G) were gathered together to plot a single graph in order to determine the complete behaviour of spread spectrum for the two signals used at different modulation indices.

To provide a useful understanding about the effects of the two modulating signals used for the SSM, the average values of all of the 100 measurements per individual case have been calculated. The graph showing the modulating index and its relationship to the BER is shown in Figure. 5.10. The resulting trend of increasing the spreading factor will increase the BER measured.

Analysing the pairs given by Sine and Random the following can be observed and discussed with regards to the minimum and maximum values in Table 5.4.

There are interesting cases in which Random and Sine driving signals

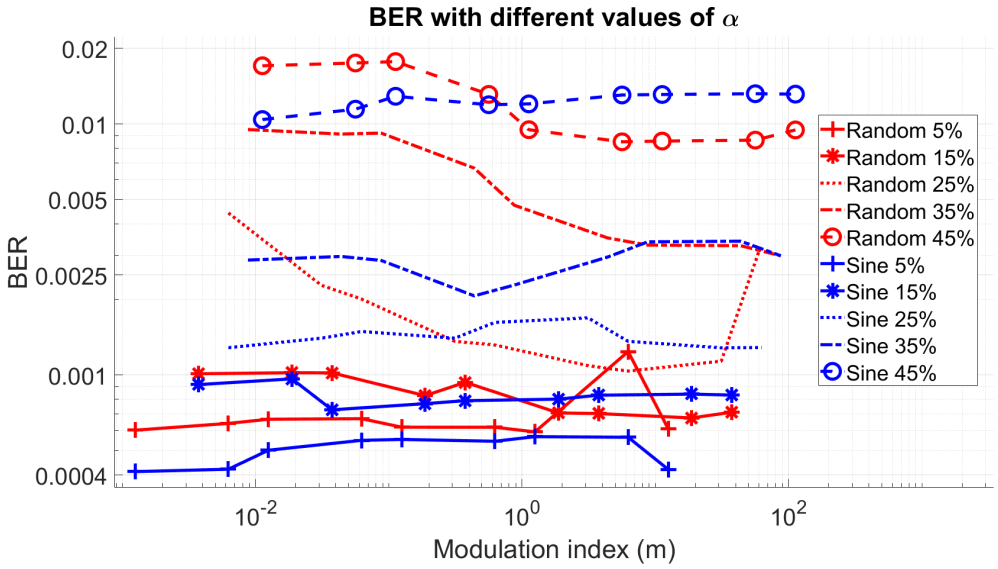

Figure 5.10: Average values of BER for the different spreading factors with different modulation indices.

perform in a similar way, especially for spreading factors lower than or equal to 25 %. In these results the trend is quite linear along the complete range of modulation indices. This minor change is due to the low value of α used, which does not compromise the complete bandwidth covered in the Spread Spectrum Modulation and the BERT measures in a similar way.

The difference in results becomes noticeable when the value of $\alpha = 25\%$. While the behaviour of the sine wave does not change within the range of modulation indices, the random starts from a high value to end on a low value: this applies for the lowest value of m to the highest m.

When both signals are analysed (Sine and Random) with $\alpha = 35\%$ it seems that they find a point at which both have similar results ($m = 8.75$). From the previous points, they are completely different with the BER measured.

Finally, for a value of $\alpha = 45\%$, a similar change of BER measured happens when the signals reach a modulation index close to one (10^0). In fact, it seems that this might be a good operating point in which both signals become similar.

Table 5.4: Minimum and maximum values for the BER measured at different values of α.

		Sine		Random	
α		min	max	min	max
5	m	0.01125	56.25	5.625	0.1125
	BER	0.010414	0.0132	0.00849	0.01772
15	m	0.4375	43.75	87.5	0.00875
	BER	0.0020676	0.0034133	0.002985	0.0095045
25	m	0.00625	3.125	6.25	0.00625
	BER	0.001285	0.00168	0.001036	0.0044235
35	m	0.0375	0.01875	18.75	0.00375
	BER	0.000727	0.000965	0.000675	0.001012
45	m	0.00125	1.25	1.25	6.25
	BER	0.0004125	0.0005683	0.0005939	0.00124

The graph used in Chapter IV is shown in here to give a better understanding with regards to the analytical process of relating both measurements in the next part of this section.

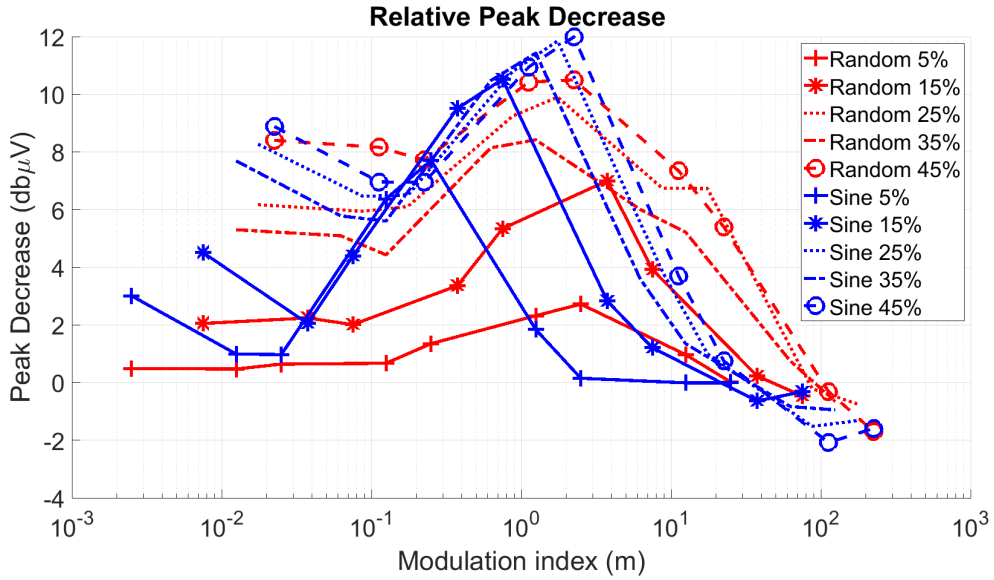

Figure 5.11: Relative Peak Decrease for different spreading factors and different modulation indices (higher is better).

5.5.2 Relative Values for Peak and BER

Considering the relationship between the BER measured and the PEAK value, it is possible to relate these measurements, at least graphically with

the data gathered in Section 5.5. To achieve this, an additional measurement has to be calculated taking into consideration the Deterministic Modulation (DetM) results obtained previously (PK = 109.74 dBμV, BER = $6.148 * 10^{-4}$). For this reason, relative values have been used. The relative value considers the substraction of the DetM modulation case (as a reference value) to the SSM values for both measurements, the Peak decrease and the BER values as seen in (5.5) and (5.6). A table showing the relative values can be seen in Appendix H.

Relative values for PEAK

$$PK_{rel} = PK_{DetM} - PK_{SS_i} \tag{5.5}$$

where PK_{rel} is the relative PK, PK_{DetM} is the result obtained when the converter was using Deterministic modulation at 50 kHz, and PK_{SS_i} considers the different i values of modulation indices used according to the value of α.

Relative values for BER

The same procedure for PK decrease value is considered for the BER measurement. The converter using Deterministic modulation at (50 kHz).

$$BER_{rel} = BER_{DetM} - BER_{SS_i} \tag{5.6}$$

In Figure 5.12 and Figure 5.13 the measurements from Section 5.5 are considered. It can be seen that the sine modulating signal (Figure 5.12) shows a steady performance and stability with regards to BER and EMI Peak decrease from 5 % to 35 %. This is seen if a straight line is considered individually for a single case. What is interesting is the big change when the spreading factor is changed to 45 %. Both indices increase but BER increases considerably. It is worth noting that every cross symbol represents one individual value of modulation index (m).

The Random modulating signal (Figure 5.13) is used, and an interesting trend develops with the increasing values of the spreading factor and its impact on the Relative Peak Decrease. There is a continuous increase of the relative BER. From 5 % to 25 % the effect of mitigation is steady, while this trend changes sharply from 35 % to 45 %.

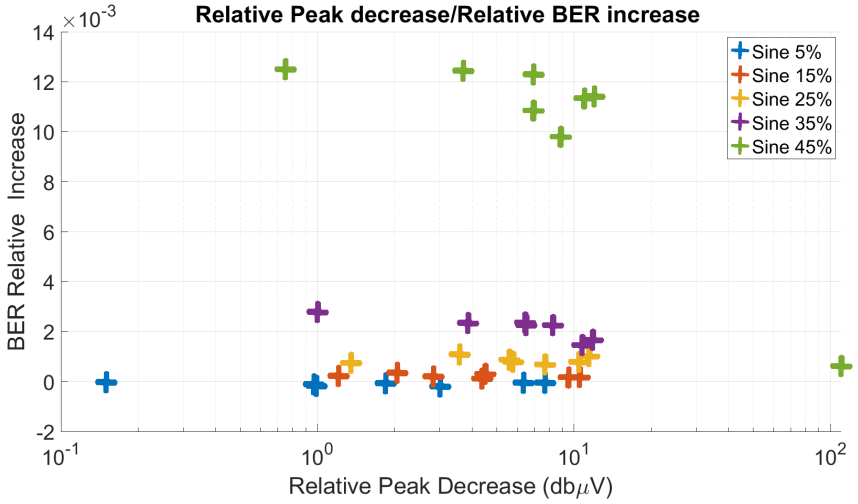

Figure 5.12: Sine wave, relative Peak decrease and relative BER increase.

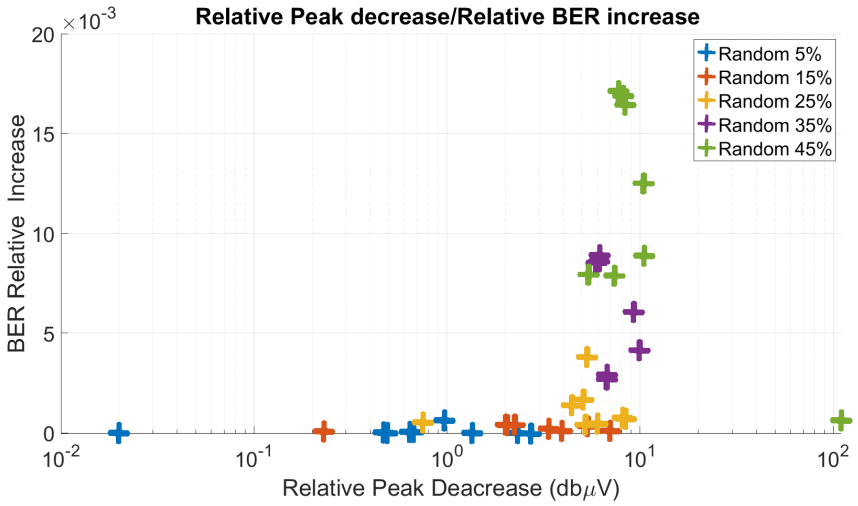

Figure 5.13: Random wave, relative Peak decrease and relative BER increase.

5.6 Statistical Correlation of the Modulations

The correlation of parameters is not a recent topic with regards to Spread Spectrum Modulation, in fact many researchers have been working on several theories such as structural properties, functions, methods of generation and its application to various electronic systems problems [98]. Having considered this, a simple method is used for correlation by applying the Pearson correlation factor [99]. This correlation factor has been chosen as it is a straightforward method to determine a value that can state how well two variables are linked. The calculations were carried out using a Matlab script.

To provide an interesting analysis of how the different modulation schemes behave, it was decided to calculate the correlation value of both cases, the Sine and the Random for the relative values obtained. It was interesting to see how the correlation changes according to the measured values. The correlation factor is obtained as follows [99],

$$r = \frac{\sum_{i=1}^{n}(x_i - \overline{x})(y_i - \overline{y})}{\sqrt{\sum_{i=1}^{n}(x_i - \overline{x})^2(y_i - \overline{y})^2}}, \tag{5.7}$$

where, n is the number of elements, x_i and y_i are the sampled points (measured), while $\overline{x}$ and $\overline{y}$ are the mean of x and y values, respectively.

According to the correlation factor analysis there are three possible outcomes with regards to the correlation; Positive correlation, Negative correlation and No correlation. Considering the two cases (Sine and Random) the results are shown in Figure 5.14. The relative values are presented using a similar scale for both signals (Random and Sine) to determine the relationship of both measurements (BER and PK), and determine how they are or are not related.

The correlation factor obtained for a random modulating signal is 0.5 which represents a positive correlation, not too strong but this effect can be

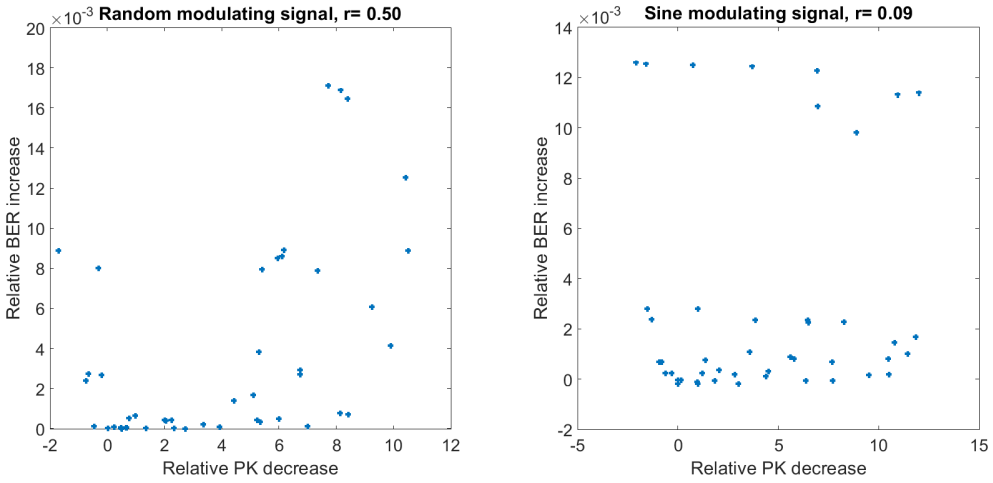

Figure 5.14: Comparison of correlation factors for the modulating signals (Random and Sine).

improved by the usage of more modulation indices. As for for the sine wave modulating signal, the value of correlation factor is 0.09 which represents a very low correlation almost close to a no correlation case.

5.7 Chapter Conclusion

This chapter has analysed and demonstrated an important drawback in the application of Spread Spectrum Modulation for DC power converters with a nearby communication channel. In this process, the Confidence Level parameter has been considered in the measurement process to provide a common point of reference for different measurements.

The measurement procedure followed in this Chapter has shown an useful method to account for the interference generated from the DC converter and how this is translated into the communication channel. The most important recommendation is to determine a suitable value of spreading factor (α) for the switching frequency used. In the results obtained, α close to 25% do not increase the BER in a major way.

It was demonstrated that the BER increases with an increase of the spreading factor (α). However, this is not the case for increasing the modulation index because when both signals (Sine and Random) are compared they behave differently. In a few cases (from 25% to 45%), when one modulating scheme presents a decrease the other scheme increases with different values of modulation index.

The correlation factor between the two variables was calculated in an effort to determine a relationship or a trend in the modulating signals used. An interesting value of 0.5 from the random modulating signal was obtained. This means a strong relationship between the variables under test i.e. the PEAK decrease and the BER increase. The resulting value of correlation is a good parameter for addressing the random effects over a certain point of interest. From the results obtained it seems that this point of interest is when the modulation index is close to one. This considers Figure 5.10 and Figure 4.24 in Chapter IV.

Chapter 6

Pseudorandom Clocking Spread Spectrum

In this chapter the development of a modified generation for a Spread Spectrum random profile is contemplated only focused on the effects in the frequency domain (from the EMI Receiver) seen at the converter specifically. The important point that is under consideration in this chapter is to develop a pseudorandom Spread Spectrum modulation with a control of switching repetitions.

To achieve this, a similar measurement framework is used as the one presented in Chapter IV. The modulation presented here considers a controlled, clocked random generation of values as shown previously in Figure 4.2. However, it should be noticed that when a signal of this nature is used there is no modulation index (m), hence the understanding and the measurement procedure becomes a difficult task and it must rely on the measurement from the EMI Receiver and its programmed parameters.

6.1 Repetition Rate Clocking Driving Signal

In DC/DC converters, Spread Spectrum techniques are often implemented with regards to basic frequency modulation assumptions, and a comparison is carried out with the reference case of Deterministic Modulation. However, the generation of switching frequency streams can be controlled to define the number of possible repetitions of a given switching frequency, i.e. the generation of the same switching frequency for a defined or random number of periods. As a starting point, a periodical generation of frequencies with a predefined rate of switching frequency change has been analysed in [100] and expanded to control the repetition pattern of a driving switching frequency for the mitigation of EMI by employing a Sigma Delta Modulator ($\Sigma\Delta$M). A simple FFT algorithm is used in combination with a Hanning window to determine the characteristics of these type of modulations. Two cases are presented: one based on the control of fixed separation and other based on fixed bandwidth; these are analysed as strategies to control the number of repetitions for a Spread Spectrum modulation scheme based on a previous programmed signal profile. An example of the time domain repetition control is shown in Figure 6.1. For one repetition, the graphs are shown in the top panel. In this figure a change from 19 kHz to 20 kHz can be noticed. In the case of two repetitions, the change from 19 kHz to 20 kHz requires to repeat the same frequency twice.

The results of [100] have demonstrated the important effect of defining a measuring window for a signal in the time domain to account for its results in the frequency domain and how the bandwidth is an important parameter to consider. Two cases are presented, the usage of Fixed Bandwidth and Fixed Separation test cases were analysed. As a conclusion with regards to EMI mitigation, the number of repetitions should be high enough and the number of frequencies must increase in a similar manner to be able to

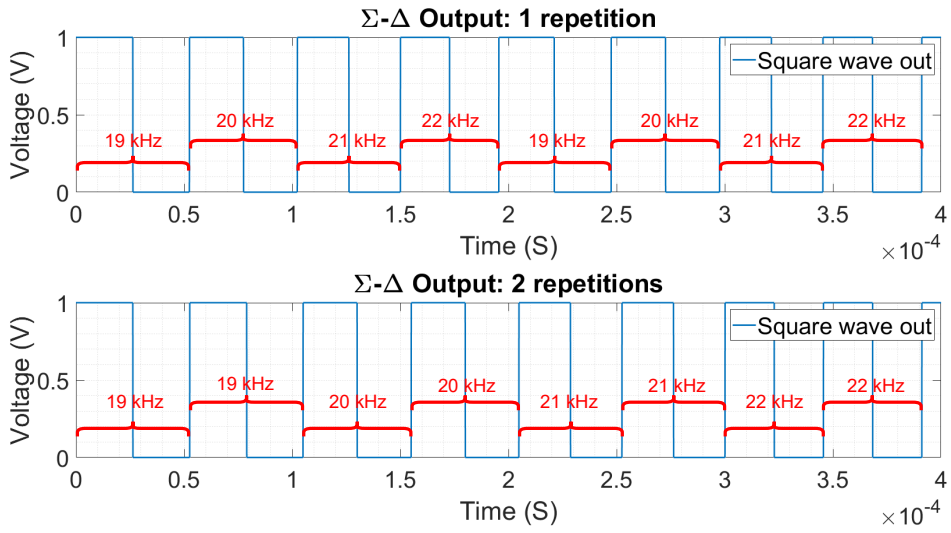

Figure 6.1: A time domain example of the repetition effect for a switching frequency.

demodulate them from the FFT algorithm, otherwise beating frequencies will generate undesired effects. The results with regards peak decrease will show different behaviour as shown in Figure 6.2 for the two strategies. The increase in the X axis refers to the increase of the number of frequency repetitions for the same switching frequency applied to the SSM.

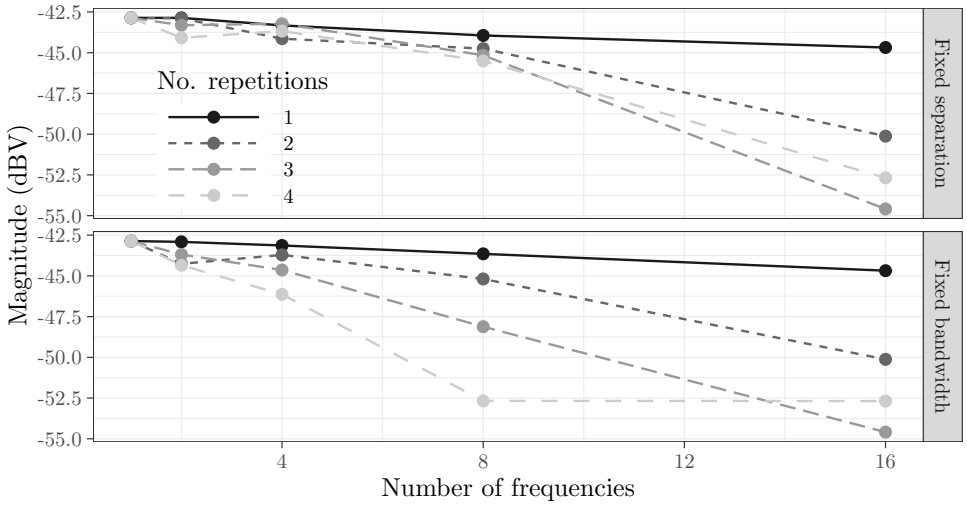

Figure 6.2: Switching harmonic results obtained considering the modification of frequency repetition, top - Fixed separation, bottom - Fixed Bandwidth.

A similar procedure for the generation of a given signal can be applied for a random modulating signal generated by means of an FPGA in order to

control the repetition of a certain switching frequency. Similar approaches can be implemented to other modulation techniques such as the ones presented in [82, 84] to achieve EMI mitigation as was shown previously in Chapter IV.

As mentioned in Chapter IV, there exist important parameters to define the modulating signal such as the carrier frequency (f_c) and the frequency deviation (Δf). These considerations also apply for the scheme proposed based on a random generation of switching frequencies with controlled rate of change (or repetitions). Considering the equipment used to measure the interference, the number of repetitions must be determined for a given resolution time of the EMI receiver, hence a tuning procedure such as the one proposed in [76] has to be considered. This chapter proposes another modulation scheme which controls the number of repetitions with a random generation of switching frequencies. The experimental validation presented and its results were carried out as a collaboration between the author in [82] and the author in [100] during a Summer School of the European Projects (Scent and Etopia).

6.1.1 Pseudorandom Modulation

Typically, the generation of pseudorandom numbers for digital systems is often carried out by means of microcontrollers (as presented in Chapter IV) or an FPGA. In these devices, there are dedicated blocks that can provide pseudorandom streams of numbers which can be periodic in time. For this reason, the word pseudorandom is often used to refer a random generation of numbers by means of hardware.

Considering the usage of an FPGA to generate the random stream of switching frequencies, the number of clock cycles must be understood before going further. On a continuous operation cycle there will be N values of

clock values required to generate a particular frequency, for example, the desired carrier frequency f_c. In a similar manner, the deviation must be related to N as the minimum and maximum limits i.e. $N \pm \Delta N/2$, hence the same equation as show in Chapter IV with regards the generation of Spread Spectrum is shown in (6.1) in terms of clocking cycles for the output Random Frequency (f_{out}).

$$f_{out} = f_c(N) \pm \frac{\Delta N}{2} \cdot \epsilon(t), \tag{6.1}$$

in which ϵ(t) represents the driving signal. An interesting approach is shown in [76] in which a random Pulse Amplitude Modulation (PAM) is employed as is shown in (6.2).

$$\epsilon(t) = \sum_k x_k g(t - kT), \tag{6.2}$$

where $x_k \in [-1, 1] \subset \mathbf{R}$, and represents the transition point between $-1 < t < 0$ and $0 < t < 1$ of the $g(\cdot)$. $g(\cdot)$ is the normalized rectangular pulse train, where $g(t) = 1$ for $0 < t < 1$ and 0 elsewhere, and T is the duration of the pulse [76]. If a hardware point of view is assumed, for every iteration of $\epsilon(t)$ one iteration count (i) is performed, as can be seen in Figure. 6.3.

When x_k is randomly generated by any desired distribution such as $k = 0,1...$, the spectrum can be considered continuous. The generation of different values with a defined sampling ratio can then generate stochastically a stream of numbers for the switching frequency of the power converter. Indeed, the value of x_k can be repeated by means of an i value which is controlled outside the main frequency calculation.

The i value defines the N value needed to generate one unique f_{out} as presented in [84]. The lower and higher limits of f_{out} are calculated using the frequency deviation formula in (6.1). This is translated in the lower

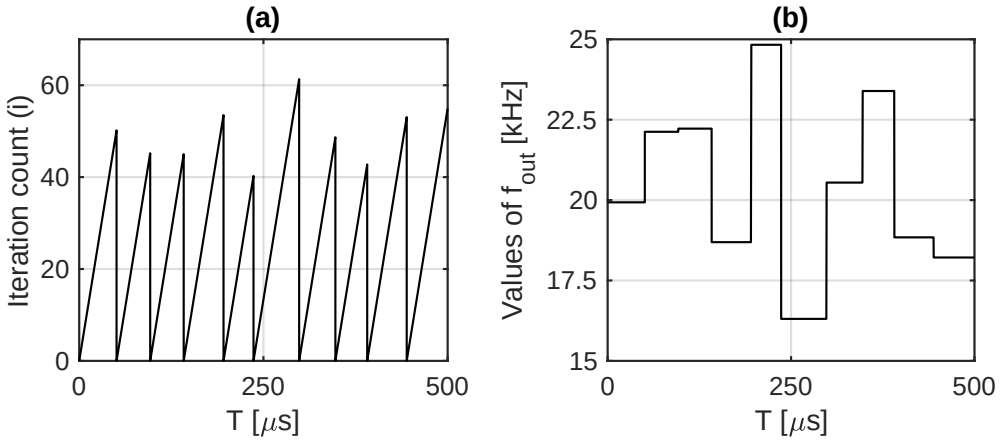

Figure 6.3: The relation between i (a) and f_{out} (b) for a set of 10 $\epsilon(t)$. The Δf_{out} is approximately 20 kHz, and the ΔT is approximately 50 μs. Also, considering in both cases $k = 1$, and $f_b = 20$ kHz with a $\Delta f = 10$ kHz.

limit as $-\frac{\Delta f}{2} \cdot \epsilon(t)$ and the higher limit as $+\frac{\Delta f}{2} \cdot \epsilon(t)$. The execution rate of i is related to the features of the control hardware available. To explain the concept of RanM repetition rate control, it is assumed that $k = 1$ means allocating all control hardware features to execute just one i. In this context, (6.2) shows that when considering constant but broader values for k, one unique $\epsilon(t)$ can be repeated more times, i.e., broader values for k make the i slow.

The implementation of the PWM technique can make use of several i for different purposes. For example, Figure 6.4-B illustrates how i becomes slow for $k = 3$, in comparison with Figure 6.4-A (with $k = 1$). For one period of $t = 1500$ μs with $k = 1$, the set of 10 $\epsilon(t)$ was performed three times, in the case of Figure 6.4-A. For the same period of $t = 1500$ μs, with $k = 3$, the same set of 10 $\epsilon(t)$ was performed just once, in the case of Figure 6.4-B.

For the correct implementation, the values Δf_{out} and ΔT must remain approximately in correspondence for frequency and time, i.e.,, $f_{out} = 20$ kHz and $T = 50$ μs (see Figure 6.3). Figure 6.4-C shows that regardless of the influence of k in the set of 10 $\epsilon(t)$, the number of turn-on and turn-off switching actions (T_{PWM}), and consequently the Δf_{out} and ΔT are not

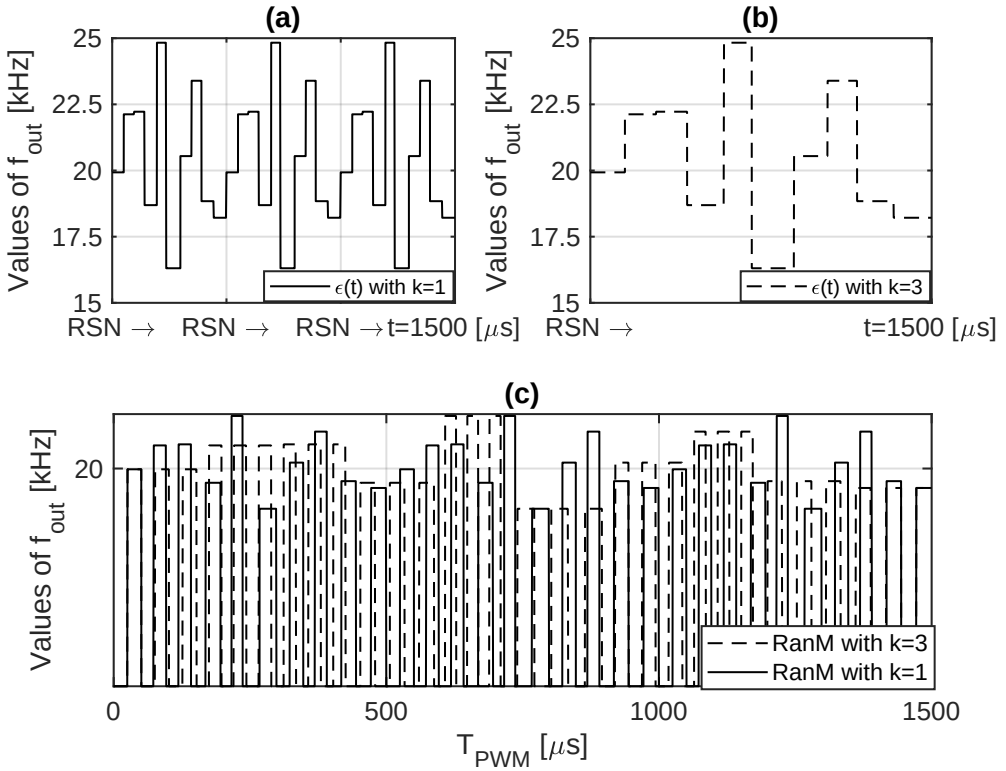

Figure 6.4: The RanM repetition rate control based on k value: (a) $\epsilon(t)$ with $k = 1$, (b) $\epsilon(t)$ with $k = 3$, and (c) both RanM with $k = 1$ and $k = 3$.

drastically changed in both approaches, i.e., RanM with $k = 1$ and RanM with $k = 3$. Furthermore, Figure 6.4-C also shows that instead of ten T_{PWM}, where each one is based on one $\epsilon(t)$ (RanM with $k = 1$), the RanM with $k = 3$ assumes the same $\epsilon(t)$ value for a set of three consecutive T_{PWM}.

From a practical point of view, implementing the RanM repetition rate control is possible since it is assumed that one i is dedicated to $\epsilon(t)$, and another i is committed to T_{PWM}. In this way, the PWM time is not influenced by k. In other words, the broader the range of values assigned to k, the longer it takes to randomly alternate the frequencies considered in the random pattern of the RanM.

This section explained the main concepts for a pseudorandom generation of switching frequencies to drive the DC converter. It has shown how the repetition rate of a certain frequency can be controlled with a simple background proposed by using a fixed profile. The same idea has been

extended to generate the random switching frequencies with a previously defined repetition rate with its application based on an FPGA.

6.2 Test Set-up: Random Clocking Driving Signal

6.2.1 Random PWM Control Generator

The PWM control algorithm has been implemented using the LabView environment for the embedded controller NI PXIe-8135, and of the FPGA PXI-7854R. The Labview block diagram is shown in Figure 6.5 and is based on two important blocks to generate the pseudorandom stream of numbers to be used as switching frequencies. Initially, this generation of switching frequencies is based on the Labview program implemented in [82] with few modifications to control the pulse repetition. In this implementation the Output Frequency (f_{out}) and the Duty Cycle (D) can be modified by considering (6.3) and (6.4).

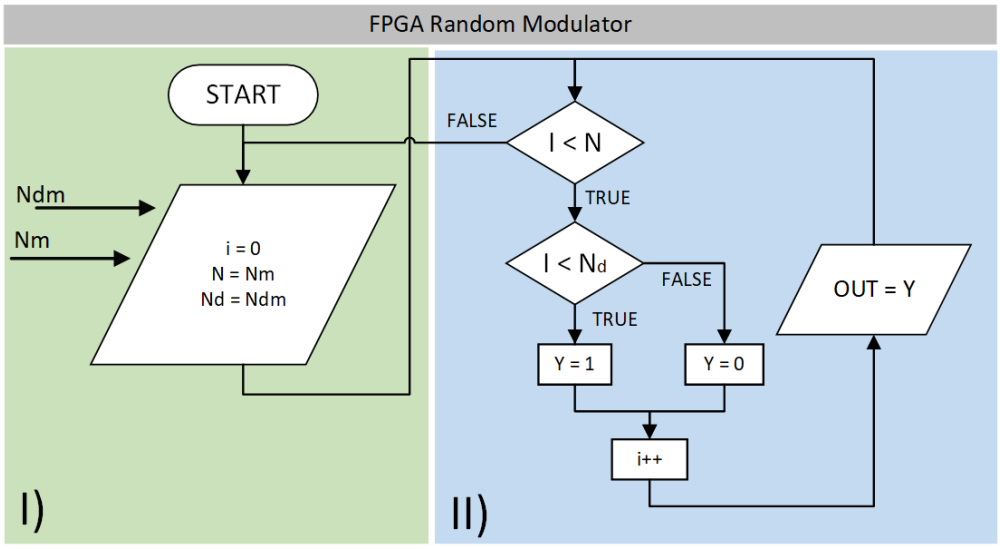

Figure 6.5: Labview block diagram based on [82].

$$N = f_{FPGA}/(f_b \cdot SC_{TL}) \tag{6.3}$$

$$N_d = D \cdot N \tag{6.4}$$

In (6.3) and (6.4), f_{FPGA} represents the master clock frequency of the FPGA, f_c is the carrier switching frequency and $SCTL$ is the Single Cycle Time Loop (in clock cycles) to divide the master clock.

To achieve the pseudorandom generation the FPGA has a clock frequency of 40 MHz (f_{FPGA}). There is a division by 10 given by $SCTL$ to achieve lower frequencies. The control of the duty cycle in relation to N is obtained by the parameter D and it can be controlled from 0 to 100 %. It is worth mentioning that there is a process to scale the values due to the use of a fixed point operation in the FPGA. The complete explanation of Figure 6.5 is as follows,

- I) Defines the Linear Congruential Generator (LCG) that generates a stream of pseudorandom variables along the desired time of execution. In this part the initialisation of the clock cycles is made to calculate the desired frequency needed with the low and high limits defined by Carson's rule.

- II) Controls the duty cycle parameters with regards to the previous calculation of switching frequency, the ramp profile is then generated with regards to the desired scaled frequency to be used for the power converter.

6.2.2 Modified Random PWM Control Generator

Having a simple method to control the generation of random switching frequencies (Figure 6.5) the modification (seen in Figure 6.6) to control the repetition rate is carried out by controlling the execution of II) with an external value provided by k as mentioned in Subsection 6.1.1. At every step of k, the N_m and N_{dm} values are recalculated for the m'th PWM period (T_{PWMm}). In the same process, the duty cycle is dynamically changed. The RanM repetition rate implementation is only possible because each environment considers one iteration count (i). With the randomisation made by considering Carson's rule the distribution will be close to a Gaussian distribution. This distribution is often chosen due to the favourable results in terms of the average frequency and converter losses. The modified block diagram for the control of random repetition rates is shown in Figure 6.6.

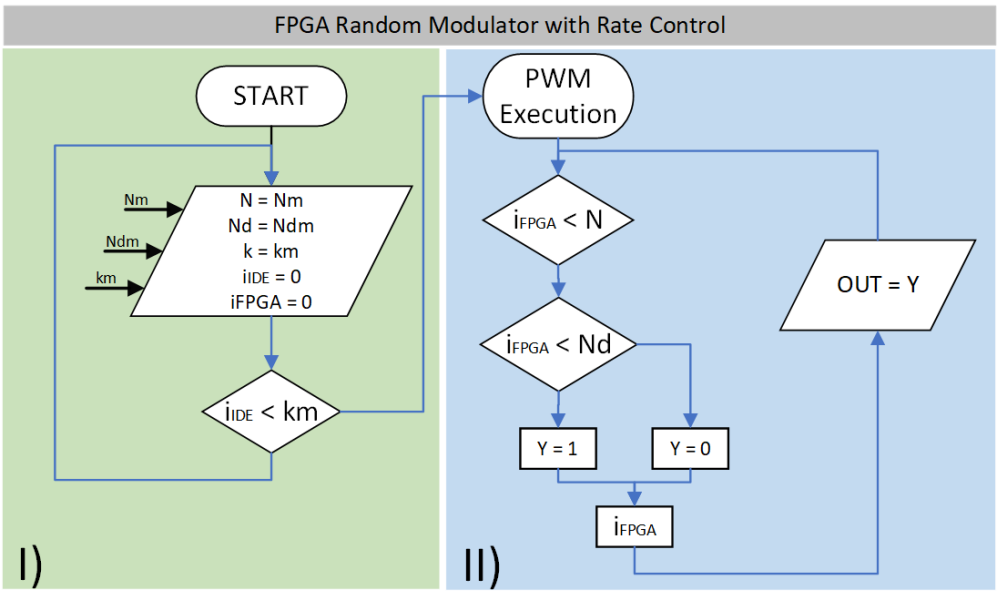

Figure 6.6: Labview block diagram based on [82] with controlled rate of change.

Some important changes were made in comparison of the previous block, these changes are explained as follows,

- I) Defines the modified Linear Congruential Generator (LCG) to gen-

erate the same pseudorandom stream of data for the control of repetition rate. An important point worth noticing is the control of the rate repetition given by i_{IDE} with its value of k (k_m) to define the number of repetitions.

- II) The generation of the ramp profile with regards to the desired scaled frequency is calculated for every value of k, in fact the parameter k is the one responsible for defining the number of repetitions in the modified random modulation block as defined in the part I) of the flowchart.

To demonstrate the usage of the modifications with regards to the repetition rates, a result with three and five repetition is shown in Figure 6.7a and Figure 6.7b in a simulation for the Labview environment. Red rectangles are used to demonstrate the switching frequency repetition effect generated from the Labview environment. The two block diagrams used to achieve the implementation of the pseudorandom modulation can be found in Appendix I.

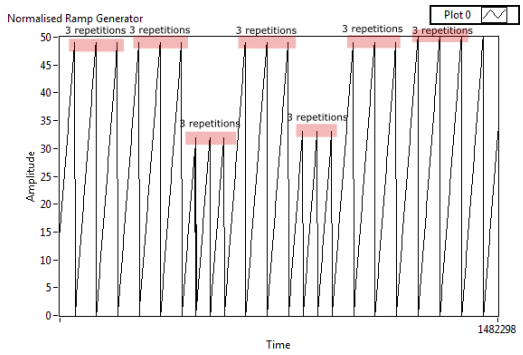

(a) Ramp control for 3 repetitions.

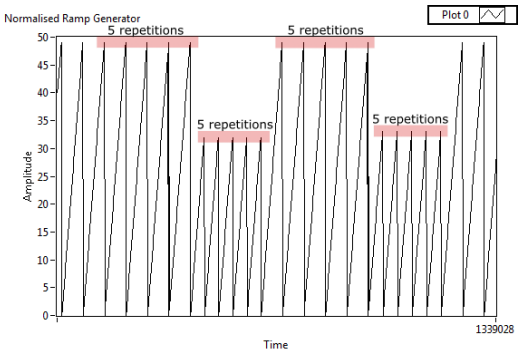

(b) Ramp control for 5 repetitions.

Figure 6.7: Labview generator for the control of repetitions.

6.2.3 Experimental Test Set-up for the Modified Algorithm

Having defined the modifications for the algorithm presented to control the repetition rate, the experimental test set-up is shown in Figure 6.8.

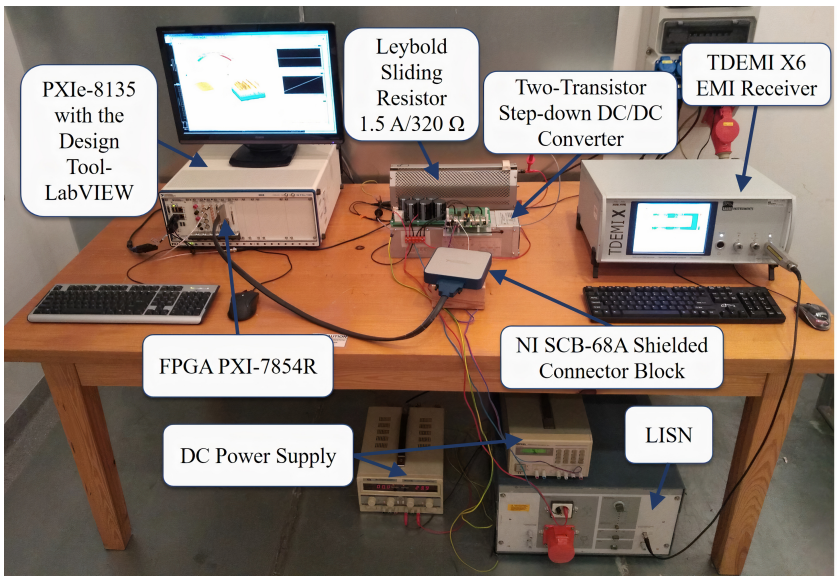

Figure 6.8: Experimental setup.

The description of the equipment is as follows,

- PXIe-8135 and PXI-7854R. The programmable modules used respectively to generate the Random modulated signal to drive the converter used. All these equipment is manufactured by National Instruments (NI).
- DC Power Supply. The power supply provides the required energy for the drivers used in the converter used; the other power supply is the one used to fed the converter at its input.
- Leybold Sliding Resistor. This resistor is used as converter load, the maximum resistance is 320 Ω.
- DC Converter. The DC converter uses IGBTs. The important parameters of the converter are summarised in Table 6.1.

- TDEMI X6 EMI, is the measuring equipment i.e. the test receiver with a dwell time of 100 ms. The dwell time in the EMI receiver can be configured by using the user interface at different values. More information about this EMI receiver can be found in [101].

Table 6.1: The main parameters of the two-transistor step-down DC/DC converter.

Component/function	**Specification**
Transistors type	IXGH40N60C2D1
I_C (max)	40 A
t_{on}	40 ns
t_{off}	180 ns
Transistor Gate Drivers	HCPL-316J
Diode rectifier	KBPC3506
Converter Power	1800 W (max)
Capacitor	1 μF
Max DC voltage	450 V
Load	Leybold sliding resistor

In this section the implementation of the algorithm designed in Section 6.1 has been presented, the main block diagram programmed in Labview has been presented as well as important assumptions to program this algorithm in the FPGA. The graphical demonstration of the pulse generation was shown by using the formula as well as the result obtained by means of Labview resources.

6.3 Conducted EMI Measurements

Tests have been performed on the converter to determine the mitigation results of the Random modulation strategy. The comparison of performance is by measuring the Random modulated case and the DetM case. The measurements carried out in this work are considering the reference case of Deterministic modulation, then the case with Fast Switching Rate of Change is analysed to conclude with the case with Slow Switching Rate of

change.

Due to the fast processing of data in the EMI receiver the three main indices are measured, (PK, QP and AV), to provide more information to compare the designed algorithm.

6.3.1 Deterministic Modulation Results

The results will be given by the Spectrogram of the TDEMI Receiver, it is important to notice that the interval of sampled values (N) discretised in the STFT (4.3) are much smaller than the dwell time [37].

As was mentioned in Chapter IV, defining a dwell time is an important task to have stable and steady signals, in fact, some standards suggest specific dwell time values to measure the interference of specific signals. Having mentioned these important points, the measurements are presented in this section for the Deterministic Modulation case with a switching frequency of 90 kHz. This frequency is chosen due to the maximum frequency covered for the Prime PLC standard (42 - 90 kHz) to have a reference.

The PK spectrogram generated from the EMI Receiver is shown in Figure 6.9, with the highest magnitude of 0 dBμV at $f_b = 90$ kHz.

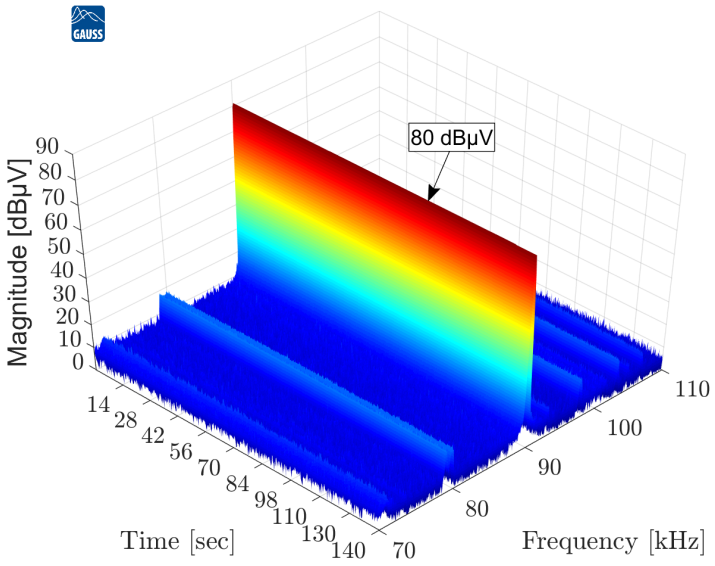

Figure 6.9: DetM with $f_b = 90$ kHz and PK detector.

In Figure 6.10, it can be seen the Quasi-Peak (QP) detector spectrogram for the EMI shape of DetM, with also the highest magnitude of 80 dBμV at $f_b = 90$ kHz.

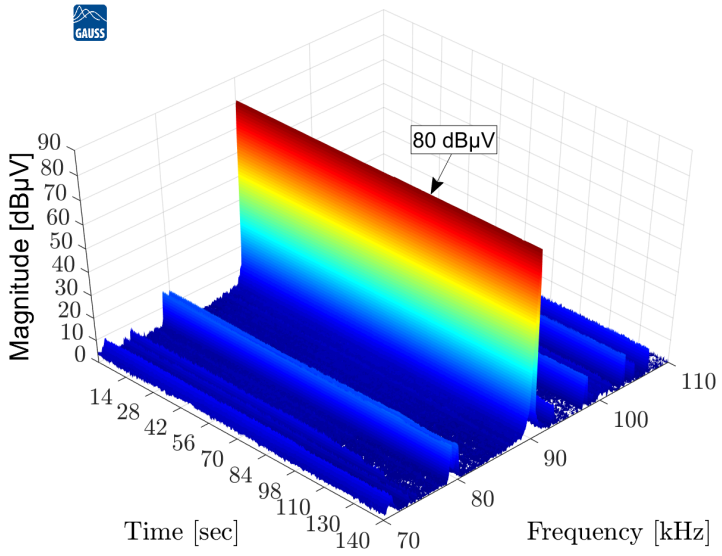

Figure 6.10: DetM with $f_b = 90$ kHz and QP detector.

Finally, the average (AV) detector spectrogram for the EMI shape of DetM can be seen in Figure 6.11, with also the highest magnitude of 80 dBμV at $f_b = 90$ kHz.

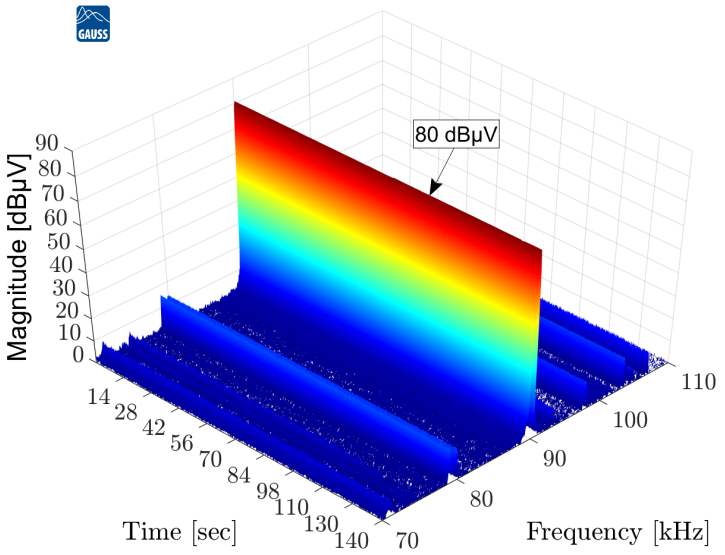

Figure 6.11: DetM with $f_b = 90$ kHz and AV detector.

Therefore, in the case of DetM, the given rule for detectors: $PK = QP = AV$,

is demonstrated for Figure 6.9, Figure 6.10, and Figure 6.11. The noise floor of the three indices is close to 0 dBμV and the characteristic peak shape for one switching frequency is seen in the spectrograms. Smaller peaks develop across the frequency band but these are not considered important if they are compared to the magnitude of the switching frequency.

6.3.2 RanM with Fast Switching Rate of Change

When a modification in the algorithm is applied to achieve the Random Repetition Rate Control, the expected behaviour for the signal spreading for the spectrum is achieved. For the specific case to determine the suitability of this technique, a value of $\Delta N = 30\%$ is chosen along with the parameter $k = 1$, which means a very fast rate of change for a centre frequency of 90 kHz. The results of the spectrogram for this case are shown in the following figures.

Figure 6.12 shows the result for the PK detector. The highest magnitude of 64 dBμV at $f_b = 90$ kHz is measured when the parameter $k = 1$ and the $\Delta N = 30\%$.

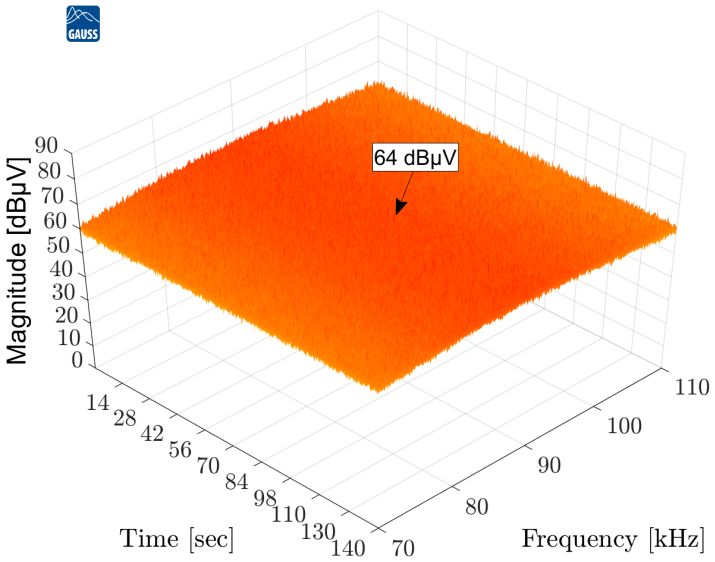

Figure 6.12: RanM with $\Delta N = 30\%$, $k = 1$, $f_b = 90$ kHz, and PK detector.

Figure 6.13 presents the QP detector spectrogram which has a highest

magnitude of 60 dBμV at $f_b = 90$ kHz.

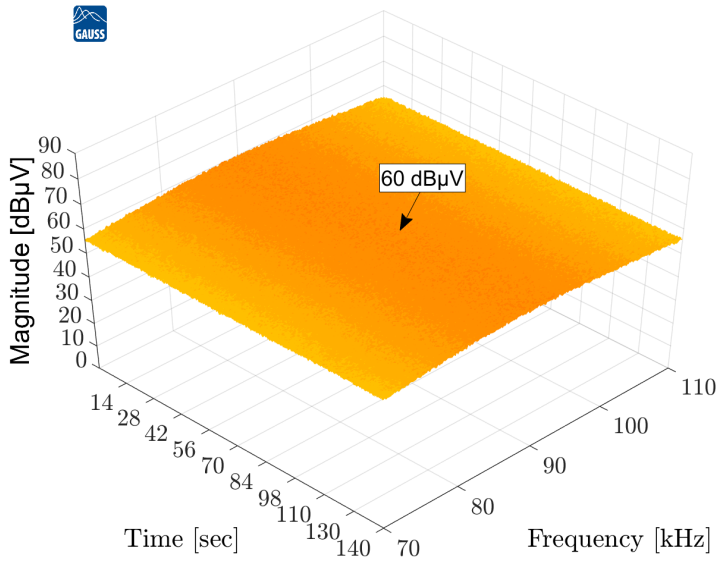

Figure 6.13: RanM with $\Delta N = 30\%$, $k = 1$, $f_b = 90$ kHz, and QP detector.

Figure 6.14 presents the AV detector spectrogram with 57 dBμV at $f_b = 90$ kHz.

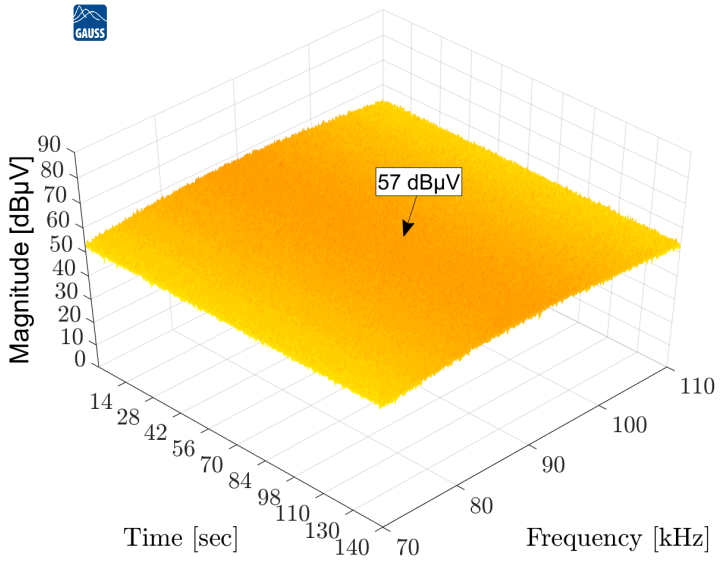

Figure 6.14: RanM with $\Delta N = 30\%$, $k = 1$, $f_b = 90$ kHz, and AV detector.

For all the three indices, the signals develop a flat and stable surface across the bandwidth under analysis. Interestingly, the noise floor has increased to similar levels to the maximum index values measured. This is the well-know trade-off when considering any SSM either periodical or random.

Nevertheless, the following should be noted:

- The spreading of the spectrum components will always be a consequence of the RanM;
- The spreading of the EMI noise levels as presented in Figure 6.12, Figure 6.13 and Figure 6.14 does not mean EMI noise level or even power spectrum have been reduced;
- The RanM provides changes in the frequency of a given PWM signal and provides random changes between the frequencies considered in this PWM signal. It then becomes imperative to find the trade-offs between RanM, dwell time and RBW to achieve a stable EMC measurement.

6.3.3 RanM with Slow Switching Rate of Change

For the slow switching rate of change used, the EMI receiver is allowed to have more time to properly characterise the non-periodic signal without increasing the dwell time, as presented by Figure 6.15, Figure 6.16, and Figure 6.17.

Therefore, by using $k = 4 * 10^5$, it takes longer to randomly alternate the frequencies considered in the pseudorandom control used by RanM.

Considering the dwell time equal to 100 ms for all the results obtained, it is possible to define what are the stable EMI measurements by comparing the two cases presented.

The highest magnitudes presented in Figure 6.15, Figure 6.16 and Figure 6.17 of 80 dBμV are the same as those presented in Figure 6.9, Figure 6.10, and Figure 6.11, respectively. This is mainly caused by the switching nature of the carrier frequency of the RanM and the EMI receiver resolution parameter mismatch. Which in reality are not spreading the noise and represents a non-reliable measurement.

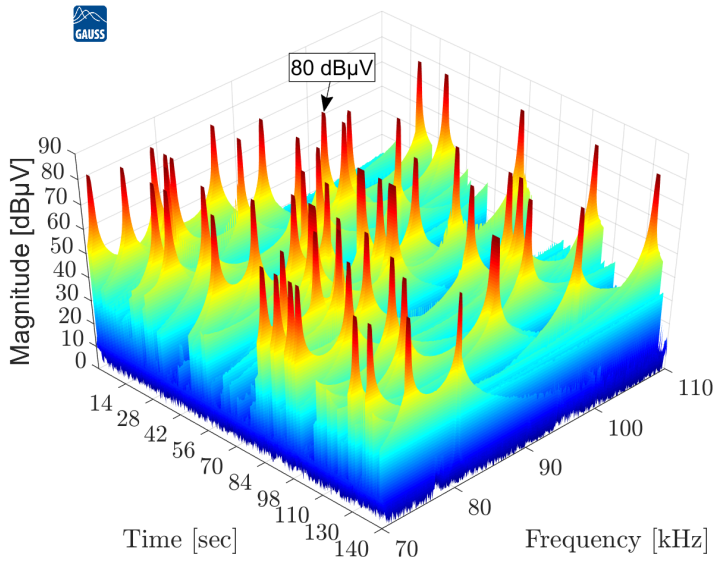

Figure 6.15: RanM with $\Delta N = 30\%$, $k = 4 * 10^5$, $f_b = 90$ kHz, and PK detector.

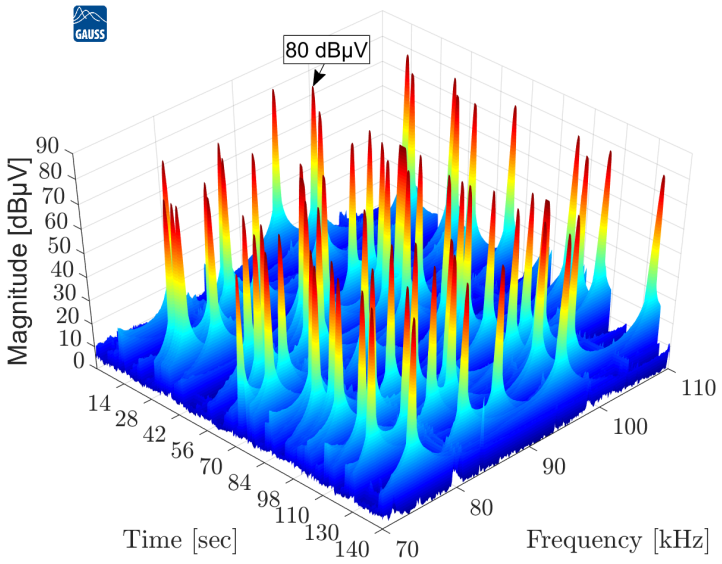

Figure 6.16: RanM with $\Delta N = 30\%$, $k = 4 * 10^5$, $f_b = 90$ kHz, and QP detector.

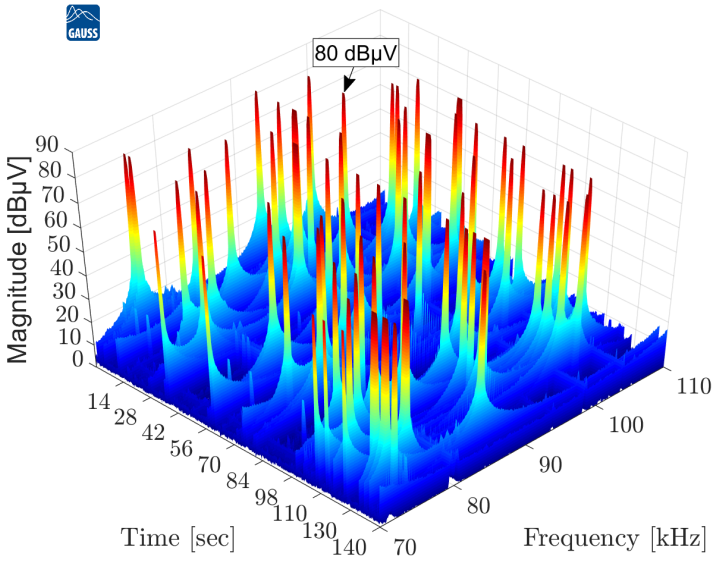

Figure 6.17: RanM with $\Delta N = 30\%$, $k = 4 * 10^5$, $f_b = 90$ kHz, and AV detector.

All of the results obtained for the three testing cases were shown. An interesting conclusion that can be obtained from the results is that only one repetition could be enough to mitigate the effect of the switching frequency. However different frequencies can be tested for further work in order to determine the advantages and disadvantages of controlling the repetition rate.

In addition, the effect of using Random Modulation is entirely dependant on the equipment configuration and how it is measured as an increase in the dwell time can indicate that there is no improvement in the maximum peak values emission of the interference.

6.4 Chapter Conclusion

The use of pseudorandom modulation techniques for spreading the spectrum components of a signal in DC/DC converters is a topic that must be considered according to particular needs. In the past, many authors have suggested that it was a misleading way of complying with EMC standards. This holds true if there is not enough information about all the

pseudorandom modulation parameters as well as the functioning of the TD-EMI test receiver. In other words, it is not enough to just determine the pseudorandom modulation parameters. In addition, the control of the rate of change of switching can be used as a parameter to control the EMI generated by switching power converters.

The results in this chapter have demonstrated the application of the repetition rate control for the pseudorandom modulation. From the results obtained it seems that a fast repetition is enough to have a reasonable decrease of about 16 dBμV for Peak, a decrease of 20 dBμV for Quasi-Peak and, 23 dBμV for Average. These results seem to be a good indicator since a $\Delta N = 30\%$ was used with a frequency of 90 kHz. The dwell time for all the measurements was 100 ms. These tests clearly show a way of shaping the spectrum.

In general, many power electronic researchers are not looking at the potential EMI effects of fixed modulated converters nor the system emissions in combination. Therefore can be considered the main contribution of the pseudorandom repetition rate control presented here is as a possible solution for future standards.

Furthermore, as was explained in the previous sections (Section III), the stability of a signal measured by the TD-EMI test receiver depends on the STFT calculation. The Fast Fourier Transform calculation relies on essential parameters such as the resolution bandwidth, dwell time, and the IF filter. Thus, finding the trade-offs with the dwell time and resolution bandwidth to achieve a stable EMC measurement with pseudorandom modulation becomes imperative to understand how to comply with restrictive standards.

Chapter 7

Summary and Reflections

7.1 Importance of EMI Analyses

This thesis has presented an analysis to assess for the most common Power Converter EMI mitigation techniques which use Spread Spectrum Modulation in the frequency domain, and demonstrates the important drawback seen when analysing EMI in the time domain.

The theoretical background of SSM was presented and the important parameters were highlighted with regards to signal generation. A time domain simulation was carried out with a modulator designed to generate different modulation profiles to understand and to control the EMI generated by a switching frequency of a buck converter. The results were analysed by both of time and frequency domain techniques with a defined sampling ratio. The modulation was then implemented using a bespoke laboratory experiment. The CISPR-16 standard was used to define the measurements and analyses focused on the Low Frequency band A (9 kHz - 150 kHz).

It has been shown that there probably exists a best point for reducing the EMI generated by a Buck Converter when Spread Spectrum Modulation is used with the proposed parameters, this value is given by the Modulation Index (m) which has to be close to one. However, the spreading factor

along with the frequency of the modulating signal play an important role in defining this and must be considered as a part of the holistic analysis as presented in the experiments of this thesis.

The conclusions of every chapter can provide important guidance or rules of thumb for EMI/EMC engineers who are looking for solutions to improve certain undesired switching frequency related emissions from a power converter. However, these methods are not enough to completely understand the nature of a signal which has either a periodic or random nature. In the frequency domain analyses made, the Resolution Bandwidth of the measuring equipment is a key component in the process of understanding the emissions of a specific device.

In this work, two different random distributions were used as a part of the SSM process (in Chapter IV), Random Linear and Random Gaussian. The former was used for the research as it has a flat distribution across the switching frequencies applied to the converter. Random Gaussian distribution was also analysed but experimental tests were not carried out. However, in the Random distribution usage for SSM a Peak shaped signal was seen in the frequency domain measurements, this is due to the central frequency used according to the limits defined.

Finally, special mention should be made of the additional method presented in Chapter VI in which the generation of a random signal can follow a repetition rate control. In this analysis, it can be difficult to determine the best point to be used but the generation of random numbers and its repetitions must be high enough to guarantee a process of demodulation from the EMI receiver side. By applying a technique based on these points a tuning procedure might be needed to find the best operating point. In a similar way, the distribution also plays an important role in spreading the signal to reduce peaks to an acceptable level. When a point close to this was found, an interesting value of 18 dbμV was measured in comparison to

the previous method presented (with clocked cycles) in Chapter IV which decreased the noise of a similar converter by 14 dbμV. Better results for the EMI reduction were found in Chapter VI due to the higher switching frequency 90 kHz, when compared against 50 kHz when both experimental tests are compared.

7.2 Time Domain Importance

This thesis has presented a simple method for measuring the effect of EMI in the time domain by means of measuring BER i.e., direct measurements of the performance of the communication system. The resolution of the measurement (time recorded) is a key parameter that must be chosen carefully to have reliable and reproducible results. In Chapter V, a method considering statistical parameters for measuring BER was presented. Most of the values are defined considering the modulation index that controls the effect of the SSM algorithm to show a relationship to the BER measured, and to other measurements of EMI.

The clocking signal used for the experimental tests should be highlighted. For the first analysis, the converters used a fixed frequency (from the microcontroller). This means that most of the EMI generated will come directly from the converter itself and from the devices to which it is connected.

It has been shown in Chapter IV that different signals can generate different shapes in the frequency domain when the DUT is analysed. This introduces the idea of a complete understanding of a time domain signal to fully decompose the noise measured in the frequency domain. In fact, the CISPR-16 standard was explained in Chapter IV to have a broad knowledge of the time domain operations and its relationship with the results measured from the EMI receiver perspective.

Finally, the use of measured BER has demonstrated the disadvantages

of modulating the switching frequency of a converter, which is to sharply increase this parameter across the whole measurement time when compared to the reference case of Deterministic Modulation. This provides important additional data for engineers who are only looking at the frequency domain measurements and not considering the important drawbacks seen in the time domain. What is more, Crosstalk between devices in modern smart grids is becoming a considerable problem, and few engineers are being trained in this technical area.

7.3 Frequency Domain Importance

When EMI is analysed in the frequency domain important indices are required which change according to different standards. In Chapter IV, the PK index has been taken as the main index for this research topic, as other indices (Quasi-Peak and Average) required large demodulation time for the EMI receiver available for this PhD work. However, the measurement of just the PK value still allowed to determine interesting trends. Interpolation methods were used to determine the best parameters (spreading factor, modulating signal frequency) to decrease the interference caused by clocked signals. In addition, the correlation between the BER and PK has been determined with an interesting value of correlation of 0.5 for a Linear Random distribution for SSM. This can provide an interesting starting point future studies to investigate different spreading factors and their relationships.

The frequency domain analyses have shown that there exist a best point of EMI Peak reduction for the switching frequency of a power converter with regards to the modulation index close to one ($m = 1$). However many of the assumptions made for these analyses are tailored to specific conditions, and they must be tested extensively for complex grids in which many power

converters are interacting with each other.

7.4 Final Conclusion

Finally, this thesis has provided useful considerations with regards to the time and frequency domains to understand EMI in microgrids specially focused on DC converters that can generate high levels of interference. In fact this interference can compromise a whole system if mitigation actions are not considered.

This thesis has informed the effects generated with a mitigation technique in bottle the time and the frequency domains and the highlighted drawbacks that are not often addressed in current EMI research.

Considering the method presented with regards to the theoretical and experimental background, it can be proposed as an idea for future standard development to address a different way of measuring EMI.

7.5 Future Work

Considering the knowledge gathered from the literature review and experimental tests, it is clear that the effort to relate time domain analyses to frequency domain analyses still needs more development. For this reason, future work continuing this thesis should be focused on different statistical indices that correlate the same data measured over the same time window. However, the same question arises for both domains: what is the allowable value or what is the appropriate time window to be measured for a signal. This has to be chosen carefully as the results will rely on it.

For future consideration is the analysis of a multiconverter case in which plenty of devices can coexist together with different modulation techniques. This is a challenging work as different devices will generate different EMI

levels. For this reason new methods or even more complex computational methods may bring solutions to problems such as the multiconverter case.

Finally, the idea of standardisation can be taken as a good starting point to define limits in conditions or environments when Crosstalk can cause major issues. The analysis carried out in this thesis can provide a good way of analysing the advantages and disadvantages of Spread Spectrum Modulation techniques and turn these ideas into an accepted framework for frequency modulation techniques.

Bibliography

[1] D. Kumar, F. Zare, and A. Gosh, "DC Microgrid Technology: System Architectures, AC Grid Interfaces, Grounding Schemes, Power Quality, Communication Networks, Applications, and Standardizations Aspects," *IEEE Access: Special Section on Power Quality and Harmonics Issues of Future and Smart Grids*, pp. 12230 – 12256, 2017. DOI: 10.1109/ACCESS.2017.2705914.

[2] "World Energy Investment 2019," *International Energy Agency - IEA May 2019*, p. 19, 2019. `https://iea.blob.core.windows.net/assets/c299fa1e-f2f4-4b81-bfb2-672d3a50ccab/WEI2019.pdf`.

[3] S. K. Rönnberg, M. H. Bollen, H. Amaris, G. W. Changc, I. Y. Gud, Łukasz H. Kocewiake, J. Meyerf, M. Olofssong, and J. D. Paulo F. Ribeiro, "On Waveform Distortion in the Frequency Range of 2 kHz – 150 kHz: Review and Research Challenges," *Electric Power Systems Research 150*, pp. 12230 – 12256, 2017. DOI: 10.1016/j.epsr.2017.04.032.

[4] "IEEE Approved Draft Standard for Low Frequency (less than 500 kHz) Narrow Band Power Line Communications for Smart Grid Applications," *P1901.2/D0.11.00, August, 2013*, pp. 1–271, 2013.

[5] R. T. Albertson, J. Arthur, and M. H. Rashid, "Overview of Electromagnetic Interference," in *2006 38th North American Power Symposium*, pp. 263–266, 2006. DOI: 10.1109/NAPS.2006.360154.

[6] A. E. Shadare, M. N. Sadiku, and S. M. Musa, "Electromagnetic Compatibility Issues in Critical Smart Grid Infrastructure," *IEEE Electromagnetic Compatibility Magazine*, vol. 6, no. 4, pp. 63–70, 2017. DOI: 10.1109/MEMC.0.8272283.

[7] R. Smolenski, A. Kempski, J. Bojarski, and P. Lezynski, "EMI generated by Power Electronic Interfaces in Smart Grids," in *International Symposium on Electromagnetic Compatibility - EMC EUROPE*, pp. 1–6, 2012. DOI: 10.1109/EMCEurope.2012.6396771.

[8] "IEEE Recommended Practice for Monitoring Electric Power Quality," *IEEE Std 1159-2019 (Revision of IEEE Std 1159-2009)*, pp. 1–98, 2019. DOI: 10.1109/IEEESTD.2019.8796486.

[9] CENELEC, "EN 50160 Voltage Characteristics of electricity supplied by public distribution systems," tech. rep., 2005.

[10] G. T. Heydt, *The Electrical Engineering Handbook*. Elsevier Inc, 2005.

[11] I. Ciornei, M. Albu, M. Sanduleac, L. Hadjidemetriou, and E. Kyriakides, "Analytical Derivation of PQ Indicators Compatible with Control Strategies for DC Microgrids," in *2017 IEEE Manchester PowerTech*, pp. 1–6, 2017. DOI: 10.1109/PTC.2017.7981179.

[12] Paul Lee, "Pre-compliance Testing the Conducted Line Emissions of DC Supplied Circuits,"

[13] X. Ye and C. Ye, "Transmission lines and signal integrity fundamentals," in *2017 IEEE International Symposium on Electromagnetic Compatibility Signal/Power Integrity (EMCSI)*, pp. 1–46, 2017. DOI: 10.1109/ISEMC.2017.8078017.

[14] Gary Breed, "Signal Integrity Basics: Digital Signals on Transmission Lines," 2005.

[15] L. Sandrolini and A. Mariscotti, "Waveform and Spectral Characteristics of Supraharmonic Unsymmetrical Conducted EMI of Switched-Mode Power Supplies," *Electronics*, vol. 11, no. 4, 2022. DOI: 10.3390/electronics11040591.

[16] D. A. Martínez and A. Pavas, "Current supraharmonics identification in commonly used low voltage devices," in *2015 IEEE Workshop on Power Electronics and Power Quality Applications (PEPQA)*, pp. 1–5, 2015. DOI: 10.1109/PEPQA.2015.7168230.

[17] M. Bollen, M. Olofsson, A. Larsson, S. Rönnberg, and M. Lundmark, "Standards for Supraharmonics (2 to 150 kHz)," *IEEE Electromagnetic Compatibility Magazine*, vol. 3, no. 1, pp. 114–119, 2014. DOI: 10.1109/MEMC.2014.6798813.

[18] S. K. Ronnberg, M. H. J. Bollen, and M. Wahlberg, "Interaction Between Narrowband Power-Line Communication and End-User Equipment," *IEEE Transactions on Power Delivery*, vol. 26, no. 3, pp. 2034–2039, 2011. DOI: 10.1109/TPWRD.2011.2130543.

[19] S. K. Rönnberg, A. G.-d. Castro, M. H. Bollen, A. Moreno-Munoz, and E. Romero-Cadaval, "Supraharmonics from power electronics converters," in *2015 9th International Conference on Compatibility and Power Electronics (CPE)*, pp. 539–544, 2015. DOI: 10.1109/CPE.2015.7231133.

[20] C. R. Paul, *Introduction to Electromagnetic Compatibility.* New Jersey: John Wiley Sons, 2nd ed., 2006.

[21] Clayton R Paul, *Transmission Lines In Digital and Analog Electronic Systems: Signal Integrity and Crosstalk.* Hoboken, New Jersey: IEEE Press - A John Wiley and Sons Inc, 2010.

[22] Mark I. Montrose and Edward M. Nakauchi, *Testing for EMC Compliance: Approaches and Techniques*. Piscataway, New Jersey: IEEE Press - Wiley-Interscience, 2004.

[23] C. Smartt *et al.*, *User Guide SACAMOS: State of the Art CAble MOdels for Spice Open Souce Cable Models for EMI Simulations*. University of Nottingham, 2018. http://128.243.70.77/UoN/SACAMOS/raw/master/DOCUMENTATION/SACAMOS_UserGuide.pdf.

[24] C. Smartt *et al.*, *Theory Manual SACAMOS: State of the Art CAble MOdels for Spice Open Souce Cable Models for EMI Simulations*. University of Nottingham, 2018. http://128.243.70.77/UoN/SACAMOS/raw/master/DOCUMENTATION/SACAMOS_TheoryManual.pdf.

[25] A. Devices, "Ltspice version 17.1.6," 2023. `https://www.analog.com/en/design-center/design-tools-and-calculators/ltspice-simulator.html`.

[26] A. E. Pena-Quintal, M. J. Basford, K. Niewiadomski, S. Greedy, M. Sumner, and D. W. P. Thomas, "Data links modelling under radiated emi and its impact on sampling errors in the physical layer," in *2020 International Symposium on Electromagnetic Compatibility - EMC EUROPE*, pp. 1–5, 2020. DOI: 10.1109/EMCEUROPE48519.2020.9245670.

[27] J. Balcells, A. Santolaria, A. Orlandi, D. Gonzalez, and J. Gago, "EMI Reduction in Switched Power Converters Using Frequency Modulation Techniques," *IEEE Transactions on Electromagnetic Compatibility*, vol. 47, no. 3, pp. 569–576, 2005. DOI: 10.1109/TEMC.2005.851733.

[28] S. A. Q. Mohammed and J.-W. Jung, "A State-of-the-Art Review on Soft-Switching Techniques for DC–DC, DC–AC, AC–DC, and AC–AC Power Converters," *IEEE Transactions on Industrial Informatics*, vol. 17, no. 10, pp. 6569–6582, 2021. DOI: 10.1109/TII.2021.3058218.

[29] IEC, "Industrial, scientific and medical equipment - Radio-frequency disturbance characteristics - Limits and methods of measurement," tech. rep., International Electrotechnical Commission, 2015.

[30] IEC, "Vehicles, boats and internal combustion engines - Radio disturbance characteristics - Limits and methods of measurement for the protection of off-board receivers," tech. rep., International Electrotechnical Commission, 2009.

[31] IEC, "Electromagnetic compatibility - Requirements for household appliances, electric tools and similar apparatus," tech. rep., International Electrotechnical Commission, 2020.

[32] IEC, "Limits and methods of measurement of radio disturbance characteristics of electrical lighting and similar equipment," tech. rep., International Electrotechnical Commission, 2018.

[33] CISPR16-1, "Specification for radio disturbance and immunity measuring apparatus and methods – Part 1-1: Radio disturbance and immunity measuring apparatus – Measuring apparatus," tech. rep., International Electrotechnical Commission, 2019.

[34] CISPR25, "Vehicles, boats and internal combustion engines – Radio disturbance characteristics – Limits and methods of measurement for the protection of on-board receivers," tech. rep., 2021.

[35] CISPR32, "Electromagnetic compatibility of multimedia equipment – Emission requirements," tech. rep., 2021.

[36] Pico Technology, *PicoScope® 5000D Series - FlexRes® oscilloscopes and MSOs*. https://www.picotech.com/download/datasheets/picoscope-5000d-series-data-sheet.pdf.

[37] P. Russer, "EMC Measurements in the Time-domain," in *2011 XXXth URSI General Assembly and Scientific Symposium*, pp. 1–35, 2011. DOI: 10.1109/URSIGASS.2011.6050792.

[38] Dieter Schwarzbeck, "The EMI-Receiver According to CISPR 16-1-1." https://www.schwarzbeck.de/appnotes/EMIRcvrCISPR16.pdf.

[39] S. Braun, M. Al-Qedra, and P. Russer, "A Novel Realtime Time-domain EMI Measurement System Based on Field Programmable Gate Arrays," in *2006 17th International Zurich Symposium on Electromagnetic Compatibility*, pp. 501–504, 2006. DOI: 10.1109/EMCZUR.2006.214981.

[40] S. Braun, "A Novel time-domain EMI Measurement System for Measurement and Evaluation of Discontinuous Disturbance According to CISPR 14 and CISPR 16," in *2011 IEEE International Symposium on Electromagnetic Compatibility*, pp. 480–483, 2011. DOI: 10.1109/ISEMC.2011.6038359.

[41] F. Krug, S. Braun, Y. Kishida, and P. Russer, "A Novel Digital Quasi-Peak Detector for Time-Domain Measurements," in *2003 33rd European Microwave Conference*, pp. 1027–1030, 2003. DOI: 10.1109/EUMA.2003.340834.

[42] T. Williams, *EMC for Product Designers*. Elsevier Science, 5th ed., 2016.

[43] M. J. Basford, C. Smartt, D. W. P. Thomas, and S. Greedy, "On the Disruption of Wired Serial Communication Links by Time

Domain Interference," *2018 IEEE International Symposium on Electromagnetic Compatibility and 2018 IEEE Asia-Pacific Symposium on Electromagnetic Compatibility (EMC/APEMC)*, pp. 183–186, 2018. DOI: 10.1109/ISEMC.2018.8393763.

[44] Li, Ke-Jie and Xie, Yan-Zhao and Zhang, Fan and Chen, Yu-Hao, "Statistical Inference of Serial Communication Errors Caused by Repetitive Electromagnetic Disturbances," *IEEE Transactions on Electromagnetic Compatibility*, vol. 62, no. 4, pp. 1160–1168, 2020. DOI: 10.1109/TEMC.2019.2932855.

[45] Li, Yadong and Li, Danlan and Cui, Wenqiang and Zhang, Rui, "Research Based on OSI Model," pp. 554–557, 2011. DOI: 10.1109/ICCSN.2011.6014631.

[46] A. J. Jerri, *The Gibbs Phenomenom in Fourier Analysis, Splines and Wavelet Approximations*. Postdam, New York, USA: Springer Sicence Bussines Media B.V., 1st ed., 1998.

[47] N. Marda, G. Vaishnav, and U. S. N. Rao, "Bit Error Rate Testing Scheme for Digital Communication Devices," in *Proceedings of The 2014 International Conference on Control, Instrumentation, Energy and Communication (CIEC)*, pp. 490–493, 2014. DOI: 10.1109/CIEC.2014.6959137.

[48] M. Jeruchim, "Techniques for Estimating the Bit Error Rate in the Simulation of Digital Communication Systems," *IEEE Journal on Selected Areas in Communications*, vol. 2, no. 1, pp. 153–170, 1984. DOI: 10.1109/JSAC.1984.1146031.

[49] "BER – Is it Bit Error Rate or Bit Error Ratio?." `https://blogs.keysight.com/blogs/tech.entry.html/2019/03/10/ber_is_it_bit_erro-PlIE.html`.

[50] M. A. Mannah, N. Ginot, and C. Batard, "Effect of the Power Cable on Data Transmission Over a Pulse Width Modulated Network," *IEEE Transactions on Industrial Electronics*, vol. 61, no. 8, pp. 4238–4245, 2014. DOI: 10.1109/TIE.2013.2288189.

[51] K. Mainali and R. Oruganti, "Conducted EMI Mitigation Techniques for Switch-Mode Power Converters: A Survey," *IEEE Transactions on Power Electronics*, vol. 25, no. 9, pp. 2344–2356, 2010. DOI: 10.1109/TPEL.2010.2047734.

[52] D. Thomas, "Conducted Emissions in Distribution Systems (1 kHz–1 MHz)," *IEEE Electromagnetic Compatibility Magazine*, vol. 2, no. 2, pp. 101–104, 2013. DOI: 10.1109/MEMC.2013.6550941.

[53] A. Nagel and R. De Doncker, "Systematic design of EMI-filters for power converters," in *Conference Record of the 2000 IEEE Industry Applications Conference. Thirty-Fifth IAS Annual Meeting and World Conference on Industrial Applications of Electrical Energy (Cat. No.00CH37129)*, vol. 4, pp. 2523–2525 vol.4, 2000. DOI: 10.1109/IAS.2000.883177.

[54] C. Wenjie, Y. Xu, and W. Zhaoan, "Design and evaluation of an input active emi filter for integrated power electronics modules," in *2005 IEEE 36th Power Electronics Specialists Conference*, pp. 309–312, 2005. DOI: 10.1109/PESC.2005.1581640.

[55] M. Hartmann, H. Ertl, and J. W. Kolar, "EMI Filter Design for a 1 MHz, 10 kW Three-Phase/Level PWM Rectifier," *IEEE Transactions on Power Electronics*, vol. 26, no. 4, pp. 1192–1204, 2011. DOI: 10.1109/TPEL.2010.2070520.

[56] M. Caponet, F. Profumo, and A. Tenconi, "EMI filters design for power electronics," in *2002 IEEE 33rd Annual IEEE Power*

Electronics Specialists Conference. Proceedings (Cat. No.02CH37289), vol. 4, pp. 2027–2032 vol.4, 2002. DOI: 10.1109/PSEC.2002.1023112.

[57] Y. Zhenyang, W. Shishan, S. Zheng, and B.-L. Lee, "The reviews of integrated EMI filters applied in power electronic system," in *2015 Asia-Pacific Symposium on Electromagnetic Compatibility (APEMC)*, pp. 227–230, 2015. DOI: 10.1109/APEMC.2015.7175240.

[58] S. Ye, W. Eberle, and Y.-F. Liu, "A novel EMI filter design method for switching power supplies," *IEEE Transactions on Power Electronics*, vol. 19, no. 6, pp. 1668–1678, 2004. DOI: 10.1109/TPEL.2004.836629.

[59] C. Paul and K. Hardin, "Diagnosis and reduction of conducted noise emissions," *IEEE Transactions on Electromagnetic Compatibility*, vol. 30, no. 4, pp. 553–560, 1988. DOI: 10.1109/15.8769.

[60] A. Riccobono and E. Santi, "Comprehensive Review of Stability Criteria for DC Power Distribution Systems," *IEEE Transactions on Industry Applications*, vol. 50, no. 5, pp. 3525–3535, 2014. DOI: 10.1109/TIA.2014.2309800.

[61] T. Hegarty, "The Engineer's Guide To EMI In DC-DC Converters (Part 10): Input Filter Impact On Stability," *How 2 Power Desing Today - Exclusive Technology Feature*, 2019.

[62] H. A. Huynh, S. Joo, and S. Kim, "An experimental study of EMI reduction of DC-DC converter with frequency hopping technique," in *2016 IEEE Electrical Design of Advanced Packaging and Systems (EDAPS)*, pp. 107–109, 2016. DOI: 10.1109/EDAPS.2016.7893138.

[63] L. Comstock, H. Rakouth, and J. Ruiz, "Reduction in radio interference through pwm frequency dithering," in *2006 IEEE International*

Symposium on Electromagnetic Compatibility, 2006. EMC 2006., vol. 3, pp. 615–619, 2006. DOI: 10.1109/ISEMC.2006.1706384.

[64] R. Scholtz, "Notes on Spread-Spectrum History," *IEEE Transactions on Communications*, vol. 31, no. 1, pp. 82–84, 1983. DOI: 10.1109/TCOM.1983.1095718.

[65] R. Scholtz, "The Origins of Spread-Spectrum Communications," *IEEE Transactions on Communications*, vol. 30, no. 5, pp. 822–854, 1982. DOI: 10.1109/TCOM.1982.1095547.

[66] R. John, G. Dirk, and S. Mike, "Understanding Noise-Spreading Techniques and their Effects in Switch-Mode Power Applications," 2008.

[67] Texas Instruments, *LM62460, LM61480, and LM61495 Pin-Compatible 6-A/8-A/10-A Buck Converter Optimized for Power Density and Low EM*. SNVSBZ4A – FEBRUARY 2020 – REVISED NOVEMBER 2021.

[68] Texas Instruments, *LM25148-Q1 42-V Automotive Synchronous Buck DC/DC Controller with Ultra-Low IQ and Dual Random Spread Spectrum*. SNVSC03 – JUNE 202.

[69] N. Sudhakar, N. Rajasekar, and S. A. Shanmuga, "FPGA Based Chaotic PWM Combined with Soft Switching for Effective EMI Mitigation in Boost Converter," in *2016 International Conference on Energy Efficient Technologies for Sustainability (ICEETS)*, pp. 148–152, 2016. DOI: 10.1109/ICEETS.2016.7582915.

[70] G. Marsala and A. Ragusa, "Chaos PWM for EMI Reduction in a High Boost DC-DC Converter with Coupled Inductors," in *2017*

IEEE 5th International Symposium on Electromagnetic Compatibility (EMC-Beijing), pp. 1–6, 2017. DOI: 10.1109/EMC-B.2017.8260349.

[71] K. Mina, P. Hwa-Pyeong, and J. Jee-Hoon, "Spread Spectrum Technique With Random-Linear Modulation for EMI Mitigation and Audible Noise Elimination in IH Appliances," *IEEE Transactions on Industrial Electronics*, vol. 69, no. 8, pp. 8589–8593, 2022. DOI: 10.1109/TIE.2021.3102405.

[72] O. Trescases, G. Wei, A. Prodic, and W. T. Ng, "An EMI Reduction Technique for Digitally Controlled SMPS," *IEEE Transactions on Power Electronics*, vol. 22, no. 4, pp. 1560–1565, 2007. DOI: 10.1109/TPEL.2007.901911.

[73] A. Pena-Quintal, K. Niewiadomski, V. Muneeswaran, S. Greedy, M. Sumner, and D. W. P. Thomas, "The Effect of Spread Spectrum Modulation for a Buck Converter Coupled with a Single Wired Communication Link," in *2021 IEEE International Joint EMC/SI/PI and EMC Europe Symposium*, pp. 445–450, 2021. DOI: 10.1109/EMC/SI/PI/EMCEurope52599.2021.9559276.

[74] H. Skinner and K. Slattery, "Why Spread Spectrum Clocking of Computing Devices is not Cheating," in *2001 IEEE EMC International Symposium. Symposium Record. International Symposium on Electromagnetic Compatibility (Cat. No.01CH37161)*, vol. 1, pp. 537–540 vol.1, 2001. DOI: 10.1109/ISEMC.2001.950699.

[75] R. Mukherjee, A. Patra, and S. Banerjee, "Impact of a Frequency Modulated Pulsewidth Modulation (PWM) Switching Converter on the Input Power System Quality," *IEEE Transactions on Power Electronics*, vol. 25, no. 6, pp. 1450–1459, 2010. DOI: 10.1109/TPEL.2009.2037421.

[76] F. Pareschi, R. Rovatti, and G. Setti, "EMI Reduction via Spread Spectrum in DC/DC Converters: State of the Art, Optimization, and Tradeoffs," *IEEE Access*, vol. 3, pp. 2857–2874, 2015. DOI: 10.1109/ACCESS.2015.2512383.

[77] Uluişik and L. Sevgi, "A Tutorial on Bessel Functions and Numerical Evaluation of Bessel Integrals," *IEEE Antennas and Propagation Magazine*, vol. 51, no. 6, pp. 222–233, 2009. DOI: 10.1109/MAP.2009.5433159.

[78] B. Deutschmann, G. Winkler, and T. Karaca, "Emission Reduction in Class D Audio Amplifiers by Optimizing Spread Spectrum Modulation," in *2015 10th International Workshop on the Electromagnetic Compatibility of Integrated Circuits (EMC Compo)*, pp. 1–6, 2015. DOI: 10.1109/EMCCompo.2015.7358320.

[79] B. Deutschmann, B. Auinger, and G. Winkler, "Spread Spectrum Parameter Optimization to Suppress Certain Frequency Spectral Components," in *2017 11th International Workshop on the Electromagnetic Compatibility of Integrated Circuits (EMCCompo)*, pp. 39–44, 2017. DOI: 10.1109/EMCCompo.2017.7998078.

[80] Francesco Vasca and Luigi Iannelli, *Dynamics and Control of Switched Electronic Systems - Advanced Perspectives for Modeling, Simulation and Control of Power Converters*. Springer, 2012.

[81] IEC, "Electromagnetic Compatibility (EMC) - Part 4-7: Testing and Measurement Techniques – General Guide on Harmonics and Interharmonics Measurements and Instrumentation, for Power supply systems and equipment connected thereto," tech. rep., International Electrotechnical Commission, 2002.

[82] H. Loschi, P. Lezynski, R. Smolenski, D. Nascimento, and W. Sleszynski, "FPGA-Based System for Electromagnetic Interference Evaluation in Random Modulated DC/DC Converters," *Energies*, vol. 13, no. 9, 2020. DOI: 10.3390/en13092389.

[83] P. Lezynski, R. Smolenski, H. Loschi, D. Thomas, and N. Moonen, "A Novel Method for EMI Evaluation in Random Modulated Power Electronic Converters," *Measurement*, vol. 151, p. 107098, 2020. DOI: 10.1016/j.measurement.2019.107098.

[84] H. Loschi, R. Smolenski, P. Lezynski, W. El Sayed, and D. Nascimento, "Reduction of Conducted Emissions in DC/DC Converters with FPGA-based Random Modulation," in *2020 International Symposium on Electromagnetic Compatibility - EMC EUROPE*, pp. 1–6, 2020. DOI: 10.1109/EMCEUROPE48519.2020.9245684.

[85] H. Loschi, R. Smolenski, P. Lezynski, D. Nascimento, and G. Demidova, "Aggregated Conducted Electromagnetic Interference Generated by DC/DC Converters with Deterministic and Random Modulation," *Energies*, vol. 13, no. 14, 2020. DOI: 10.3390/en13143698.

[86] Mathias Keller, "Comparison of Time Domain Scans and Stepped Frequency Scans in EMI Test Receivers," tech. rep., Rohde & Schwarz. "`https://cdn.rohde-schwarz.com/pws/dl_downloads/dl_application/application_notes/1ee24/1EE24_1e_ESR_Time_Domain_Scan.pdf`".

[87] BK Precision Corp, *Datasheet - Programmable DC Power Supplies XLN Series*. `https://docs.rs-online.com/40bf/A700000007848399.pdf`.

[88] Schwarzbeck Mess, *NSLK 8127 Artificial Mains Network - Rev. A*. `https://schwarzbeck.de/Datenblatt/k8127.pdf`.

[89] Rohde and Schwarz, *RS®ESL EMI Test Receiver Compact, cost-effective measuring receiver.* https://scdn.rohde-schwarz.com/ur/pws/dl_downloads/dl_common_library/dl_brochures_and_datasheets/pdf_1/ESL_dat-sw_en_5214-0430-22_v0300.pdf.

[90] Cree Wolfspeed, "KIT8020CRD8FF1217P-1 CREE Silicon Carbide MOSFET Evaluation Kit." https://media.digikey.com/pdf/Data%20Sheets/CREE%20Power/KIT8020CRD8FF1217P-1_UM.pdf.

[91] Musolino, Francesco and Crovetti, Paolo S., "Interference of Spread-Spectrum Switching-Mode Power Converters and Low-Frequency Digital Lines," in *2018 IEEE International Symposium on Circuits and Systems (ISCAS)*, pp. 1–5, 2018. DOI: 10.1109/ISCAS.2018.8351815.

[92] P. S. Crovetti and F. Musolino, "Interference of Spread-Spectrum EMI and Digital Data Links under Narrowband Resonant Coupling," *Electronics*, vol. 9, no. 1, 2020. DOI: 10.3390/electronics9010060.

[93] W. E. Sayed, P. Lezynski, R. Smolenski, N. Moonen, P. Crovetti, and D. W. P. Thomas, "The Effect of EMI Generated from Spread-Spectrum-Modulated SiC-Based Buck Converter on the G3-PLC Channel," *Electronics*, vol. 10, no. 12, 2021. DOI: 10.3390/electronics10121416.

[94] Keysight, "How to Measure Bit Error Rate (BER)?." Accessed Apr. 18, 2017 [Online]. https://www.keysight.com/zz/en/assets/7018-06435/white-papers/5992-3524.pdf.

[95] Anritsu, "MP8931A Bit Error Rate Tester Operation Manual," 2003. https://usermanual.wiki/m/f17801b27f27b8f13fcf7b7d066a9e986f17e80573b81827e4a1eca8ef32fe8a.pdf.

[96] National Instruments, "Labview," 2018. https://www.ni.com/en-gb/support/downloads/software-products/download.labview.html#460283.

[97] Pierre Morel, "Gramm: Grammar of Graphics Plotting in Matlab," *The Journal of Open Source Software*, vol. 3, p. 568, mar 2018. DOI: 10.21105/joss.00568.

[98] Sarwate, D.V. and Pursley, M.B., "Crosscorrelation properties of pseudorandom and related sequences," *Proceedings of the IEEE*, vol. 68, no. 5, pp. 593–619, 1980. DOI: 10.1109/PROC.1980.11697.

[99] Ashish Kumar Srivastav, "Pearson Correlation Coefficient." https://www.wallstreetmojo.com/pearson-correlation-coefficient/.

[100] A. Pena-Quintal, K. Niewiadomski, S. Greedy, M. Sumner, and D. Thomas, "The Influence of the Number of Frequencies and the Frequency Repetitions Rates in Spread Spectrum Sigma-Delta Modulated DC-DC Converters," in *2021 Asia-Pacific International Symposium on Electromagnetic Compatibility (APEMC)*, pp. 1–4, 2021. DOI: 10.1109/APEMC49932.2021.9597184.

[101] GAUSS INSTRUMENTS International GmbH, "TDEMI X - 64000 Times Faster Than Conventional EMI Receivers," 2022. https://www.gauss-instruments.com/images/datasheets/TDEMI_X_series_productcatalog.pdf.

Appendix A

Cispr 16 Main parameters

Table A.1: CISPR 16 Band Parameters.

CISPR Band	A	B	C	D	E
Frequency Range	9 kHz - 150 kHz	150 kHz - 30 MHz	30 MHz - 300 MHz	300 MHz - 1 GHz	1 GHz - 18 GHz
BW B6	200 Hz	9 kHz	120 kHz	120 kHz	1 MHz - 18 GHz
QP Charge Time Constant	45 ms	1 ms	1 ms	1 ms	not defined
QP Discharge Time Constant	500 ms	160 ms	550 ms	550 ms	not defined
Meter Time Constant	160 ms	160 ms	100 ms	100 ms	not defined

Appendix B

Picoscope 5444D Main Features

Table B.1: Picoscope important parameters.

Technical specification	**Value**
Resolution Bandwidth	200 MHz
Vertical Resolution	8, 12, 14, 15 or 16 bits
Input sensitivity	2 mV/div to 4 V/div
Offset accuracy	±500 µV ±1% of full scale
Analog offset range (vertical position adjust)	±250 mV (10, 20, 50, 100, 200 mV ranges), ±2.5 V (500 mV, 1 V, 2 V ranges) ±20 V (5, 10, 20 V ranges)
Analog offset control accuracy	±0.5% of offset setting, additional to basic DC offset accuracy
Noise (on ±10 mV range)	8-bit mode: 120 μV RMS 12-bit mode: 110 μV RMS 14-bit mode: 100 μV RMS 15-bit mode: 85 μV RMS 16-bit mode: 70 μV RMS

Appendix C

Bessel Function of its First Kind

The values of J_x are obtained from the solution of the Bessel function of first kind. To provide a practical understanding the Bessel function can be represented by a second order differential equation as shown in Equation C.1,

$$x^2\frac{d^2y}{dx^2} + x\frac{dy}{dx} + (x^2 - v^2)y = 0 \tag{C.1}$$

Due to the nature of the Bessel function as a second-order differential equation, there must exist two linearly independent solutions as shown,

$$y = AJ_v(x) + BY_v(x) \tag{C.2}$$

The Bessel function can be represented as using an infinite power series expansion as follows,

$$J_v(x) = \sum_{k=0}^{\infty} \frac{(-1)^k(x/2^{v+2k})}{k!\Gamma(v+k+1)} \tag{C.3}$$

Which produces,

$$J_v(x) = \frac{1}{\Gamma(1+v)} \left(\frac{x}{2}\right)^v \left\{1 - \frac{(x/2)^2}{1(1+v)} \left(1 - \frac{(x/2)^2}{2(2+v)} \left(1 - \frac{(x/2)^2}{3(3+v)}(1 - ...\right)\right)\right\} \tag{C.4}$$

Appendix D

Measurements of Spread Spectrum at Zielona Gora

The value of β refers on how fast the signal is sampled according to a certain maximum sampling frequency. The maximum frequency is 100 kHZ.

D.1 Sine wave profile

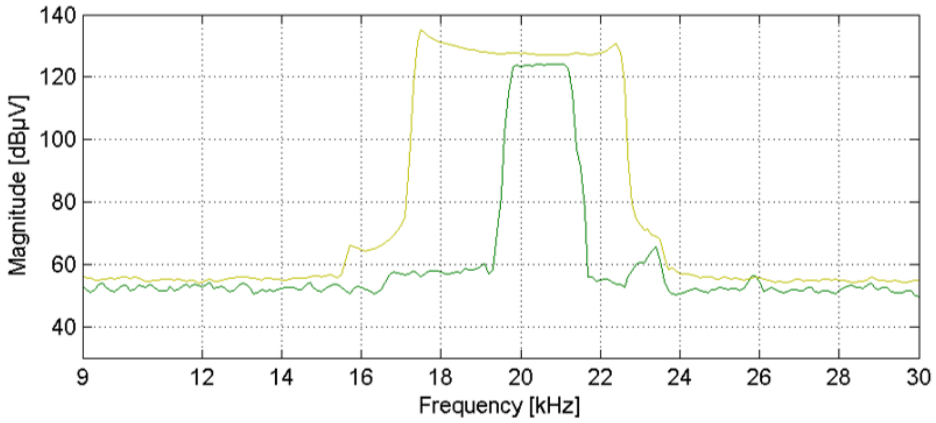

Figure D.1: Spectrum for a sine wave signal when $\beta = 5000$.

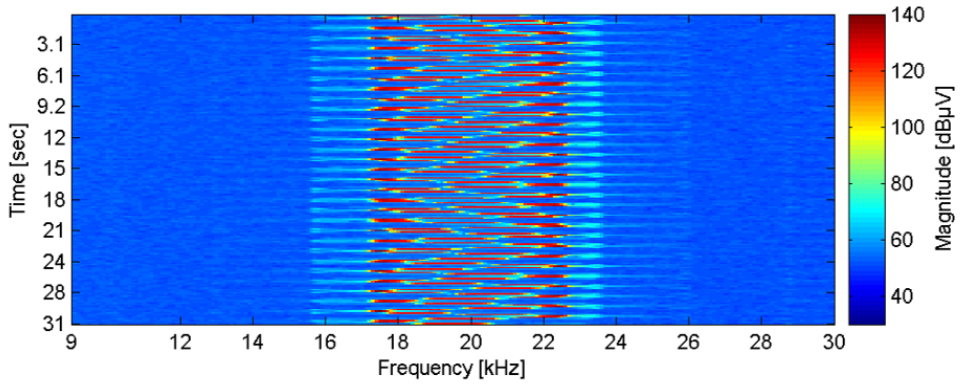

Figure D.2: Spectrogram for a sine wave signal when $\beta = 5000$.

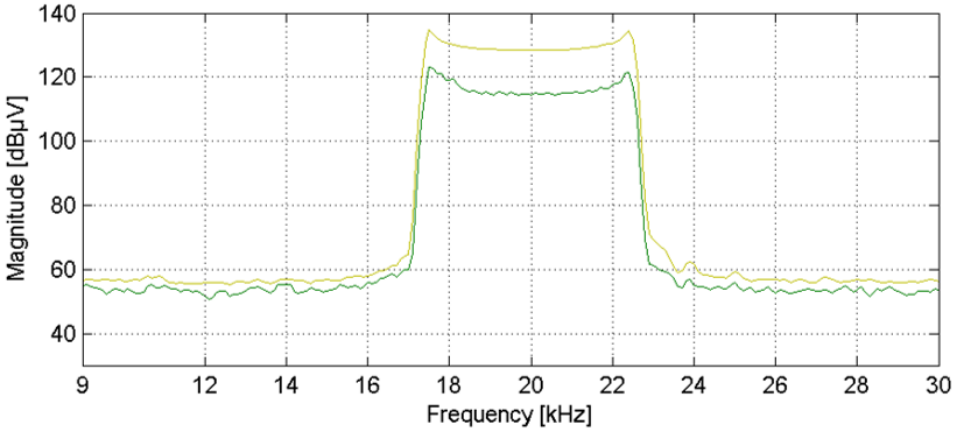

Figure D.3: Spectrum for a sine wave signal when $\beta = 500$.

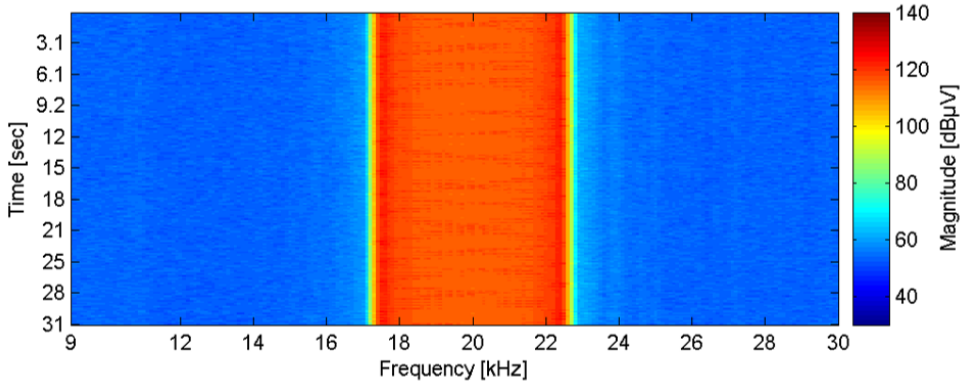

Figure D.4: Spectrogram for a sine wave signal when $\beta = 500$.

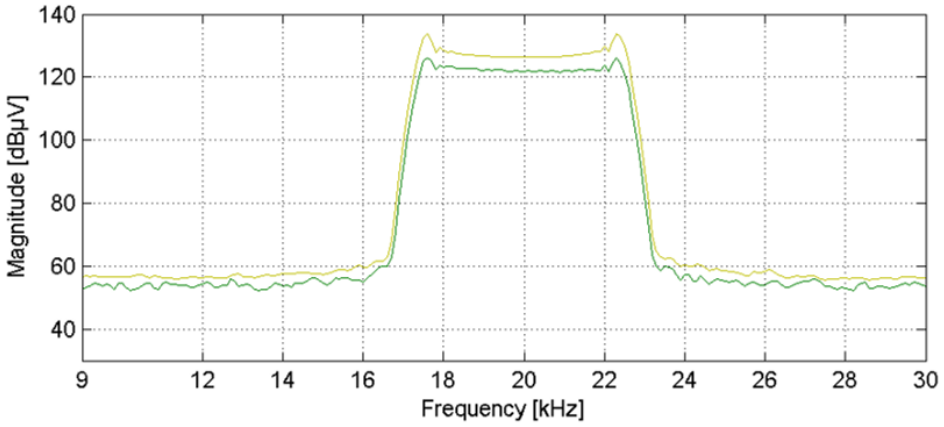

Figure D.5: Spectrum for a sine wave signal when $\beta = 100$.

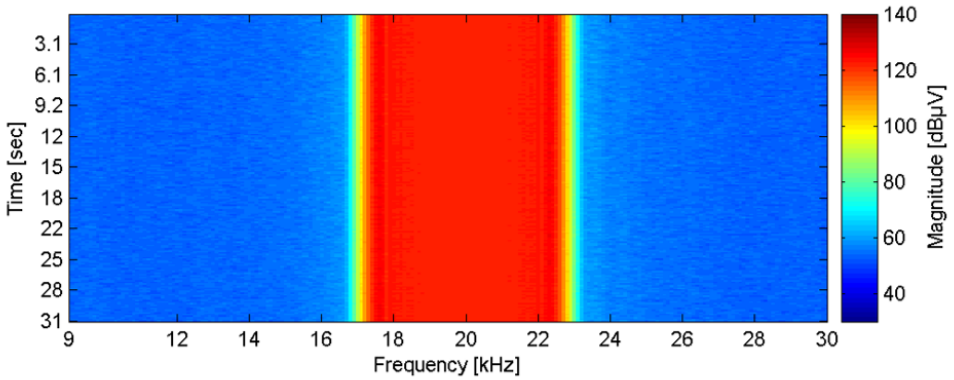

Figure D.6: Spectrogram for a sine wave signal when $\beta = 100$.

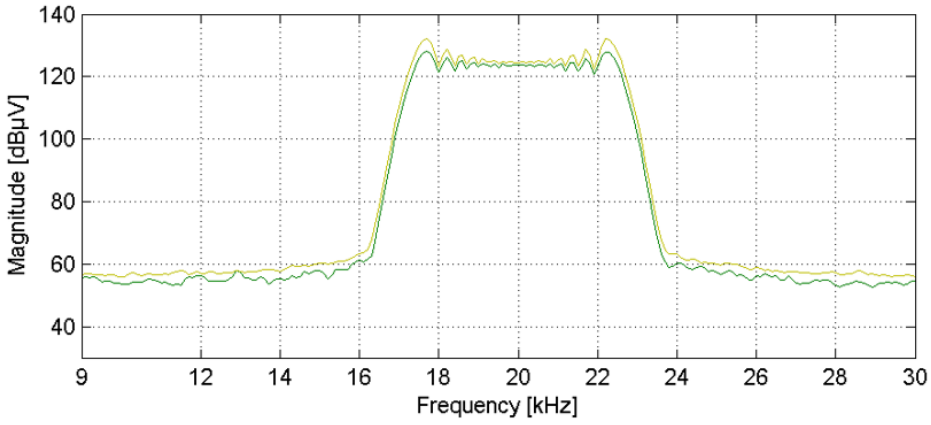

Figure D.7: Spectrum for a sine wave signal when $\beta = 50$.

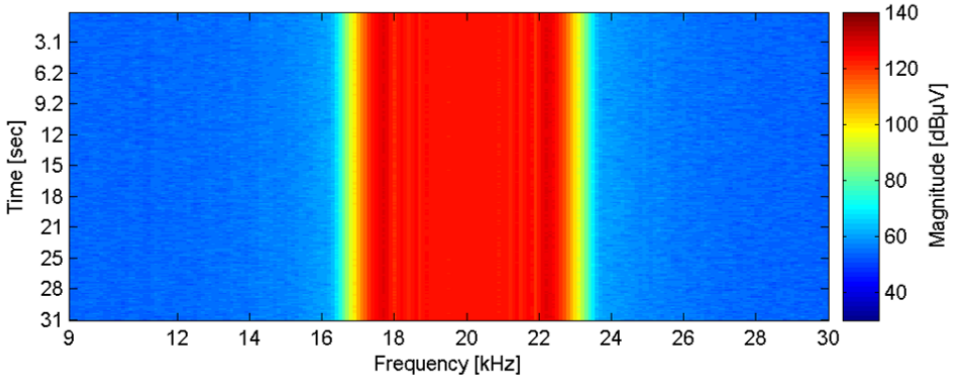

Figure D.8: Spectrogram for a sine wave signal when $\beta = 50$.

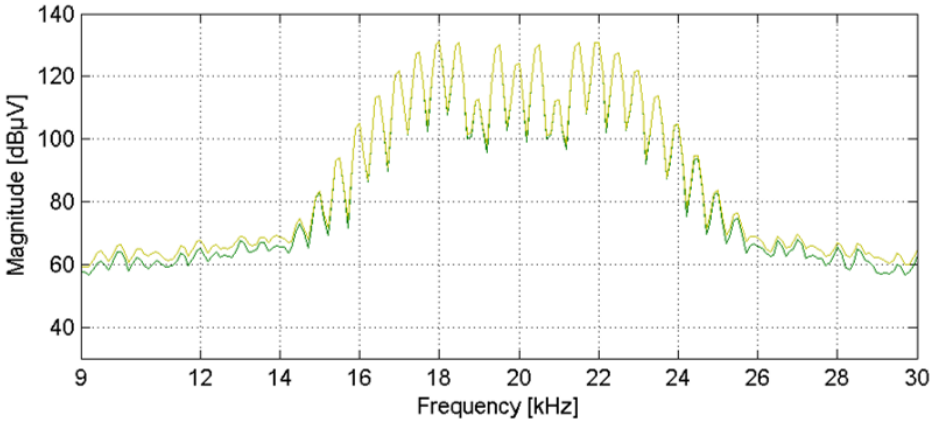

Figure D.9: Spectrum for a sine wave signal when $\beta = 10$.

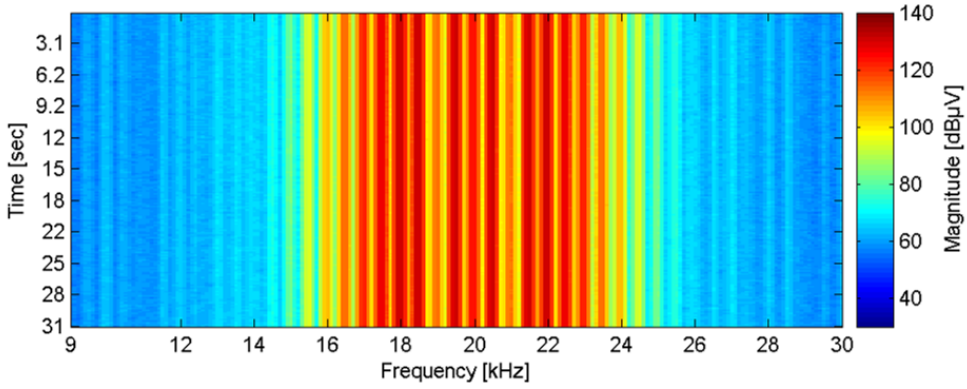

Figure D.10: Spectrogram for a sine wave signal when $\beta = 10$.

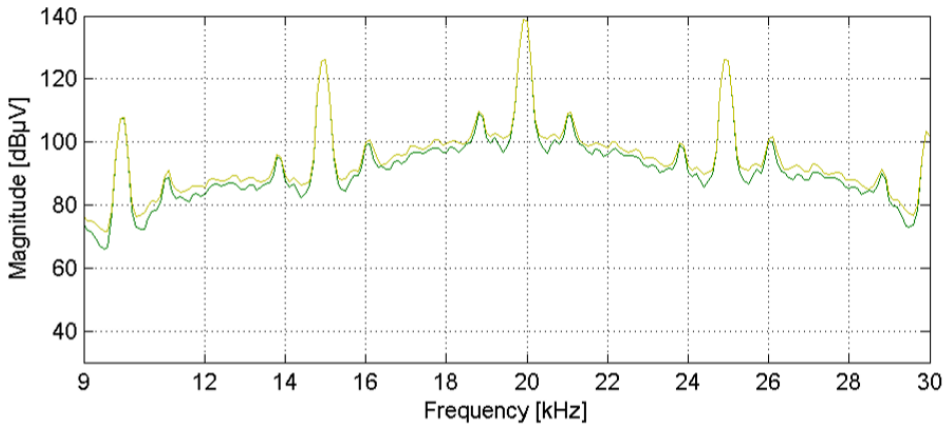

Figure D.11: Spectrum for a sine wave signal when $\beta = 1$.

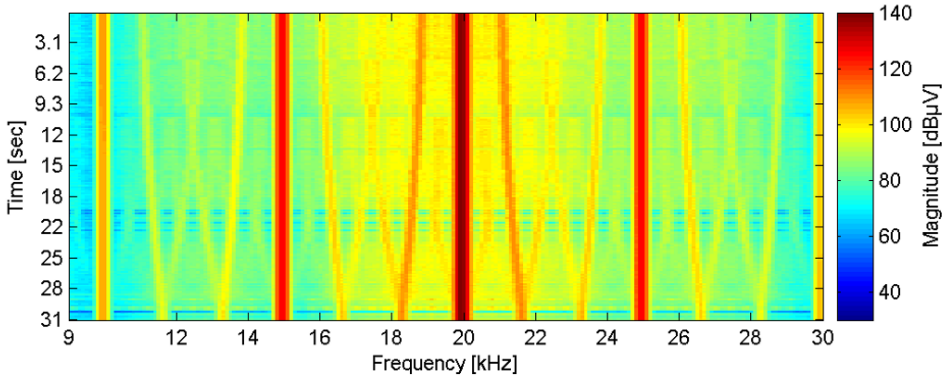

Figure D.12: Spectrogram for a sine wave signal when $\beta = 1$.

Appendix E

CREE Board Information

Table E.1: Main parameters for the CREE board development board.

Component	***Value/Specification***
Transistor	C2M0080120D
V_{DS}	1200 V
$i_{d(max)}$	36 A
t_{on}	5.2 nS
t_{off}	10.8 nS
$R_{DS(on)}$	80 mΩ
Diode	C4D20120D
V_{rrm}	1200 V
i_f	33 A
Q_c	104 nC

Appendix F

Labview Control Block for the BERT

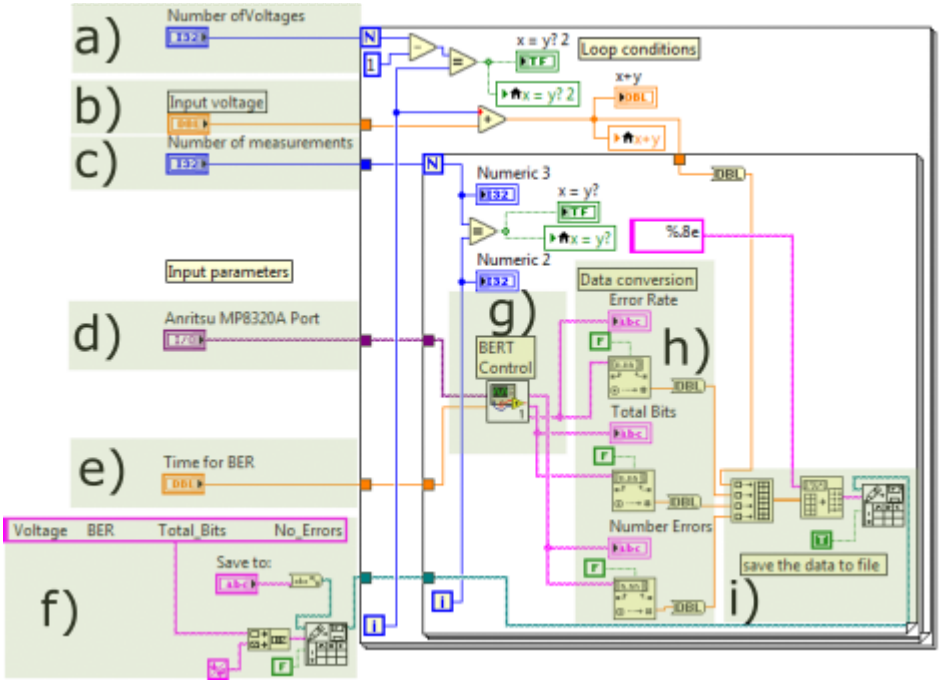

Figure F.1: Programmed flowchart block in Labview for the control of the BERT.

- a) Number of voltages. This defines the number of voltages to measure, this parameter controls the maximum count to be reached for directly controlling the power supply.

- b) Input voltage. This defines the starting value of the voltage for the power supply.

- c) Number of measurements. This value defines the number of times a measurement with the same voltage has to be obtained.

- c) Anritsu MP8320A Port. This parameter defines the Serial Port to be used by the BERT and allows the Labview interface to control the equipment.

- d) Time for BER. An important parameter to determine the effect of the interference over a desired time. The BERT program is ready to measure any time in a minute time base.

- f) Time for BER. The blank array of data is defined in this parameter, four values are taken in order to generate a list for the voltage defined.

- g) BERT Control. In this block all the registers to control the main parameters of the BERT are programmed. In this block it is possible to change the data type, frequency of data, etc.

- h) Data conversion. The measured values from the BERT are obtained and converted from text to decimal.

- i) Data save. In this part the data converted is transferred to the "txt" file generated.

Appendix G

BER and PK values Results

Table G.1: Analysis of BER for **Sine Signal** with α= **45%** and EMI Receiver result.

	Sine Wave				
m	BER Mean	Q1	Q2	Q3	PK (dBμV)
0.01125	**1.041E-02**	1.040E-02	1.040E-02	1.050E-02	100.86
0.05625	1.146E-02	1.140E-02	1.150E-02	1.150E-02	102.78
0.1125	1.289E-02	1.290E-02	1.290E-02	1.300E-02	102.80
0.5625	1.193E-02	1.190E-02	1.190E-02	1.200E-02	98.79
1.125	1.203E-02	1.195E-02	1.210E-02	1.230E-02	**97.75**
5.625	1.305E-02	1.300E-02	1.300E-02	1.310E-02	106.04
11.25	1.311E-02	1.310E-02	1.310E-02	1.310E-02	108.99
56.25	**1.320E-02**	1.320E-02	1.320E-02	1.320E-02	**111.82**
112.5	1.315E-02	1.310E-02	1.310E-02	1.320E-02	111.33

Table G.2: Analysis of BER for **Random Signal** with α= **45%** and EMI Receiver result.

	Random Wave				
m	BER Mean	Q1	Q2	Q3	PK (dBμV)
0.01125	1.706E-02	1.700E-02	1.710E-02	1.710E-02	101.34
0.05625	1.750E-02	1.750E-02	1.750E-02	1.750E-02	101.58
0.1125	**1.773E-02**	1.290E-02	1.290E-02	1.300E-02	102.02
0.5625	1.312E-02	1.190E-02	1.190E-02	1.200E-02	99.32
1.125	9.491E-03	1.195E-02	1.210E-02	1.230E-02	**99.24**
5.625	**8.493E-03**	1.300E-02	1.300E-02	1.310E-02	102.4
11.25	8.550E-03	1.310E-02	1.310E-02	1.310E-02	104.34
56.25	8.624E-3	1.320E-02	1.320E-02	1.320E-02	110.05
112.5	9.471E-3	1.310E-02	1.310E-02	1.320E-02	**111.44**

Table G.3: Analysis of BER for **Sine** Signal with α= 35% and EMI Receiver result.

	Sine Wave				
m	BER Mean	Q1	Q2	Q3	PK (dBμV)
0.00875	2.871E-03	1.040E-02	1.040E-02	1.050E-02	101.47
0.04375	2.967E-03	1.140E-02	1.150E-02	1.150E-02	103.28
0.0875	2.862E-03	1.290E-02	1.290E-02	1.300E-02	103.24
0.4375	**2.068E-03**	1.190E-02	1.190E-02	1.200E-02	98.95
0.875	2.283E-03	1.195E-02	1.210E-02	1.230E-02	**97.89**
4.375	2.950E-03	1.300E-02	1.300E-02	1.310E-02	105.88
8.75	3.393E-03	1.310E-02	1.310E-02	1.310E-02	108.74
43.75	**3.413E-03**	1.320E-02	1.320E-02	1.320E-02	111.26
87.5	2.985E-03	1.310E-02	1.310E-02	1.320E-02	**111.06**

Table G.4: Analysis of BER for **Random** Signal with α= 35% and EMI Receiver result.

	Random Wave				
m	BER Mean	Q1	Q2	Q3	PK (dBμV)
0.00875	1.706E-02	1.700E-02	1.710E-02	1.710E-02	103.57
0.04375	1.750E-02	1.750E-02	1.750E-02	1.750E-02	103.8
0.0875	**1.773E-02**	1.290E-02	1.290E-02	1.300E-02	103.63
0.4375	1.312E-02	1.190E-02	1.190E-02	1.200E-02	100.5
0.875	9.491E-03	1.195E-02	1.210E-02	1.230E-02	**99.84**
4.375	**8.493E-03**	1.300E-02	1.300E-02	1.310E-02	103.00
8.75	8.550E-03	1.310E-02	1.310E-02	1.310E-02	103.01
43.75	8.624E-3	1.320E-02	1.320E-02	1.320E-02	109.95
87.5	9.471E-3	1.310E-02	1.310E-02	1.320E-02	**110.48**

Table G.5: Analysis of BER for Sine Signal with α= 25% and EMI Receiver result.

	Sine Wave				
m	BER Mean	Q1	Q2	Q3	PK (dBμV)
0.00625	1.29E-03	1.040E-02	1.040E-02	1.050E-02	102.05
0.03125	1.40E-03	1.140E-02	1.150E-02	1.150E-02	103.96
0.0625	1.49E-03	1.290E-02	1.290E-02	1.300E-02	104.14
0.3125	1.40E-03	1.190E-02	1.190E-02	1.200E-02	99.27
0.625	1.62E-03	1.195E-02	1.210E-02	1.230E-02	**98.31**
3.125	**1.69E-03**	1.300E-02	1.300E-02	1.310E-02	106.16
6.25	1.36E-03	1.310E-02	1.310E-02	1.310E-02	108.39
31.25	**1.28E-03**	1.320E-02	1.320E-02	1.320E-02	110.57
62.5	1.29E-03	1.310E-02	1.310E-02	1.320E-02	**110.69**

Table G.6: Analysis of BER for Random Signal with α= 25% and EMI Receiver result.

	Random Wave				
m	BER Mean	Q1	Q2	Q3	PK (dBμV)
0.00625	**4.42E-03**	1.040E-02	1.040E-02	1.050E-02	104.44
0.03125	2.28E-03	1.140E-02	1.150E-02	1.150E-02	104.65
0.0625	2.01E-03	1.290E-02	1.290E-02	1.300E-02	105.31
0.3125	1.36E-03	1.190E-02	1.190E-02	1.200E-02	**101.31**
0.625	1.32E-03	1.195E-02	1.210E-02	1.230E-02	101.60
3.125	1.09E-03	1.300E-02	1.300E-02	1.310E-02	103.74
6.25	**1.04E-03**	1.310E-02	1.310E-02	1.310E-02	104.52
31.25	1.14E-03	1.320E-02	1.320E-02	1.320E-02	108.99
62.5	3.33E-03	1.310E-02	1.310E-02	1.320E-02	**110.40**

Table G.7: Analysis of BER for Sine Signal with α= 15% and EMI Receiver result.

	Sine Wave				
m	BER Mean	Q1	Q2	Q3	PK (dBμV)
0.00375	**9.17E-04**	1.040E-02	1.040E-02	1.050E-02	105.23
0.01875	9.66E-04	1.140E-02	1.150E-02	1.150E-02	107.69
0.0375	**7.27E-04**	1.290E-02	1.290E-02	1.300E-02	105.36
0.1875	7.69E-04	1.190E-02	1.190E-02	1.200E-02	100.23
0.375	7.91E-04	1.195E-02	1.210E-02	1.230E-02	**99.22**
1.875	8.02E-04	1.300E-02	1.300E-02	1.310E-02	106.53
3.75	8.31E-04	1.310E-02	1.310E-02	1.310E-02	108.53
18.75	8.40E-04	1.320E-02	1.320E-02	1.320E-02	**110.38**
37.5	8.32E-04	1.310E-02	1.310E-02	1.320E-02	110.06

Table G.8: Analysis of BER for Random Signal with α= 15% and EMI Receiver result.

	Random Wave				
m	BER Mean	Q1	Q2	Q3	PK (dBμV)
0.00375	3.974E-04	1.040E-02	1.040E-02	1.050E-02	107.69
0.01875	**4.068E-04**	1.140E-02	1.150E-02	1.150E-02	107.5
0.0375	4.056E-04	1.290E-02	1.290E-02	1.300E-02	107.73
0.1875	2.128E-04	1.190E-02	1.190E-02	1.200E-02	106.38
0.375	3.209E-04	1.195E-02	1.210E-02	1.230E-02	104.40
1.875	9.170E-05	1.300E-02	1.300E-02	1.310E-02	**102.74**
3.75	8.764E0-05	1.310E-02	1.310E-02	1.310E-02	105.82
18.75	**6.008E-05**	1.320E-02	1.320E-02	1.320E-02	109.51
37.5	9.651E-05	1.310E-02	1.310E-02	1.320E-02	**110.20**

Table G.9: Analysis of BER for Sine Signal with α= 5% and EMI Receiver result.

	Sine Wave				
m	BER Mean	Q1	Q2	Q3	PK (dBμV)
0.00125	**4.12E-04**	1.040E-02	1.040E-02	1.050E-02	106.73
0.00625	4.22E-04	1.140E-02	1.150E-02	1.150E-02	108.75
0.0125	5.02E-04	1.290E-02	1.290E-02	1.300E-02	108.77
0.0625	5.50E-04	1.190E-02	1.190E-02	1.200E-02	103.37
0.125	5.54E-04	1.195E-02	1.210E-02	1.230E-02	**102.03**
0.625	5.45E-04	1.300E-02	1.300E-02	1.310E-02	107.9
1.25	**5.68E-04**	1.310E-02	1.310E-02	1.310E-02	108.53
6.25	5.65E-04	1.320E-02	1.320E-02	1.320E-02	**109.75**
12.5	4.21E-04	1.310E-02	1.310E-02	1.320E-02	**109.75**

Table G.10: Analysis of BER for Random Signal with α= 5% and EMI Receiver result.

	Random Wave				
m	BER Mean	Q1	Q2	Q3	PK (dBμV)
0.00125	6.03E-04	1.040E-02	1.040E-02	1.050E-02	109.25
0.00625	6.42E-04	1.140E-02	1.150E-02	1.150E-02	109.27
0.0125	6.67E-04	1.290E-02	1.290E-02	1.300E-02	109.1
0.0625	**6.70E-04**	1.190E-02	1.190E-02	1.200E-02	109.07
0.125	6.20E-04	1.195E-02	1.210E-02	1.230E-02	**108.39**
0.625	6.20E-04	1.300E-02	1.300E-02	1.310E-02	107.42
1.25	5.94E-04	1.310E-02	1.310E-02	1.310E-02	107.02
6.25	**1.24E-03**	1.320E-02	1.320E-02	1.320E-02	108.77
12.5	6.10E-04	1.310E-02	1.310E-02	1.320E-02	**109.72**

Appendix H

Relative Values of BER and PK

	Sine		Random	
α	Relative PK	Relative BER	Relative PK	Relative BER
0.5	3.01	-2.02E-04	0.49	-1.16E-05
	0.99	-1.93E-04	0.47	2.70E-05
	0.97	-1.13E-04	0.64	5.21E-05
	6.37	-6.52E-05	0.67	5.53E-05
	7.71	-6.07E-05	1.35	5.14E-06
	1.84	-6.99E-05	2.32	4.80E-06
	0.15	-4.65E-05	2.72	-2.09E-05
	-0.01	-4.96E-05	0.97	6.25E-04
	-0.01	-1.94E-04	0.02	-4.58E-06
0.15	4.51	3.02E-04	2.05	3.97E-04
	2.05	3.51E-04	2.24	4.07E-04
	4.38	1.12E-04	2.01	4.06E-04
	9.51	1.54E-04	3.36	2.13E-04
	10.52	1.76E-04	5.34	3.21E-04
	2.83	1.87E-04	7	9.17E-05
	1.21	2.16E-04	3.92	8.76E-05
	-0.64	2.25E-04	0.23	6.01E-05
	-0.32	2.17E-04	-0.46	9.65E-05
0.25	7.69	6.70E-04	5.3	3.81E-03
	5.78	7.88E-04	5.09	1.66E-03
	5.6	8.76E-04	4.43	1.39E-03
	10.47	7.88E-04	8.14	7.47E-04
	11.43	1.01E-03	8.42	7.03E-04
	3.58	1.07E-03	6	4.75E-04
	1.35	7.477E-04	5.22	4.221E-04
	-0.83	6.692E-04	0.75	5.214E-04
	-0.95	6.720E-04	-0.66	2.711E-03
0.35	8.27	2.256E-03	6.17	8.890E-03
	6.46	2.352E-03	5.94	8.504E-03
	6.5	2.247E-03	6.11	8.587E-03
	10.79	1.453E-03	9.24	6.056E-03
	11.85	1.669E-03	9.9	4.132E-03
	3.86	2.335E-03	6.74	2.903E-03
	1	2.778E-03	6.73	2.680E-03
	-1.52	2.799E-03	-0.21	2.660E-03
	-1.32	2.370E-03	-0.74	2.370E-03
0.45	8.88	9.799E-03	8.4	1.645E-02
	6.96	1.084E-02	8.16	1.688E-02
	6.94	1.228E-02	7.72	1.711E-02
	10.95	1.132E-02	10.42	1.250E-02
	11.99	0.01141123	10.5	0.00887593
	3.7	0.01243423	7.34	0.00787853
	0.75	0.01249323	5.4	0.00793523
	-2.08	0.01258523	-0.31	0.00800923
	-1.59	0.01253523	-1.7	0.00885653

Appendix I

Pseudorandom Algorithms Used in Labview

I.1 Random Modulation Scheme

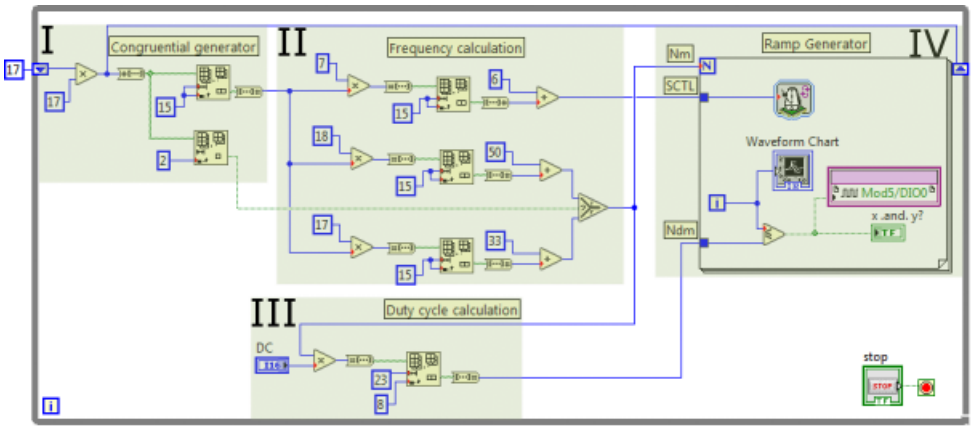

Figure I.1: Programmed block in Labview for generating simple random modulation streams.

- I) Defines the linear congruential generator (LCG) that generates a stream of pseudo-random variables along the desired time of execution.
- II) Generates the clock cycles to generate the desired frequency needed with the low and high limits defined by Carson's rule.

- III) Controls the duty cycle parameters with regards to the previous calculation of switching frequency.

- IV) Generates the ramp profile with regards to the desired scaled frequency to be used for the power converter.

I.2 Random Modulation Scheme with Rate Control

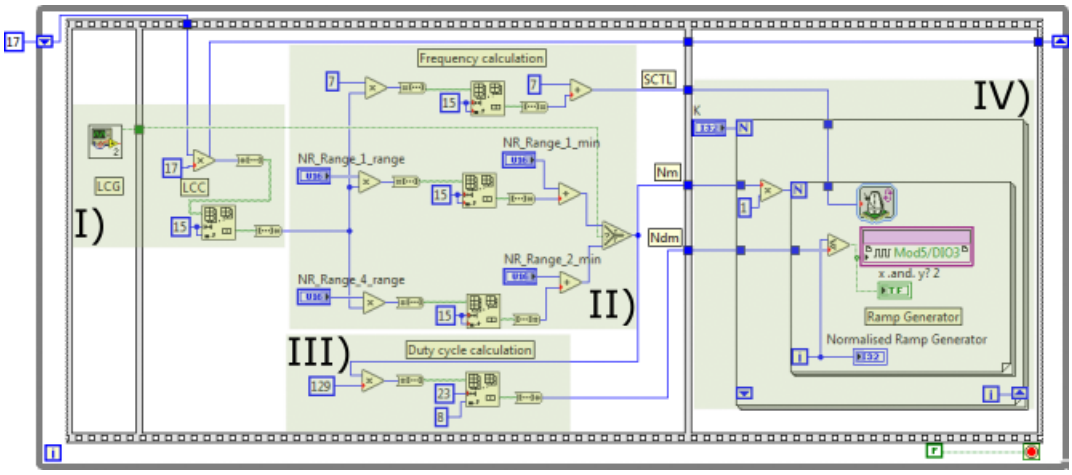

Figure I.2: Programmed block in Labview for generating simple random modulation streams.

- I) Defines a modified linear congruential generator (LCG) to generate the same pseudo-random stream of data for the control of repetition rate.

- IV) The generation of the ramp profile with regards to the desired scaled frequency is calculated for every value of, in fact the parameter k is responsible for defining the number of repetitions in the modified random modulation block.